METHUEN'S
MONOGRAPHS ON
PHYSICAL SUBJECTS

General Editor: B. L. WORSNOP, B.SC., PH.D.

MAGNETIC MATERIALS

Magnetic Materials

F. BRAILSFORD

PH.D.(LONDON), WH.SCH., M.I.E.E.

Research Department, Metropolitan-Vickers Electrical Company Ltd., Manchester

WITH 86 DIAGRAMS

LONDON: METHUEN & CO. LTD.
NEW YORK: JOHN WILEY & SONS, INC.

First Published March 11th 1948
Second Edition, Revised, June 1951
Reprinted 1954

2.2
CATALOGUE NO. 3977/U (METHUEN)

PRINTED IN GREAT BRITAIN

PREFACE

In this short book the aim has been to give to the advanced student, the research worker and those concerned with the technological applications of magnetic materials, a comprehensive outline of the present state of knowledge of the subject. The information given is necessarily brief, but it is hoped that lack of detail is remedied to some extent by the provision with each chapter of references to original work.

A list of books and summarizing articles which the author has found helpful while writing this monograph is given on the following page, and acknowledgment is made to these and to the original sources, quoted as references, which have been consulted. The author is also indebted to the Metropolitan-Vickers Electrical Company for permission to include some information not hitherto published, and to his wife for assistance with the manuscript.

F. BRAILSFORD

TIMPERLEY
CHESHIRE

PREFACE TO SECOND EDITION

In presenting a second edition of this book the opportunity has been taken to correct and amend the text in several minor respects and to add some recent references.

F. B.

LIST OF BOOKS AND SUMMARIZING ARTICLES

BOOKS

1. *Magnetic Induction in Iron and Other Metals*, J. A. Ewing ('Electrician Series', London, 1900).
2. *Die Ferromagnetischen Legierungen*, W. S. Messkin and A. Kussmann (Julius Springer, Berlin, 1932).
3. *Magnetism and Matter*, E. C. Stoner (Methuen, London, 1934).
4. *Magnetism*, E. C. Stoner (Methuen, London, 1936).
5. *Introduction to Ferromagnetism*, F. Bitter (McGraw-Hill, New York, 1937).
6. *Modern Magnetism*, L. F. Bates (Cambridge University Press, 1939).
7. *Ferromagnetismus*, R. Becker and W. Döring (Julius Springer, Berlin, 1939).

SUMMARIZING ARTICLES

1. 'Stand der Forschung und Entwicklung auf dem Gebiet der ferromagnetischen Werkstoffe', A. Kussmann, *Arch. f. Elek.*, 1935, **29**, 297.
2. 'Present Status of Ferromagnetic Theory', R. M. Bozorth, *Elec. Engg.*, 1935, **54**, 1251.
3. 'Directional Ferromagnetic Properties of Metals', R. M. Bozorth, *Journ. App. Phys.*, 1937, **8**, 575.
4. 'Recent Developments in Magnetic Materials', C. E. Webb, *Journ. I.E.E.*, 1938, **82**, 303.
5. 'Wege und Ergebnisse der ferromagnetischen Werkstofforschung', A. Kussmann, *Z.V.D.I.*, 1939, **83**, 445.
6. 'The Physical Basis of Ferromagnetism', R. M. Bozorth, *Bell Syst. Tech. Journ.*, 1940, **19**, 1.
7. 'A Survey of Electrical Sheet Steels for Power Plant and the Factors affecting their Magnetic Properties,' F. Brailsford, *Journ. I.E.E.*, 1943, **90**, Part 2, 307.
8. 'Magnetism in Theory and Practice', E. C. Stoner, *Journ. I.E.E.*, 1944, **91**, Part 1, 340.

CONTENTS

CHAPTER I

INTRODUCTORY

1.1. MAGNETIZATION

THE term 'magnetic materials' may be said to embrace all substances since all exhibit some magnetic effect, but in those known either as diamagnetics or paramagnetics, the effect is exceedingly feeble and, by the technologist, they are commonly regarded as 'non-magnetic'. In this book we shall be concerned mainly with that class of elements and alloys, of which iron is the most important, which display magnetism to an extraordinary degree and which are said to be 'ferro-magnetic'.

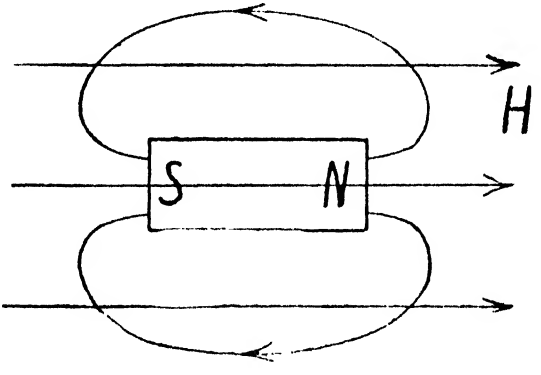

FIG. 1.1

If a piece of soft iron is placed in a magnetic field as shown in Fig. 1.1, magnetism is induced in it and north and south poles appear at its ends. The effect of these induced poles is to increase the field strength in the medium near the poles external to the iron, but to reduce it around the sides and, indeed, also within the space now occupied by the iron. Unless the iron specimen is of special form it will not be uniformly magnetized from end to end but,

for present purposes, we may disregard this. If the induced poles are each of pole strength m and the length of the iron is l, its magnetic moment $M = ml$. We may define the intensity of magnetization of the iron, denoted by J, as the magnetic moment per unit volume. Whence, if the volume is V and the section A, clearly

$$J = \frac{M}{V} = \frac{m}{A}$$

so that the intensity of magnetization may also be defined as the pole strength per unit area.

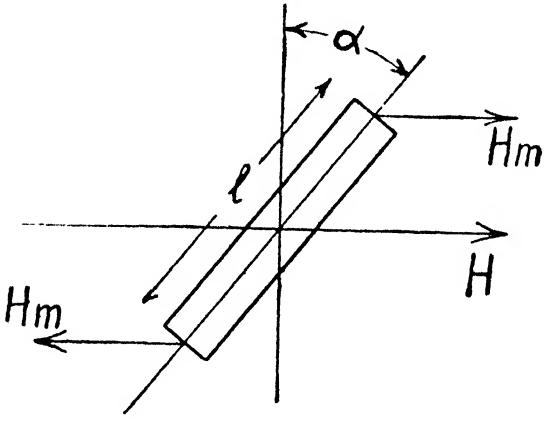

FIG. 1.2

Now a pole is said to have unit strength if, when concentrated at a point, it repels an equal and similar pole at 1 cm. distance, in a vacuum, with a force of 1 dyne. If such a pole is placed in a magnetic field the intensity of the field, or the field strength, at the point may be defined as the force in dynes experienced by the unit pole.

Let us now substitute a permanent magnet, which we assume free to rotate, in place of the soft iron of Fig. 1.1. We suppose the material of this magnet is so magnetically hard that the field H has no appreciable effect on its permanent magnetism. If the poles are of strength m, each is acted on by a force Hm as shown in Fig. 1.2, and

if the length of the magnet is l and it is inclined to the field as shown, the torque L per unit volume acting on it is given by

$$L = H.\frac{ml}{V}.\cos\alpha$$

or

$$L = HJ_m \cos\alpha$$

where J_m is the permanent intensity of magnetization of the magnet. It will be clear that, on account of this torque, the magnet is capable of doing work in turning into the field direction, and therefore for any angle α the magnet in the field possesses potential energy. If we take as our datum level of energy that corresponding to $\alpha = 0$, the potential energy then being assumed zero, the potential energy per unit volume for the angle α is given by

$$E = -\int_0^\alpha L\, d\alpha = -HJ_m \sin\alpha$$

Of if $J = J_m \sin\alpha$ is the resolved component of the intensity of magnetization in the field direction, the potential energy is given by

$$E = -HJ$$

Clearly, if by a small movement $d\alpha$ of the magnet, J increases by dJ there is a change in potential energy $dE = -H\,dJ$. If the magnet moves in a viscous medium this fall in the potential energy may reappear as heat in the medium, or again if the medium is conductive the movement of the magnet may set up eddy currents in it which will dissipate the energy. The medium might, however, be purely elastic, and in this case the decrease of potential energy would be exactly balanced by additional energy stored in the medium. In any case the sum of energy stored and heat dissipated is given by

$$E = \int_{J_1}^{J_2} H\, dJ$$

Let us now consider a long uniform rod of iron magnetized by a parallel applied field, for example, by a long solenoid carrying a current. Magnetic conditions near the centre of the rod will be uniform since the induced poles at the ends will be very remote. Consider a unit cube of the material in the rod separated by a very thin void on all sides as shown in Fig. 1.3. This gap might be of infinite thinness so that it would have no effect on the uniform magnetic conditions in the rod. The effect of the applied field H would be to induce north and south

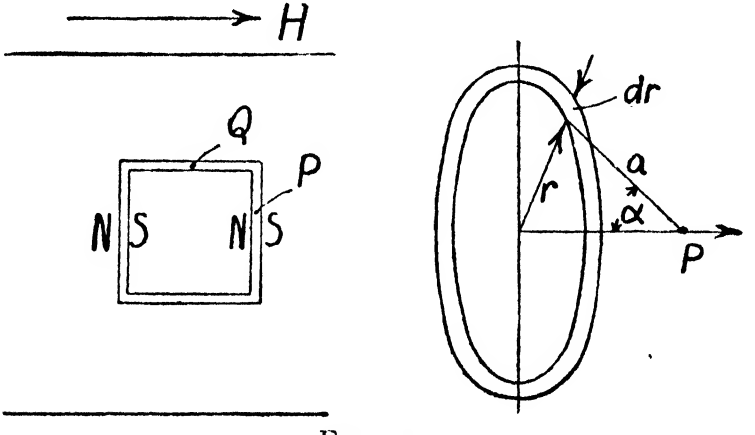

FIG. 1.3

magnetic poles on either end of the cube and on either side of the corresponding gaps as shown in the figure. If J is the intensity of magnetization in the rod the pole strength of each end of the cube and on either side of the gaps will be J. Suppose now we insert a unit pole into the gap at P. The pole strength of an annular element of the surface of the cube of radius r and width dr will clearly be $2\pi rJ\,dr$ and if this subtends a semi-vertical angle α at P it will be clear that the total force due to this element on the unit pole at P, in the axial direction, is given by dF where

$$dF = \frac{2\pi rJ \cos\alpha \; dr}{a^2}$$

which may be written

$$dF = 2\pi J \sin \alpha \, d\alpha$$

Since P is very near the surface the total force on the unit pole due to the whole of the surface is obtained by integrating this between the limits of α, 0 and $\frac{\pi}{2}$, whence

$$F = \int_0^{\frac{\pi}{2}} 2\pi J \sin \alpha \, d\alpha$$

$$= 2\pi J$$

Thus the force on unit pole at P due to the cube face is $2\pi J$, and since P lies between two faces of equal and opposite pole strength the total force due to these surfaces is $4\pi J$. Now in the gaps at the sides of the cube such as at the point Q there are no free poles and the total force on unit pole there is only that due to and equal the applied field H, and this field is also existing at P. The total force on a unit pole at P is therefore $H + 4\pi J$. This is known as the induction and represented by B. Whence

$$B = H + 4\pi J$$

which may also be written

$$(B - H) = 4\pi J$$

The ratio $\frac{B}{H}$ is called the permeability of the material and the ratio $\frac{J}{H}$ the susceptibility, denoted by μ and κ respectively. Therefore it is clear that

$$\mu = 1 + 4\pi\kappa$$

Magnetization curves may be plotted with B as ordinate and H as abscissa, or alternatively with J or $(B - H)$ as ordinate. The former curves are in the most useful form for the technologist who requires to know the induction for his calculations, but in investigating and comparing

magnetic materials J or $(B - H)$, the latter sometimes called the ferric induction, is usually of greater interest. The electromagnetic unit of induction is the gauss, a name which will be applied in this book also to the unit of field strength, so that $(B - H)$ or $4\pi J$ is also in gauss.

The magnetization curve for a sample of ordinary dynamo sheet is shown in Fig. 1.4. This is typical in form of that of any magnetic material which, having

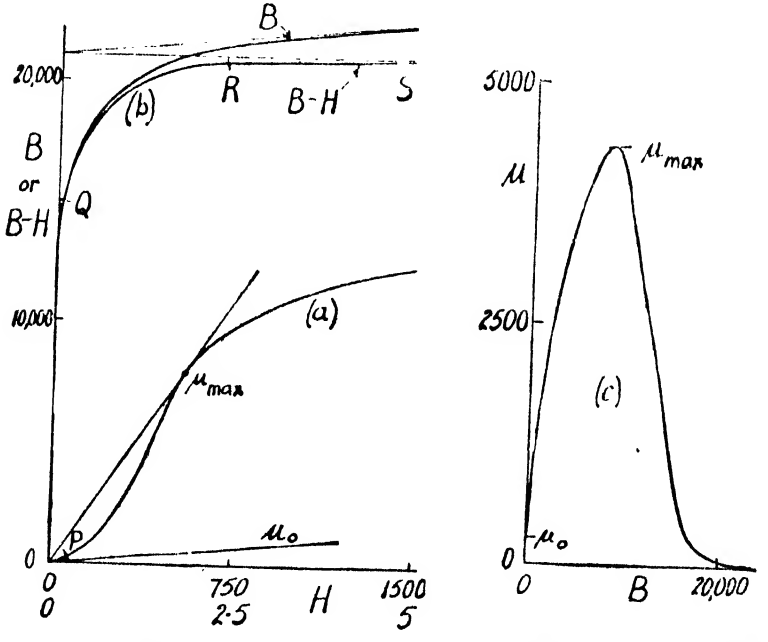

FIG. 1.4.—Magnetization Curves of Annealed Dynamo Sheet

reasonable purity and being well annealed, is in the 'soft' condition, and its characteristic features may be seen in the curves at (*a*) and (*b*) drawn to different scales of H. Two curves are drawn at (*b*), one to a scale of B and the other with $4\pi J$ or $(B - H)$ as ordinate. The magnetization curve may be divided into four parts overlapping somewhat indefinitely at the points P, Q, and R. The first part OP, corresponding to low values of H, is found to be reversible and B increases only very slowly with H

in this region. The slope of a tangent to the curve at the origin gives the permeability at $H = 0$ or the initial permeability μ_0. Over the region PQ the induction increases at a much more rapid rate as H is increased, and a tangent to the curve fixes the point of maximum permeability $\mu_{max.}$ as shown. This part of the magnetization curve is irreversible in character, that is, if at any point on it H is reduced the curve for increasing H is not retraced. Beyond Q a further increase of B is obtained only with a very large increase of H, and it is apparent that a change in the mechanism of the magnetization process occurs in the region of the point Q, a point usually referred to as the knee of the curve. As H is still further increased the curve for $(B - H)$ eventually becomes almost horizontal, as shown by RS, and $(B - H)$ or $4\pi J$ reaches a saturation value $(B - H)_{sat.} = 4\pi J_s$. It will be noted that it is the intensity of magnetization J_s which has a saturation value and that the induction B can continue increasing without limit. The permeability curve in Fig. 1.4(*c*) serves to emphasize the non-linear relation between B and H. The permeability in this example rises from $\mu_0 = 250$ to $\mu_{max.} = 4{,}000$ and at $B = 23{,}000$ gauss falls again to $\mu = 11.5$. The curves shown in the figure are, as already stated, representative in form, although not, of course, in the actual magnitudes of B and H which vary considerably with different materials, of those of a good well-annealed material. A much inferior curve, rising eventually, however, to the same saturation value, would be obtained for the same material in the unannealed work-hardened condition.

1.2. HYSTERESIS

As already mentioned in the previous section, the magnetization curve over certain portions, particularly the region PQ of Fig. 1.4, is irreversible. This leads to the phenomenon to which Ewing gave the name of magnetic ' hysteresis ', derived from the Greek for ' to lag behind '.

Referring to Fig. 1.5(*b*), which relates to a sample of transformer sheet steel, it will be seen that if H is reduced from the point P on the initial magnetization curve the induction decreases along the path PQ. At Q, where the applied field is reduced to zero, an induction correspond-

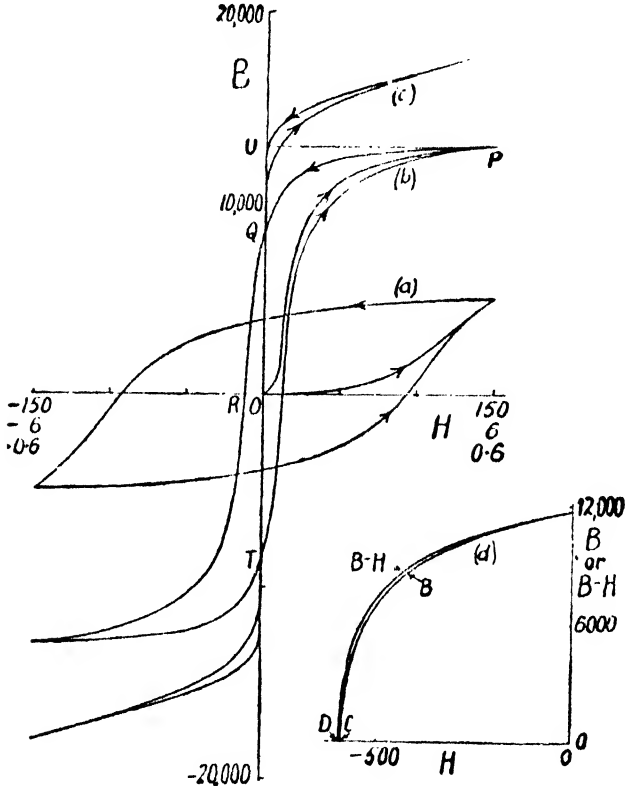

FIG. 1.5.—Hysteresis Loops of 4% Silicon Transformer Steel, (*a*), (*b*), (*c*), and Demagnetization Curve of a Permanent Magnet Material (*d*)

ing to OQ, known as the remanence, remains in the specimen, and, in order to reduce this induction to zero, a field strength corresponding to OR in the reverse direction is required. This reverse field is called the coercive force. The relation between B and H for a complete cycle of values of the latter, with the same amplitude in the for-

ward and reverse directions, is given by the hysteresis loop in which the arrows indicate the direction of traversal, as shown. The appearance of the hysteresis loop depends greatly on the amplitude of its extremities as shown at (*a*), (*b*), and (*c*) in Fig. 1.5, in which the abscissa scales in the three diagrams cover a wide range of H. In the case of that hysteresis loop in which the amplitude of the applied H is sufficient to produce saturation, the value of the induction at the remanent point is called the retentivity, while the corresponding coercive force is known as the coercivity.

It has already been shown that the energy required to raise the intensity of magnetization by an applied field is given by $\int H\,dJ$ over the appropriate limits. Thus referring to Fig. 1.5(*b*), it will be clear that if this loop had been plotted with J for the ordinate scale instead of B, the total energy put into the specimen per unit volume, in traversing the loop from T to P, would be measured by the area TPU. On returning from P to Q energy is restored by the specimen, which, with ordinates plotted in terms of J, would be represented by the area PQU. Thus in passing round one half of the hysteresis loop from T to Q, energy has been put into the specimen in excess of that recovered corresponding to the area TPQ. In fact in encompassing the complete loop this energy, which is dissipated as heat in the specimen and known as hysteresis loss, is measured by the area of the whole hysteresis loop when this is plotted to scales of J and H. If the ordinate scale is $(B - H)$ or $4\pi J$ the area has clearly to be divided by 4π to obtain the hysteresis loss. In the latter case a little consideration will show that no change to the area of the loop is caused by changing the ordinate scale from $(B - H)$ to B. Thus the area of the hysteresis loop to scales of B and H is a measure of 4π times the hysteresis loss, which, in C.G.S. units, will be in ergs per c.c. per cycle.

In transformers and in parts of rotating electrical

machines the magnetic materials employed are subjected to rapidly alternating induction. Thus in such apparatus the hysteresis cycle is repeated, in the case of a transformer at the normal power supply frequency, 50 times per second. The hysteresis loss thus produced leads to a loss in efficiency and adds to the temperature rise produced in the equipment, and thus for such apparatus materials of low hysteresis loss are required. Fig. 1.5(*d*) shows, however, by way of contrast, part of the saturation hysteresis loop of a permanent magnet material. In this particular class of magnetic material the highest possible hysteresis effect, with high coercivity and retentivity, is required for reasons which will be described in more detail in Chapter 7, and that part of the hysteresis loop shown, known as the demagnetization curve, is the characteristic on which the quality of a permanent magnet material is judged. If the demagnetization curve is plotted to an ordinate scale of $4\pi J$ or $(B - H)$ the curve will, bearing in mind that H is here negative, lie higher than the B curve as shown. This cuts the H axis at a point D to the left of the point C, which latter gives, according to the definition above, the true coercivity of the material. The difference between the points C and D is not very great with the commercial permanent magnet materials but can be very great with certain alloys. This difference should be remembered when comparing demagnetization curves which may have either J or B as ordinates.

In Fig. 1.6(*a*) are shown [1], for a sample of soft iron, the subsidiary hysteresis loops which may be formed when, in the course of increasing an applied field, this is reduced to zero and then reapplied. Similar subsidiary loops formed while traversing the principal loop for another sample of iron are shown at (*b*). It will be clear that a sample subjected to such irregular cycles of magnetization will have additional hysteresis loss corresponding to the additional areas of the subsidiary loops.

These curves also serve to emphasize the further point

that the observed relations between B and H depend upon the previous magnetic history of the specimen. The initial magnetization curves and subsequent hysteresis loops shown in Figs. 1.4 and 1.5 relate to specimens which before the test had been demagnetized in order to reduce the remanent magnetization to zero. Demagnetization is commonly carried out by subjecting the sample in the testing apparatus to repeated reversals of the induction

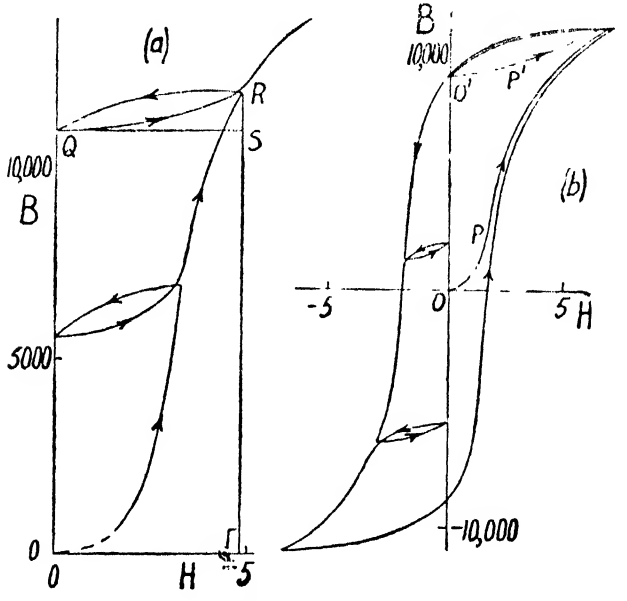

FIG. 1.6.—Subsidiary Hysteresis Loops for Samples of Iron (Ewing)

from a high value down to zero. If this procedure is not carried out we might start with a specimen with an initial residual magnetization corresponding, for example, to the point O' in Fig. 1.6(b). The apparent initial magnetization curve, if this were determined step by step, would then be along $O'P'$, with O' as origin, a curve quite different from the true curve OP. Also if the test were continued in order to delineate a normal hysteresis loop, it would be found that this did not close on itself and

many cycles would require to be completed before the material reached a ' cyclic state ' when successive hysteresis loops were coincident.

In some applications, for example in smoothing reactors and in inductor alternators, the magnetic materials may have an alternating induction where a steady, unidirectional applied field is also present. In such cases the magnetization cycles will be represented by some such subsidiary loop as that shown at QR in Fig. 1.6(a), although the extremities of the loop may be at other points than those shown. For the loop QR the apparent, or incremental permeability μ_Δ may be defined by the ratio $\mu_\Delta = \dfrac{RS}{QS}$, which is clearly lower than the permeability corresponding to the point R of the initial magnetization curve in the ratio of RS to RT. The effect of a steady applied field is not only to reduce the apparent permeability to a superimposed alternating induction, but also for a given amplitude of the latter to increase the hysteresis loss per cycle. Some data are given in Chapter 5.

The hysteresis loss corresponding to a slow traversal of the hysteresis loop, termed the static hysteresis loss, may obviously be obtained by measuring the area of the loop, although accurate determinations become more difficult at the higher inductions for the magnetically soft materials because of the relatively small difference between the ascending and descending sides of the loop. A sample in the form of a disc may, however, be taken through a cycle of alternating magnetization by rotating it in a steady field. For slow rotation the mean work done to rotate it through one revolution corresponds to the static hysteresis loss for one cycle. By using a sample consisting of several discs accurate determinations of the hysteresis loss may be made up to high inductions by measuring the torque required to rotate the sample [2].

The general form of the relation for magnetically soft materials between the static alternating hysteresis loss and

the amplitude of $(B - H)$ or $(B - H)_{max.}$, which is inappreciably different from B except at high inductions, is shown in Fig. 1.7(a) by curve P. On the lower portion the empirical equation of Steinmetz

$$w_h = \eta B_{max.}^{n} \quad . \quad . \quad . \quad (1.1)$$

where w_h is the hysteresis loss in ergs per c.c. for a single cycle and η and n are constants, can be made to fit the observed results fairly accurately. For the upper portion of the curve, however, a straight line relation is found to apply up to the highest values of $(B - H)_{max.}$ for which measurements have been made. The relation is given by

$$w_h = b\{(B - H)_{max.} - c\} \quad . \quad . \quad (1.2)$$

or by $$w_h = b'\{J_{max.} - c'\}.$$

where b, c, b', and c' are constants. Values of the Steinmetz coefficient η and the various constants are given in Chapter 5 for a number of sheet materials. The observed curve runs gradually from one form to the other, as shown in Fig. 1.7(a), the transition occurring in the region of the knee of the magnetization curve.

If a magnetic material is subjected to an induction whose vector, whilst remaining constant in magnitude, rotates continuously in one direction, it will be found that the intensity of magnetization lags by an angle in space behind the applied rotating field which produces it. Energy is, again in this case, lost as heat in the material. The relation between the rotational hysteresis loss [3] and the value of $(B - H)$ is shown in Fig. 1.7(a) by the curve Q for the same disc specimens used to obtain curve P. It will be seen that a discontinuity again occurs in the region corresponding to the knee of the magnetization curve shown by curve R. The rotational loss rises with increasing magnetization to a maximum and then, near saturation, approaches zero. The curve S shows the ratio of rotational to alternating hysteresis loss in relation to $(B - H)$ or $(B - H)_{max.}$ as a fraction of $(B - H)$ at saturation,

This relation was found by the author to hold, approximately, for a number of materials where the alternating and rotational measurements were made on identically the same disc specimens

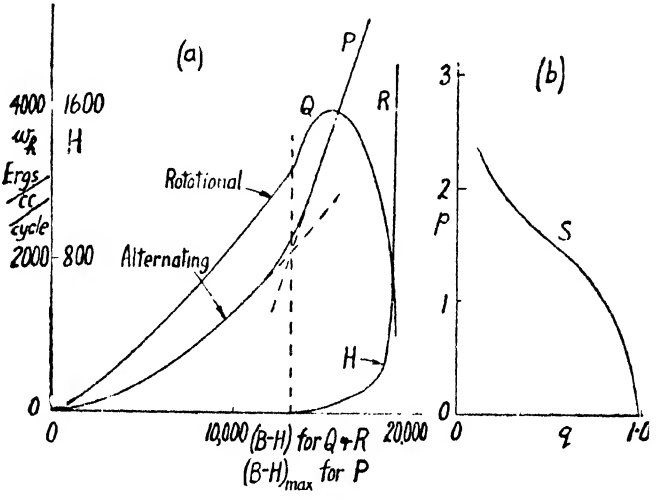

FIG. 1.7.—(*a*) Form of Alternating and Rotational Hysteresis Loss Curves for a Sample of Transformer Sheet Steel. (*b*) Relation between Rotational and Alternating Hysteresis Loss: p is ratio of Alternating to Rotational Loss and q the value of $(B - H)$ or $(B - H)_{max}$. as a fraction of its Saturation Value.

1.3. EDDY CURRENTS

In a transformer core the induction is an alternating one following, ideally, a sinusoidal wave form. The same is true for the armature of a rotating machine, except that in this case the wave form is distorted by harmonics and, in the region behind the armature teeth, a combination of alternating and rotational flux occurs. These magnetic circuits are built up of thin insulated sheets of magnetic material of varying grades according to the particular application, the materials being classed under the general title of 'Electrical Sheet Steels'. The object of thus laminating the flux path is to reduce the magnitude and effect of the Foucault or eddy currents which are set up

in the steel by the alternating flux. These currents flow parallel to the surface of the steel and perpendicular to the direction of the induction. They set up a field opposing the applied field and thus cause the flux density to decrease progressively from the surface inwards, thereby tending to reduce the flux-carrying capacity of the material for a given applied field. The currents flowing in the steel are, at the same time, a source of heating or eddy current loss.

Exact mathematical calculation of the effects cannot be made because of the extremely non-linear relation, which the hysteresis loop represents, between B and H. However, an approximate solution may be obtained by assuming the permeability to be constant, that is, the hysteresis loop is condensed to a single straight line through the origin. In this case it may be shown [4] that the instantaneous induction b at any point inside a lamination is given by the following expression:

$$b = B_0\left(\frac{\cosh 2px + \cos 2px}{\cosh 2pa + \cos 2pa}\right)^{\frac{1}{2}} . \cos(\omega t - \nu)$$

where

$$\tan \nu = \frac{\sinh p(a-x) . \sin p(a+x) + \sinh p(a+x) . \sin p(a-x)}{\cosh p(a-x) . \cos p(a+x) + \cosh p(a+x) . \cos p(a-x)}$$

In this expression the flux density in the surface layer $b_0 = B_0 \cos \omega t$, where $\omega = 2\pi f$, f being the frequency of the applied field. Also $p = 2\pi\sqrt{\frac{\mu f}{\rho}}$ where μ and ρ are the permeability and resistivity respectively of the steel, and $2a$ is the thickness of the sheet. It will be seen that both the magnitude and phase of the induction are dependent on the distance from the surface.

The calculated amplitude of the induction inside laminations of the quality of ordinary dynamo sheet for various thicknesses at a frequency of 50 cycles per second is shown in Fig. 1.8. The values assumed are $\mu = 2{,}500$, $\rho = 14{,}000$ e.m.u.

If the flux density across the section of the sheet is uniform, and it may be seen from Fig. 1.8 that for a dynamo steel of the standard thickness of 0·016 inch (0·4 mm.) working at the normal supply frequency the calculated values, at least, do not depart far from this condition, it may easily be shown that the eddy current loss is given by

$$W_e = \frac{(\pi . 2a . f . B_{max.})^2}{6 . \rho} \text{ ergs per c.c. per sec.} \quad (1.3)$$

where ρ is again in electromagnetic units.

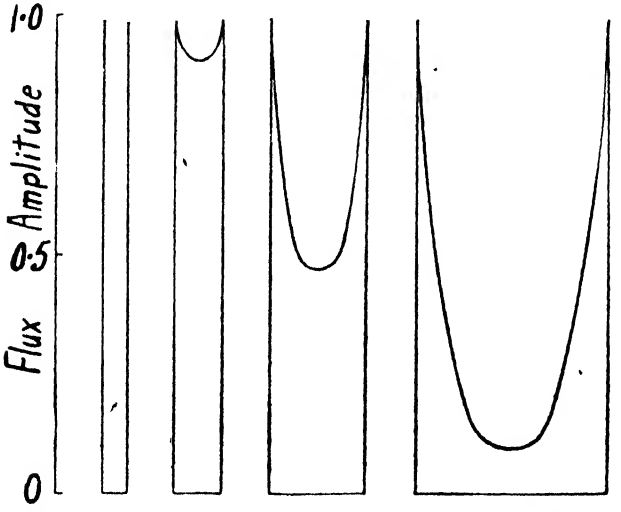

FIG. 1.8.—Calculated Amplitude of Alternating Flux in Sheets of various Thicknesses as a fraction of the value at the Surface. The curves apply to Ordinary Dynamo Steel at 50 c.p.s. for thicknesses of 0·016″, 0·032″, 0·064″, and 0·128″ respectively. Alternatively they apply to any material or frequency with $2pa = 0{\cdot}75$, 1·5, 3, and 6 respectively

This formula will in fact apply when *pa* is small, and bearing in mind this limitation to its application, it will be seen that the eddy current loss is directly proportional to the square of thickness, frequency, and induction, and inversely proportional to the resistivity. The advantage of reducing the thickness as the frequency is increased will be apparent, and also the necessity for a high elec-

trical resistivity of the material if the eddy current loss is to be kept small.

The formulae given above are based on the assumption of constant permeability, as already stated, which means that if the applied field is sinusoidal the eddy currents and induction inside the sheet will also be of sine wave form. Now, in actual fact, the relation between B and H is far from linear, and therefore if one of these quantities is

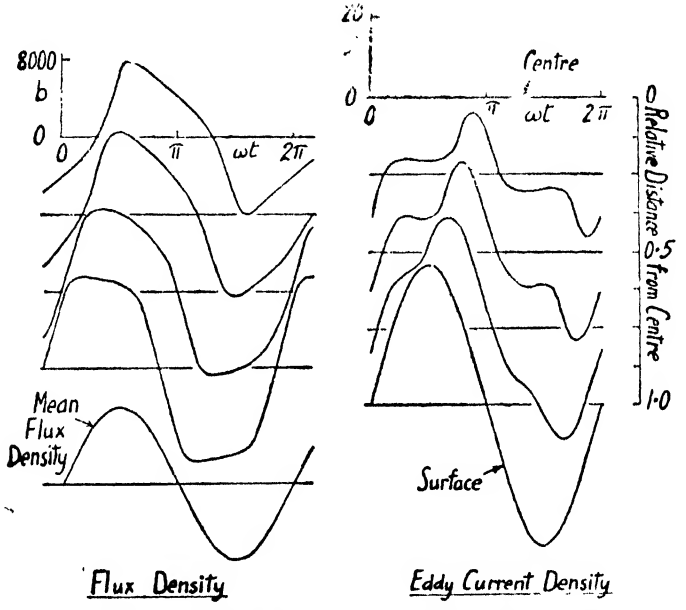

FIG. 1.9.—Probable Wave Forms of Flux and Eddy Currents inside a Sheet of Dynamo Steel 0·021″ thick at 50 c.p.s. Flux Density b is in gauss and Eddy Current Density i in amperes per sq. cm.

sinusoidal the other must be of distorted wave form. Since the effective field acting at any point inside a lamination is the resultant of the applied field and that produced by the eddy currents encircling the point, a little consideration will show that not only the amplitude and phase but the wave form also, of both induction and eddy currents, changes in passing through the sheet from the surface to the centre. In Fig. 1.9 the wave forms of the flux

density b and eddy current density i, which may be expected at various points inside a sheet of ordinary dynamo steel of 0·021 inch thickness at 50 cycles per second and with an average induction amplitude $B_{max.}$ = 8,000 gauss, the total flux being sinusoidal, are shown. These results were obtained by the author on a model, and a careful analysis of them shows that, in spite of the wave form distortion and a variation of the amplitude and phase of the waves greater than the theoretical values based on a constant permeability, the effect on either the eddy current or hysteresis components of iron loss is not very great [5].

1.4. TOTAL IRON LOSS

The total iron loss in a sample of thin sheet steel carrying a sinusoidal alternating flux thus consists of an eddy current and a hysteresis component and the total power loss per c.c. may be written

$$W_t = W_e + W_h = W_e + f.w_h \quad . \quad . \quad (1.4)$$

where w_h is as given in equations 1.1 and 1.2, and W_e is the eddy current loss component, the calculated value of which is given in equation 1.3. In writing down equation 1.4 it is assumed that the hysteresis loss per cycle is independent of frequency. We may rewrite this in the form

$$\frac{W_t}{f} = k_1 f B_{max.}^2 + w_h \quad . \quad . \quad (1.5)$$

where the calculated value of k_1 is, from equation 1.3, given by $\frac{4\pi^2 a^2}{6\rho}$.

Thus if the total iron loss is measured at a number of frequencies and, for a given value of $B_{max.}$, $\frac{W_t}{f}$ is plotted against f we obtain a relation which should conform to equation 1.5 and from which we should, clearly, be able to separate out the two components of loss. It is, how-

ever, found that when this is done the value of k_1, and thus also the value of the apparent eddy current loss, is much greater than its calculated value. The formula in equation 1.3 is derived with the assumption of a constant permeability and therefore takes no account of the wave form distortions of flux and eddy currents inside the sheet already referred to. This distortion, however, does not appear to be enough to account for the discrepancy and there appear to be no real grounds for believing that the actual eddy current loss is greatly different from the calculated value.

REFERENCES

1. J. A. Ewing, *Magnetic Induction in Iron and other Metals* (London, 1900), p. 95.
2. F. Brailsford, *Journ. I.E.E.*, 1939, **84**, 399.
3. F. G. Baily, *Phil. Trans. Roy. Soc.*, 1896, **187**, 715; F. Brailsford, *Journ. I.E.E.*, 1938, **83**, 566.
4. A Russell, *Alternating Currents*, 1914, Vol. 1, p. 490.
5. F. Brailsford, *Journ. I.E.E.*, 1948, **95**, Part 2, 38.

CHAPTER 2

FERROMAGNETISM

2.1. THE ELEMENTARY MAGNET

CONSIDER an electron with charge e circulating in an orbit of radius r as illustrated in Fig. 2.1(a). If the periodic time of rotation is τ the circular current in electromagnetic units is given by $i = \frac{e}{c\tau}$ where c is the velocity of light. Now it is well known that a circular current of strength i is

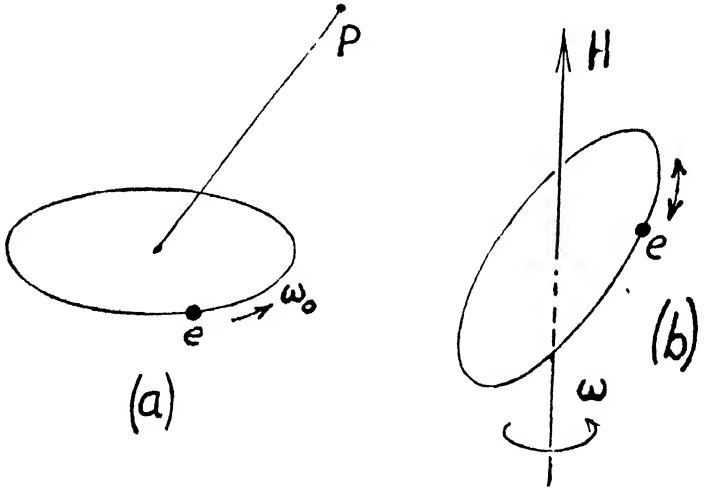

FIG. 2.1

equivalent in its external magnetic effect to a circular magnetic shell of strength σ where $\sigma = i$. Now if μ is the magnetic moment of the magnetic shell

$$\mu = S\sigma = \frac{eS}{c\tau} = \frac{e\omega_0 r^2}{2c} \quad . \quad . \quad (2.1)$$

where S is the area of the orbit and ω_0 is the angular velocity of the electron. Thus an orbital electron in a circular path will produce a field, at any external point

such as P, the same as that of a magnet of moment μ whose value is given by equation 2.1.

Now if j is the angular momentum of the electron in its orbit, then clearly

$$j = mr^2\omega_0 \quad . \quad . \quad (2.2)$$

and from equations 2.1 and 2.2 we have

$$\frac{j}{\mu} = \frac{2mc}{e} \quad . \quad . \quad (2.3)$$

Therefore the ratio of the angular momentum to the magnetic moment of the electron is clearly a fixed quantity independent of the angular velocity of the electron or the radius of the orbit.

Suppose now a field H is applied to any orbit, as shown in Fig. 2.1(*b*). It was shown by Larmor that under this condition the orbit as a whole precesses, with the direction of H as axis, and with an average angular velocity of precession ω given by

$$\omega = -\frac{e}{2mc}.H$$

It may be shown that the direction of the precessional rotation is such as to set up an opposing field to that applied. This is, in fact, the origin of the phenomenon called 'diamagnetism', and results, in those substances classed as diamagnetics, in a negative susceptibility.

The direct effect of a steady field on an electron in an orbit is thus to produce a precessional motion, but in any given material the interchange of energy between neighbouring atoms, in a state of thermal agitation, might also enable the field to turn the axes of the orbits on the average, towards the direction of the applied field and thus, in opposition to the diamagnetic effect, magnetize the material in the same direction as the field. In this event a change in magnetization, with a change in direction of the orbital axes, would clearly be accompanied by a change in the angular momentum of the specimen about the field direc-

tion as axis. Thus, if a rod suspended vertically has a field applied axially which induces a magnetic moment M in the rod and the angular momentum produced is J, then it may be shown that

$$\frac{J}{M} = \frac{j}{\mu}$$

and thus an experimental means is available to determine the ratio of the angular momentum to the magnetic moment of the elementary carrier of magnetism if this is a moving charged particle.

Moreover if these carriers are, in effect, minute gyroscopes formed by orbital electrons then, as with a gyroscope, rotation of the rod about its longitudinal axis will produce a couple on each orbit tending to turn it into the longitudinal direction, thus acting in the same way as an axially applied field. It may be shown that

$$\frac{H}{\omega} = \frac{j}{\mu}$$

where ω is the angular velocity of the rod and H is the equivalent field to produce the same magnetic effect as the rotation.

Thus experimentally the ratio may be determined, either by observing the angular momentum produced by a change of magnetization, or by observing the magnetic effect obtained by rotation of the specimen. The first successful experiments, by Barnett [1], used the latter method. He found that the direction of the effect corresponded with the magnetic carrier being a rotating negative charge, but the magnitude of the ratio $\frac{j}{\mu}$, for the magnetic specimens examined, was approximately only one half the value given by equation 2.3 for an orbital electron. His findings were subsequently confirmed by other investigators employing the rotation by magnetization method. This ' gyromagnetic anomaly ', which cast doubt on the electron orbit as the elemental magnet, is now explained by suppos-

ing the electron to spin on its own axis, in virtue of which it has an angular momentum and a magnetic moment distinct from those due to its orbital motion. The supposition that the electron had a spin with an associated angular momentum and magnetic moment, the ratio being one half that given by equation 2.3, was, in point of fact, made independently by Goudsmit and Uhlenbeck [2] to correlate the experimental data obtained from atomic spectra, and thus the observed gyromagnetic ratios came to fit naturally into the general theoretical scheme for atomic structure. The general conclusion is that the magnetization of a specimen occurs by a reorientation of the spin axes of electrons in the atom and that, in the ferromagnetics at least, the contribution due to the orbital motions is small.

Now the free atom of an element is conceived to consist of a central nucleus surrounded by a sufficient number of electrons to keep the atom neutral. By the Bohr theory these electrons were classified into groups and supposed to have their orbital motions in shells and sub-shells round the nucleus. In the further development of the theory each electron is defined by four quantum numbers, n, l, m, and s, which define the state of the electron, no two electrons having the same four numbers. n, the total quantum number, is a measure of the energy of the orbit and indicates the main shell, whilst l gives the orbital angular momentum of the electron and indicates the sub-shell. The third quantum number m, which, like n and l, is always an integer, gives the resolved component of the orbital angular momentum in a particular direction, such, for example, as the direction of an applied magnetic field. Since m is a whole number, the orbital axis can alter its direction relative to a given fixed direction only in discrete jumps. Finally s gives the angular momentum due to the electron spin and always has the value $\pm \frac{1}{2}$ corresponding to spin in either the positive or negative directions.

The distribution of the electrons in the various shells and the corresponding n and l numbers for the free atom are shown in Table 2.1 for the ferromagnetic elements iron, cobalt, and nickel, while the direction of spin is indicated by the plus or minus sign.

Now for elements coming higher in the periodic table than nickel the third shell is completed with a total of 18 electrons, and a completed shell is magnetically neutral, the orbital and spin motions giving a zero resultant magnetic moment to the atom. But the free atoms of iron, cobalt, or nickel are seen, from the table, to be incomplete in their third shells to the extent of 4, 3, and 2 electrons respectively. These electrons are missing from the $3d$ sub-shell as indicated in the table and give to the free atom the number of uncompensated electron spins shown. The atom will thus have a magnetic moment corresponding to the number of uncompensated spins in this incompleted $3d$ sub-shell.

In the metallic state, however, the average distribution of electrons in the $3d$ sub-shell, and in the outer shell of the atoms making up the metal, is slightly different and it is deduced that this average distribution is as shown in Table 2.2, which indicates a different average number of uncompensated spins from that for the free atom.

The magnetic moment μ_B of a single spinning electron, called the Bohr magneton, has the value

$$\mu_B = \frac{eh}{4\pi mc} = 9{\cdot}174 \times 10^{-21} \text{ erg/gauss}$$

where h is Planck's constant, whence it is readily shown that the number of Bohr magnetons per atom is given by

$$b = \frac{J_0 A}{d\mu_B}$$

where A is the atomic weight, d is the density of the metal and J_0 is the saturation value of the intensity of magnetization. Thus the average number of uncompensated spins,

TABLE 2.1

DISTRIBUTION OF ELECTRONS IN THE FREE ATOM

SHELL	K	L		M			N		
n	1	2		3			4		
SUB-SHELL	s	s	p	s	p	d	s	SPIN	NUMBER OF UNCOMPENSATED SPINS
l	0	0	1	0	1	2	0		
	NUMBER OF ELECTRONS								
IRON	1	1	3	1	3	5	1	+	4
	1	1	3	1	3	1	1	−	
COBALT	1	1	3	1	3	5	1	+	3
	1	1	3	1	3	2	1	−	
NICKEL	1	1	3	1	3	5	1	+	2
	1	1	3	1	3	3	1	−	

TABLE 2.2

AVERAGE DISTRIBUTION OF ELECTRONS FOR THE METALLIC STATE

SUB-SHELL	$3d$	$4s$	SPIN	AVERAGE NUMBER OF UNCOMPENSATED SPINS PER ATOM
IRON	4·8	0·3	+	2·22
	2·6	0·3	−	
COBALT	5·0	0·35	+	1·71
	3·3	0·35	−	
NICKEL	5·0	0·3	+	0·606
	4·4	0·3	−	

or Bohr magnetons per atom, may be found experimentally from the observed saturation value (extrapolated to absolute zero). The values given in Table 2.2 have been so determined and represent the average magnetic moment of the atom in Bohr magnetons for the element in the metallic state.

2.2 THE LANGEVIN-WEISS THEORY

Now if a field H is applied to a substance at a given temperature, for example to a gas, the atoms or molecules of which each have a magnetic moment, each atomic magnet will acquire a magnetic potential energy determined by the field strength, the moment and the inclination of the magnetic axis to the field direction. It may be shown that if the magnetic axes of the atoms are free to turn in any direction the average distribution of the axes relative to the field direction will, under equilibrium conditions, be of a particular kind and such as to produce a resultant intensity of magnetization in the field direction. Langevin [3], in fact, obtained the following relation

$$\frac{J}{J_0} = \coth a - \frac{1}{a} \quad . \quad . \quad . \quad (2.4)$$

where J is the intensity of magnetization due to H, J_0 is the saturation value corresponding to parallel alignment of all axes, and $a = \frac{\mu H}{kT}$ where μ is the atomic or molecular magnetic moment, k is Boltzmann's universal gas constant, and T is the absolute temperature. Equation 2.4 clearly gives the theoretical magnetization curve for a substance in which the constituent magnets are free to turn in any direction and also exert no mutual magnetic effect upon one another. If the assumption of quantum mechanics, that only certain directions of the magnetic axes relative to the field direction are permissible, is made, however, equation 2.4 is modified. If the assumption is that only

two directions are allowed, parallel or anti-parallel with H, then the equation becomes

$$\frac{J}{J_0} = \tanh a \quad . \quad . \quad . \quad (2.5)$$

These expressions are plotted in Fig. 2.2.

The Langevin theory is found to be generally satisfactory when applied to those weakly magnetic materials classed as ' paramagnetics ', but fails when applied in this form

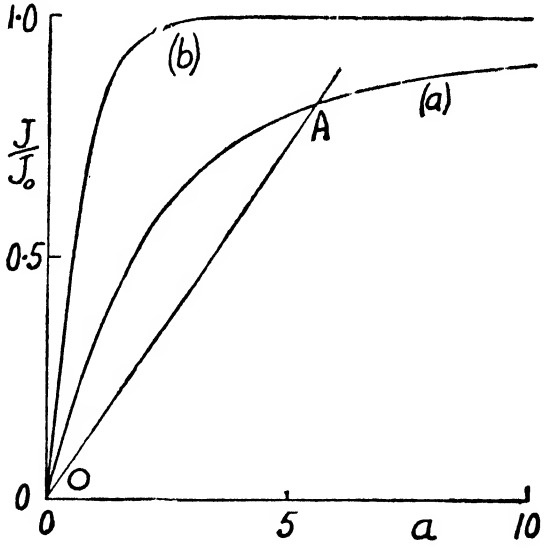

FIG. 2.2.—Magnetization Curves for a Paramagnetic: Curve (*a*) from the original Langevin Theory and Curve (*b*) as modified by Quantum Theory

to ferromagnetic materials. For, referring to curve (*b*) in Fig. 2.2, saturation is only reached when a is about 4. The corresponding value of H is given by

$$H = \frac{akT}{\mu}$$

If we substitute the appropriate value of μ for iron, by way of example, $\mu = 2{\cdot}04 \times 10^{-20}$ erg/gauss, and $T = 293°$ K. corresponding to 20° C. with $k = 1{\cdot}371 \times 10^{-16}$ erg/degree,

we find that $H = 7{\cdot}86 \times 10^6$ gauss. But it is a matter of common observation that a field strength of only a few hundred gauss is enough to bring a sample of iron near to saturation. Similarly, the permeability of iron, or any ferromagnetic, is far greater than the value deduced from the curves.

Weiss [4] overcame this difficulty by making the arbitrary assumption that, in a ferromagnetic, there was spontaneously induced a ' molecular field ' which was proportional in magnitude to, and in the same direction as the intensity of magnetization in the material. Thus, if an external field H was applied to a specimen, the effective field acting was $H + NJ$ where N was a factor of unspecified origin. Therefore if the material had a magnetization J then, even with no applied field, a molecular field $H_m = NJ$ would still be present. The relation between this molecular field and the magnetization will clearly be a straight line through the origin in Fig. 2.2 such, for example, as OA where, since $a = \frac{\mu H}{kT}$, the equation of OA is given by

$$a = \frac{J}{J_0} \cdot \frac{\mu N J_0}{kT} \quad . \quad . \quad . \quad (2.6)$$

A little consideration will show that, if the molecular field according to the line OA exists, then the material would not be stable in the unmagnetized condition represented by the point O but would, referring to curve (a), spontaneously magnetize itself to a saturation value represented by the point A. If J_s represents this saturation value then its value may clearly be obtained by eliminating a between equations 2.6 and 2.4 for the older Langevin theory and between equations 2.6 and 2.5 for the later theory. In the former case

$$\frac{J_s}{J_0} = \coth\left(\frac{J_s \cdot \mu N J_0}{J_0 \quad kT}\right) - \frac{J_0}{J_s} \cdot \frac{kT}{\mu N J_0} \quad . \quad (2.7)$$

It will be found that, in this expression, $\frac{J_s}{J_0} = 0$ when

$T = \theta = \frac{\mu N J_0}{3k}$, and we may write equation 2.7 in the form

$$\frac{J_s}{J_0} = \coth\left(\frac{J_s}{J_0}\cdot\frac{\theta}{T}\right) - \frac{J_0}{J_s}\cdot\frac{T}{\theta} \quad . \quad . \quad (2.8)$$

This is a general relation between the saturation magnetization and temperature which is plotted as curve (*a*) in Fig. 2.3, and would be valid if the axes of the elementary

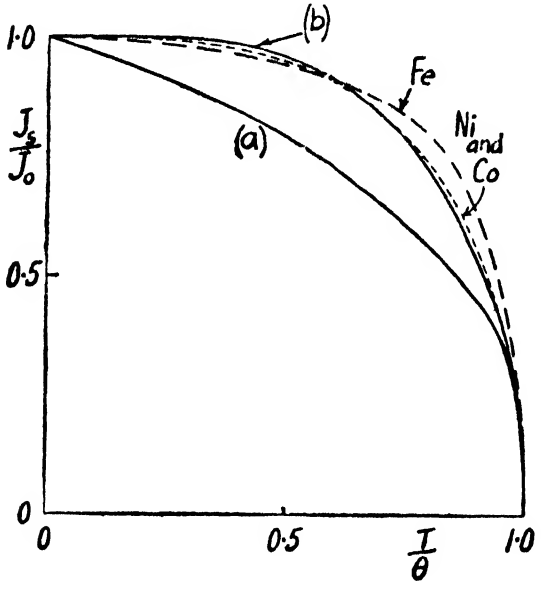

FIG. 2.3.—General Relation between Saturation Value and Temperature for Ferromagnetics

magnets were free to point in any direction. Where, however, the assumption of quantum theory is made, that only two directions are permissible, the relation between J_s and T is obtained from equations 2.5 and 2.6 and becomes

$$\frac{J_s}{J_0} = \tanh\left(\frac{J_s}{J_0}\cdot\frac{\theta}{T}\right) \quad . \quad . \quad . \quad (2.9)$$

where, however, θ is now $\frac{\mu N J_0}{k}$. Equation 2.9 is plotted as curve (*b*) in Fig. 2.3.

Now the experimentally observed saturation value of the ferromagnetics does in fact fall with rising temperature reaching substantially zero at a temperature known as the Curie temperature or magnetic change point. Thus θ represents the Curie temperature and, as has been shown, θ can be expressed in terms of the constants of the material and the Weiss molecular field constant N. The observed relations for the elements iron, cobalt, and nickel are shown in the figure and are seen to be in good agreement with the later theory.

The theory, thus far, leads to the conclusion that at any temperature below the Curie point a ferromagnetic, even in the absence of an externally applied field, is saturated to a value appropriate to the particular temperature. A sample in the demagnetized state, however, shows no external evidence of being magnetized at all and Weiss therefore made the further assumption that, although the material was everywhere self-saturated, it was also divided up by boundaries into small regions in which the directions of the magnetization vectors were, with no externally applied field, directed on the average at random. When, however, a field was applied, magnetization of the sample occurred by changes in direction of the saturation magnetization in whole domains, this process of reorienting the vectors requiring a much smaller field strength than is required in a paramagnetic.

The Weiss theory involving a molecular field of very high value—many millions of gauss—and the sub-division of a ferromagnetic into domains is now well supported by experimental evidence, and is the basis upon which the modern domain theory of ferromagnetism has been formed. Two main questions, to which, however, answers have been given, naturally arise. What is the origin of the molecular field and why are so few elements ferromagnetic?

A well-known example in quantum theory is that of the formation of the hydrogen molecule. If two hydrogen

atoms, each consisting of a positive nucleus and an electron, are brought together it may be shown that the total energy of the system can be a minimum when the distance between the nucleii has a certain value. The system is, in that case, stable with a fixed distance between the nucleii, that is, a hydrogen molecule has been formed. The condition for molecule formation in this way is that the pair of electrons belonging to the approaching nucleii shall be of opposite spin. The forces involved, known as 'exchange forces', which thus tie the atoms together as a hydrogen molecule, also give it a zero magnetic moment. The origin of the Weiss molecular field was explained by Heisenberg [5] in terms of these quantum mechanical forces of interaction which, however, in the ferromagnetic elements lead to a parallel, instead of an anti-parallel, alignment of electron spins, and thus give the spontaneous saturation believed to exist in the domains. It appears, from the calculations of Bethe [6], that the alignment of electron spins may be parallel or anti-parallel, depending on the ratio of the distance between neighbouring atoms to the diameter of the incomplete shell containing the electrons responsible for the magnetic moment of the atom. The ferromagnetic elements in the normal crystalline state are distinguished by a value of this ratio greater than 1·5, unlike other paramagnetic elements with a smaller ratio, and this appears to be the special condition necessary to cause a parallel alignment of the electron spins and to account for the occurrence of ferromagnetism in the few elements concerned.

2.3. THE DOMAIN THEORY

The first experimental evidence for the existence of self-saturated domains was provided by the Barkhausen Effect [7]. If a piece of iron or any ferromagnetic is put inside a search coil which is connected to telephones and the sample is then magnetized, for example, by slowly approaching it to the poles of a permanent magnet, then

under very quiet conditions a rustling noise is heard. With an amplifier and a loud-speaker the noise may be produced in great volume. Clearly, if the magnetization through the search coil increased smoothly nothing would be heard. The observed noise is due to the rapid succession of minute e.m.f.s in the coil induced by sudden jumps in the magnetization as the saturation magnetization suddenly changes direction in the domains. The magnetization curve, greatly magnified, would thus show discrete steps as illustrated in the diagram in Fig. 2.4.

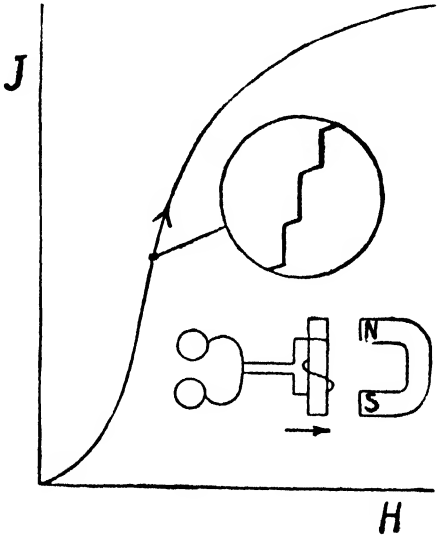

FIG. 2.4.—The Barkhausen Effect

Bozorth and Dillinger [8] carried out an elaborate series of experiments in which the e.m.f.s due to the domains were amplified and recorded. By an analysis of the records estimates were made of the domain sizes. The largest were found, for a wide variety of materials, to have a linear dimension of the order of 0·003 cm. corresponding to about 10^{15} atoms, but they were also of all sizes below this, extending beyond the range of sensitivity of the experimental apparatus. While the largest domains were opera-

tive on the steepest part of the magnetization curve or hysteresis loop, reversals of small domains were also occuring to a limited extent even above the knee of the curve. Fig. 2.5 shows the nature of the results obtained for a sample of annealed iron, and for a sample of nickel.

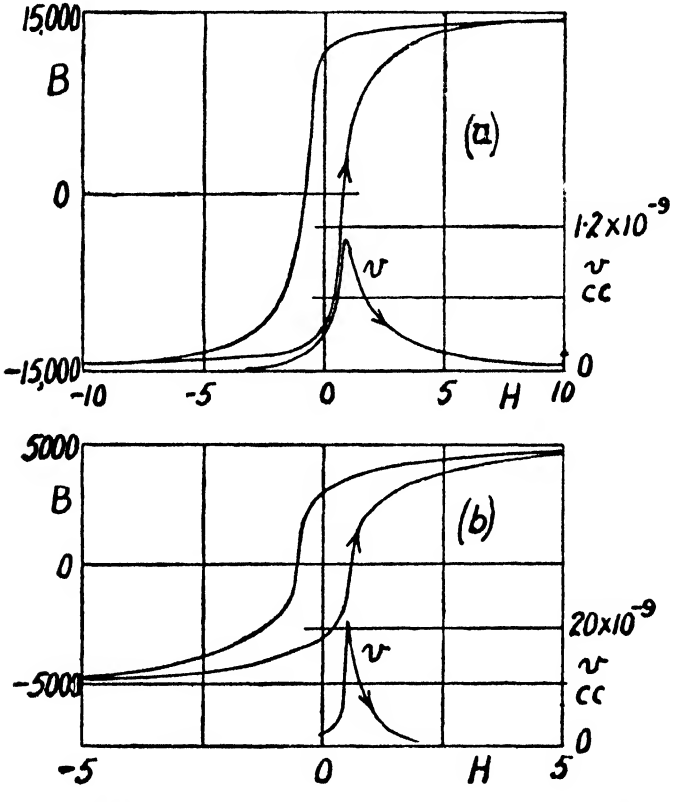

FIG. 2.5.—Size of Domains: (*a*) Annealed Iron, (*b*) Nickel (Bozorth and Dillinger)

It has already been said that the magnetization curve of a ferromagnetic may be considered to consist of four parts. This is indicated in diagrammatic and simplified form in Fig. 2.6. The magnetization processes involved will be discussed in detail in Chapter 3 in relation to single crystals. Fig. 2.6 may, however, be used to indicate in a preliminary way how, according to the domain theory, magnetization

proceeds in a magnetically soft material from the demagnetized condition up to saturation. As explained later the spontaneous magnetization in the domains will normally lie parallel to particular crystal axes in the material, and these preferred directions for four domains are indicated

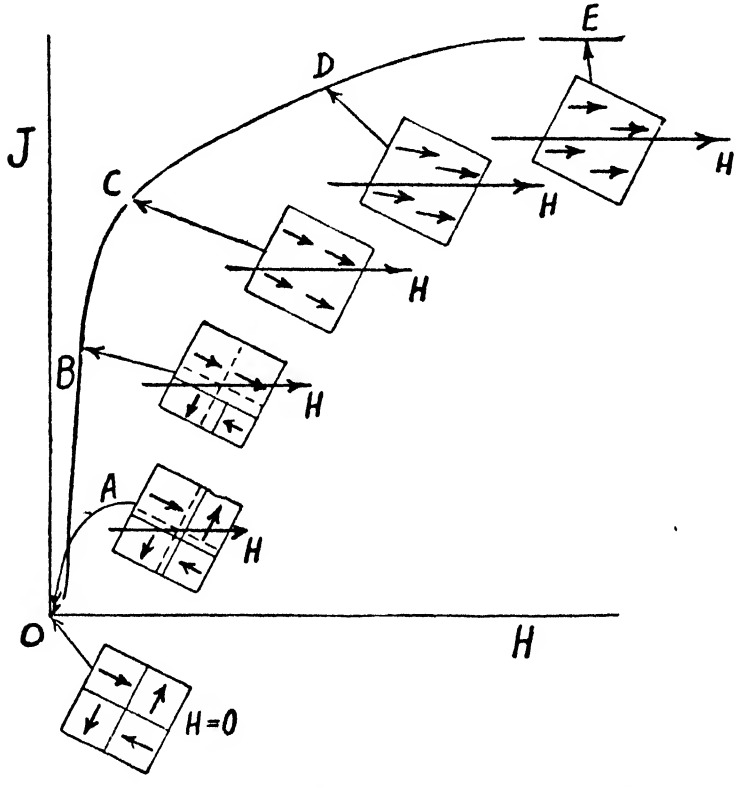

FIG. 2.6.—Diagrammatic Representation of the Magnetization Process according to the Domain Theory

by the arrows in the figure. In the demagnetized condition at *O* the average distribution over all the preferred directions is a random one making the resultant magnetization zero. The application of a small field causes an increase of the resultant field in the direction of *H* by a small, and reversible, movement of the domain boundaries, which move so that domains, in which the saturation magnetiza-

tion vector is favourably directed with respect to H, grow in volume at the expense of the remainder. This is illustrated at A. When the field is further increased Barkhausen jumps occur in which a sudden swing of one domain vector after another occurs from an unfavourable to a favourable direction, as shown at B. This process, irreversible in respect of the jumps but having also a reversible component due to the smooth boundary movements, will be about complete for a relatively low field strength at a somewhat indefinite point C which is the knee of the curve. At C most of the domain vectors have turned into the nearest preferred direction to the field direction as shown. Beyond C the magnetization increases much more slowly as H is raised, and the process now is not one of boundary movements or sudden jumps but a smooth reversible process in which the saturation magnetization of the domains is pulled gradually into the field direction as H increases. Finally, when this process is complete, technical saturation is reached as indicated at E, this having the same value as that in the individual domains.

REFERENCES

1. S. J. Barnett, *Phys. Rev.*, 1915, **6**, 239; *Rev. Mod. Phys.*, 1935, **7**, 129.
2. S. Goudsmit and G. E. Uhlenbeck, *Nature*, 1926, **117**, 264.
3. P. Langevin, *Ann. de Chim. et de Phys.*, 1905, (8), **5**, 70.
4. P. Weiss, *Journ. de Phys.*, 1907, (4), **6**, 661.
5. W. Heisenberg, *Zeits. f. Phys.*, 1928, **49**, 619.
6. H. Bethe, *Handb. d. Phys.*, 1933, **24/2**, 595.
7. H. Barkhausen, *Phys. Zeits.*, 1919, **20**, 401.
8. R. M. Bozorth and J. F. Dillinger, *Phys. Rev.*, 1930, **35**, 733

CHAPTER 3

THE PROPERTIES AND THEORY OF SINGLE CRYSTALS

3.1. PRODUCTION OF SINGLE CRYSTALS

THE ferromagnetic elements and alloys, in common with other metals, are crystalline in character. Their observed properties are due to the combined effect of all their constituent crystals, whose individual properties it is thus important to know. Frequently the crystals or grains in a polycrystalline specimen are large enough to be seen by the naked eye, but much larger single crystals may be produced by suitable technique. Honda and Kaya obtained large iron crystals by the 'strain and anneal' method. This consisted in annealing a rod, which had been carefully decarburized and stretched by about 3 per cent, for a period of several days at 880° C. Single crystal specimens were then cut from the large grains which grew in the solid rod. Nickel and silicon-iron single crystals have been made by slowly cooling the metal through the melting-point, this method being suitable for those alloys which do not undergo recrystallization at an allotropic change point during cooling from the molten state.

3.2. MAGNETIZATION CURVES

Now, at room temperature, iron crystallizes on a body-centred cubic lattice, nickel is face centred, while cobalt takes the hexagonal form. These crystal structures are illustrated in Fig. 3.1. The observed magnetization curves [1] for specimens cut from the principal crystallographic directions for these three elements are shown in Figs. 3.2 and 3.3. In the case of iron it will be seen that the cube-edge direction, denoted by the Miller

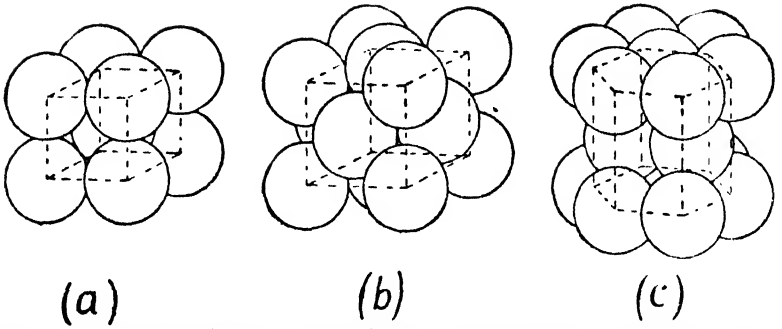

FIG. 3.1.—Crystal Structures of (*a*) Iron, (*b*) Nickel, and (*c*) Cobalt

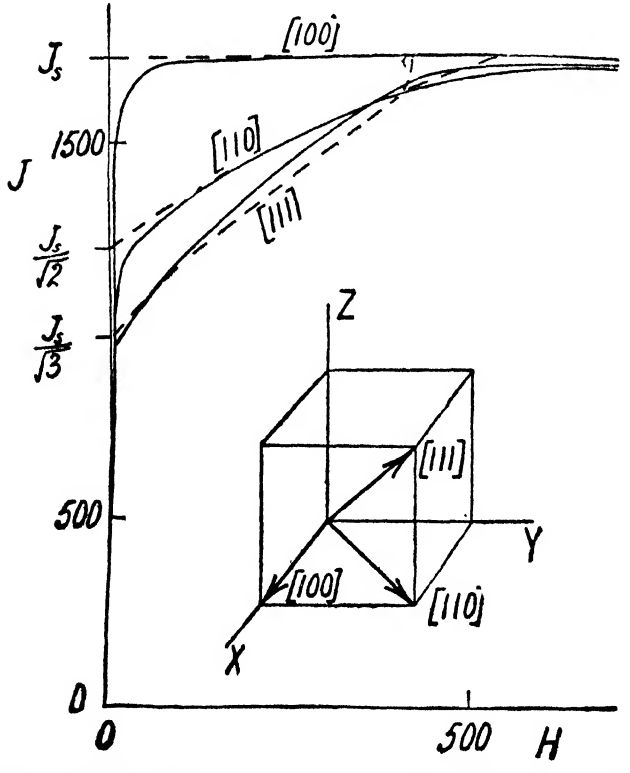

FIG. 3.2.—Magnetization Curves for Iron Single Crystal (Honda and Kaya). The broken Lines are theoretical

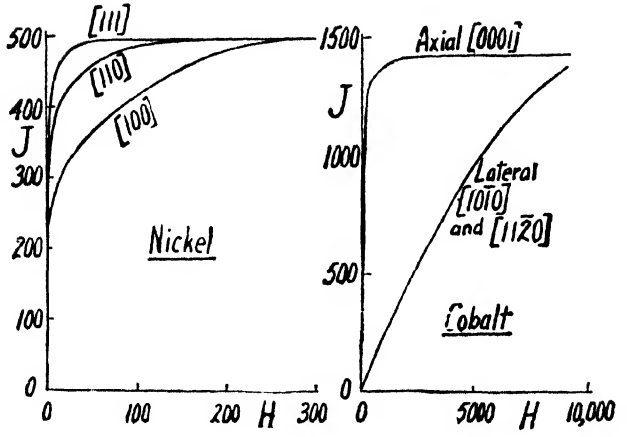

FIG. 3.3.—Magnetization Curves for Single Crystals of Nickel and Cobalt (Kaya)

Indices [100], is the easiest direction of magnetization, the [110] or cube-face diagonal direction is more difficult, whilst the [111] or long diagonal direction is most difficult. In the case of nickel the order is reversed. For cobalt the principal axis is the easy direction, whilst perpendicular to this magnetization is difficult even at low inductions.

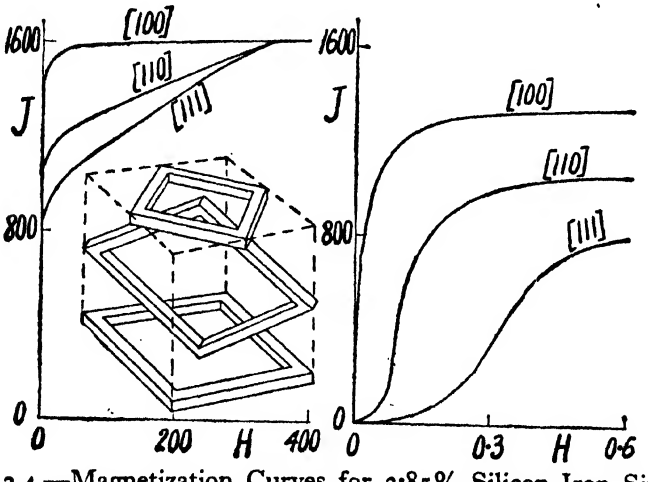

FIG. 3.4.—Magnetization Curves for 3·85% Silicon-Iron Single Crystals at High and Low Field Strengths, showing also the Form of Specimens (Williams)

Fig. 3.4 shows the magnetization curves for 3·85 per cent silicon-iron single crystal specimens made by Williams [2]. In this case each specimen was cut as a closed magnetic circuit in picture-frame form with the four sides parallel to particular crystallographic directions, as illustrated in the figure. This enabled complete magnetization curves, including the portions at low field strengths, to be measured. It will be seen that the order of ease of magnetization for the three crystal directions remains the same at low as at high field strengths, the order for 3·85 per cent silicon-iron being the same as for iron.

3.3. MAGNETOSTRICTION

When a ferromagnetic is magnetized changes in its dimensions occur. A number of effects have been observed and given the names of their discoverers, the general effect being called magnetostriction. We are here principally concerned with the Joule Effect or the change in length, either elongation or contraction, occurring in the direction of the induced magnetization. An increase in length is accompanied by a reduction of cross-section, and vice versa, the volume change being only of second order magnitude. The converse, the Villari Effect, is also observed, whereby a longitudinal deformation leads to a change in permeability in the direction of the applied strain. In general, it may be stated that a material which extends on magnetizing will have its permeability raised by a tensile strain, whereas, if its magnetostriction coefficient is negative, an externally applied pull will reduce the permeability. Examples of this are given in Chapter 4.

Magnetostriction has been measured for the principal crystallographic directions of iron [3], nickel [4], and cobalt [5], with the results shown in Fig. 3.5. It will be seen that nickel and cobalt contract when magnetized in any direction, but that the magnetostriction of iron is more complicated. Iron extends when magnetized in the

[100] or easy direction of magnetization, contracts in the [111] or most difficult direction, while for [110] it first increases in length, and then at high inductions contracts.

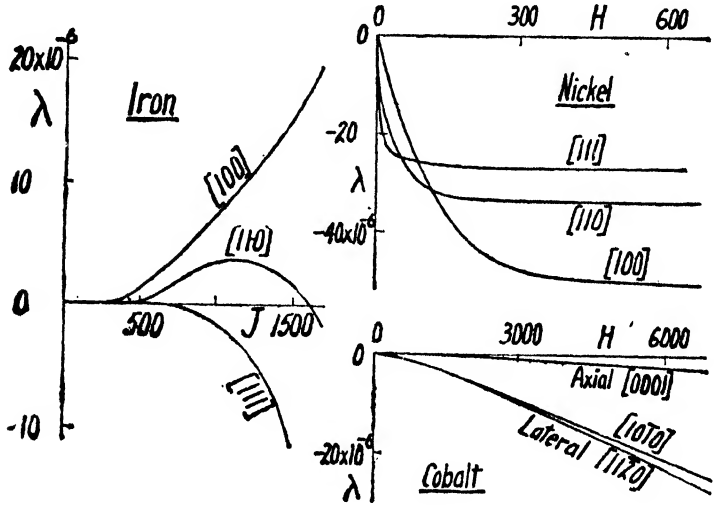

FIG. 3.5.—Magnetostriction of Single Crystals of Iron (Webster), Nickel (Masiyama), and Cobalt (Nishiyama)

3.4. CHARACTERISTICS OF THE DOMAIN

In Chapter 2 the Barkhausen Effect was described and it was stated that magnetization in a ferromagnetic proceeded in discrete steps due to the realignment of the spontaneous magnetization of the individual domains into the general direction of the applied field. This spontaneous magnetization, we said, was due to the powerful Weiss molecular field which produced almost parallel alignment of those electron spins responsible for the magnetic moments of the atoms. Now a single crystal, or indeed any crystallite or grain in a ferromagnetic, will, in general, be made up of a large number of domains. The evidence indicates that the direction of the Weiss molecular field in any domain, having no externally applied field or internal stress, will be that crystallographic direction which is the observed easy direction of magnetization of the single

crystal. Thus for such a domain the spontaneous magnetization, in the case of iron, will lie along a cube-edge direction, in fact along any one of the six possible cube-edge directions without preference.

In the direction of the spontaneous magnetization the domain will have a magnetostrictive strain λ_s, which we may call the saturation magnetostriction. Considering the case of iron, λ_s will be equal to the value observed at saturation for the multi-domain single crystal of iron in the [100] direction, provided that we may assume the

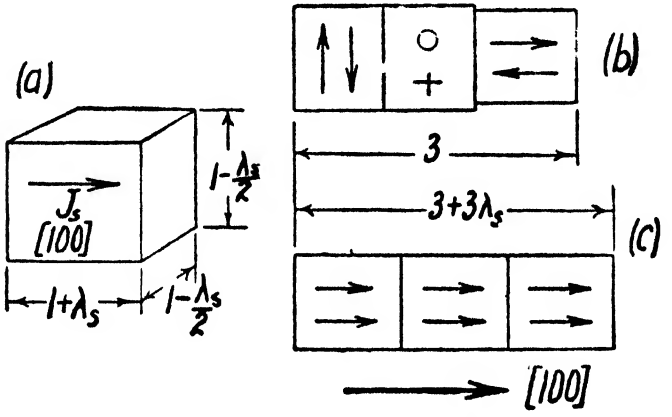

FIG. 3.6.—Diagrammatic Representation of Domains. (*a*) A unit Domain, (*b*) Demagnetized Condition, (*c*) Saturated along (100) Direction

single crystal in the initial demagnetized condition to have the domain vectors entirely randomly directed in the six possible cube-edge positions. This longitudinal strain λ_s will be accompanied by a lateral contraction which, if we neglect the small volume change accompanying magnetostriction and remember that λ_s is small compared with unity, will be equal $\frac{\lambda_s}{2}$. We may thus imagine a domain of unit volume, having positive magnetostriction, as a slightly elongated cube of length $1 + \lambda_s$ and of square section with side $1 - \frac{\lambda_s}{2}$. This is shown in Fig. 3.6, which

also shows in diagrammatic form the arrangement of the domains for an iron single crystal, firstly with the domains entirely randomly directed, the net magnetization then being zero, and then in the saturated condition. In the former case it will be clear that there are two laterally directed domains to each longitudinal one, while after saturating all the domains point in the direction of the field. The observed magnetostrictive strain in this simple picture for the saturated crystal in the [100] direction is thus λ_s, the same as the value taken for the individual self-saturated domains.

Although domains are represented diagrammatically in several figures in this book as rectangular blocks, what their precise shape may be is an open question. It seems certain that they are very variable in size and according to the theory outlined in the following sections their size and number will also depend, at any instant, on the applied field, on applied mechanical stresses, and possibly also on the past magnetic history of the specimen. Intricate patterns obtained by Bitter [6], by depositing finely divided ferromagnetic particles in colloidal suspension on the polished surfaces of ferromagnetic crystals, show a rectangular lamellar form which might possibly be related to the shape of the domain in the crystal. Theoretical considerations also indicate that, in an ideal crystal, the domains should be plane, parallel layers, but this form may not remain in the case of crystals with heterogeneous internal strain [15].

In a strain-free domain with no externally applied field the direction of both the spontaneous magnetization J_s and the saturation magnetostrictive strain λ_s is along any one of the possible easy axes of magnetization as already described. No domain in an actual crystal, which will always have many internal imperfections, will, however, be strain-free and the strain present will introduce a selected direction for J_s and λ_s. Thus if we consider iron, with λ_s positive and the cube edges as easy directions, it

may readily be shown that if a tensile strain is applied along one cube-edge direction the stored energy of the domain is a minimum when the spontaneous magnetization takes up that direction, which thus fixes the crystallographic axis along which the magnetisation vector of the domain will lie. A compressive stress, on the other hand, would dispose the vector laterally. In the case of nickel, long cube diagonals are the directions of easy magnetization, and, furthermore, the saturation magnetostriction is negative. The normal, stable position of J_s in a nickel domain is therefore along any [111] axis in the direction of which a compressive stress is applied. A tensile stress will in this case set the magnetization vector along a lateral axis.

3.5. MAGNETIZATION IN LOW FIELDS

The close dependence of magnetic properties on the magnetostriction characteristics and on mechanical stresses is shown by experimental evidence, of which some is given in Chapter 4, and Becker [7] has shown how the initial permeability may be derived in terms of J_s, λ_s, and the internal stress.

Let us consider a strip of unit section in the easy direction of magnetization of a single crystal. We assume this has positive saturation magnetostriction λ_s. The stresses included in the crystal due to its internal imperfections may be expected, on the whole, to be tensile and compressive in equal amounts, although the maximum values may vary from point to point in the crystal. Becker, however, assumed the idealized condition represented in Fig. 3.7, in which it is supposed that the internal stress varies sinusoidally along the strip, positive ordinates representing compression and negative values tension, the stresses also being assumed to be directed longitudinally. Now for the crystal in the demagnetized condition with no applied field, it will be clear from the discussion in the previous section

that the spontaneous magnetization J_s will lie laterally for those parts of the strip in compression and lengthwise for the remainder. The distribution of domains, with the arrows indicating the spontaneous magnetization, will therefore be as shown, and domain boundaries will lie at the surfaces of zero stress.

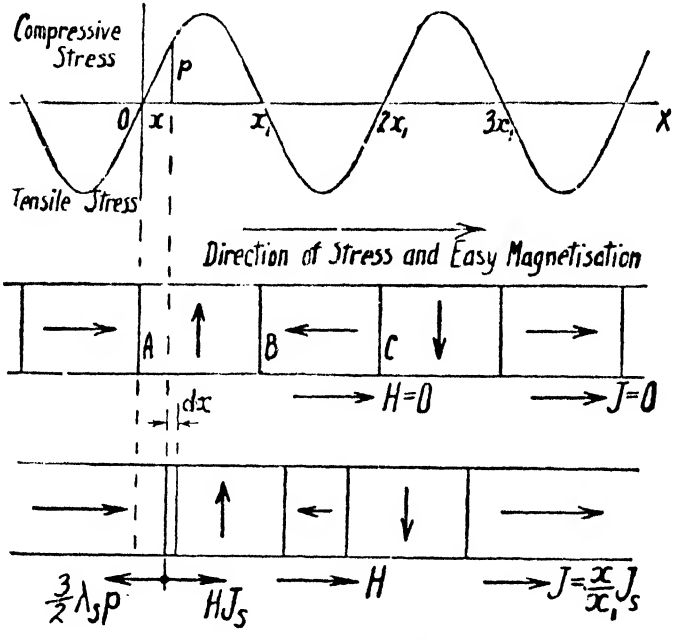

FIG. 3.7.—Initial Permeability: Movement of Domain Boundaries

In the initial demagnetized condition let the length of each domain, under these idealized conditions, be x_1. Then the variation of stress p with distance x is given by

$$p = p_m \sin \pi \frac{x}{x_1}$$

where p_m is the amplitude of the stress wave. If now a field H is applied along the strip, as shown by the arrow, this will act to move the boundaries. For, since the saturation intensity of magnetization is J_s, each boundary surface of unit area has a pole strength J_s and therefore

a force on it due to H of amount HJ_s. Under the action of this pressure each boundary moves to the right or the left, depending on its polarity, but always in a direction which increases the resultant, average intensity of magnetization in the direction of the applied field.

This boundary pressure, acting to expand the favourably directed domains and to reduce those of opposite direction, is counteracted by elastic forces in the crystal. Consider for example the boundary A, already displaced by x from its initial position, advancing by an additional distance dx. In the volume dx thus swept out the magnetization swings through a right angle from the lateral to the forward direction. The magnetostrictive strain in this element of volume thus changes from $-\frac{\lambda_s}{2}$ to $+\lambda_s$, that is the element extends magnetostrictively by $\frac{3}{2}\lambda_s$, and since at the position of the boundary there exists an internal compressive stress p, the additional elastic energy stored by this elemental movement is given by

$$dE = \frac{3}{2}.\lambda_s.p.dx$$

Therefore the force F per unit area resisting movement of the boundary at the position x is given by

$$F = \frac{dE}{dx} = \frac{3}{2}.\lambda_s.p$$

Thus the boundary reaches a stable position under the action of the field H when

$$HJ_s = \frac{3}{2}\lambda_s p$$

or

$$H = \frac{3\lambda_s p_m}{2J_s}.\sin \pi\frac{x}{x_1} \quad . \quad . \quad (3.1)$$

Similar displacements occur for each boundary. It is clear that a movement x of each boundary will lead to a

mean intensity of magnetization J in the direction of H given by

$$J = \frac{x}{x_1} J_s \quad . \quad . \quad . \quad (3.2)$$

From equations 3.1 and 3.2 we may write the susceptibility κ as

$$\kappa = \frac{J}{H} = \frac{2J_s^2}{3\pi\lambda_s p_m} \cdot \frac{\pi \frac{x}{x_1}}{\sin \pi \frac{x}{x_1}}$$

Now the initial susceptibility κ_0 is the value occurring when H, and hence x, approach zero and in this case we clearly have

$$\kappa_0 = \frac{2J_s^2}{3\pi\lambda_s p_m} \quad . \quad . \quad . \quad (3.3)$$

Also since the initial permeability $\mu_0 = 1 + 4\pi\kappa_0$, and in all important cases μ_0 is large compared with unity, we may write

$$\mu_0 = \frac{8}{3} \cdot \frac{J_s^2}{\lambda_s p_m} \quad . \quad . \quad . \quad (3.4)$$

The equation indicates that low internal stresses and low magnetostriction lead to high permeability. This is, in fact, well supported by the experimental evidence.

It will not, in general, be known what the values of the internal stresses in a ferromagnetic are, and therefore μ_0 may not be calculated directly from equation 3.4. A ferromagnetic may, however, by careful purification and heat-treatment have the main sources of internal strains removed, leaving only the unavoidable internal stresses due to magnetostriction. We may consider how the latter are induced and, following Kersten [8], assign an approximate value to them. A ferromagnetic heated above the Curie temperature changes to the paramagnetic condition, and therefore it is only on cooling through this magnetic change point that the domains form and magnetostriction occurs. Since the domains will not be free to expand on

formation in the solid metal, internal stresses will be set up in them of which the order of magnitude will be $\lambda_s E$, where E is Young's Modulus. If we substitute this value for p_m in equation 3.4, we have an expression giving the highest value of μ_0 we might ever expect to be able to obtain. If this value is μ_{0u}, we have

$$\mu_{0u} = \frac{8}{3} \cdot \frac{J_s^2}{\lambda_s^2 E} \quad . \quad . \quad . \quad (3.5)$$

For iron at 20° C. we may write the following values: $J_s = 1{,}717$, $\lambda_s = 20 \times 10^{-6}$, and $E = 20 \times 10^{11}$ dynes per sq. cm., whence

$$\mu_{0u} = 10{,}000 \text{ approximately.}$$

Equation 3.5 can be expected to give only the order of magnitude for initial permeability on account of the assumptions made in deriving it, and Kersten, with slightly different assumptions, has derived a value of 16,000 for the theoretical upper limit of the initial permeability of iron. Experimentally the highest value so far obtained is 14,000, due to Cioffi [9]. Thus Becker's theory as outlined above may be said to be in this respect in satisfactory agreement with observation.

The initial portion of the magnetization curve with which we have so far dealt is, according to the theory, perfectly reversible in character. This is also a well-known experimental fact, and the formula

$$J = aH + bH^2$$

due to Baur and Rayleigh is found to apply at sufficiently low field strengths [10]. In this expression a and b are constants with a numerically equal to κ_0 which, according to Becker, is given by equation 3.3.

3.6. MAGNETIZATION AT INTERMEDIATE FIELD STRENGTHS

The process of magnetization at very low field strengths has been described in Section 3.5, and is entirely reversible in character. As H is further increased the magnetization

increases at a much more rapid rate and the Barkhausen jumps described in Section 2 occur. These jumps are largest, according to the experimental evidence, on the steepest part of the curve. They cause the curve to become irreversible and lead to hysteresis loss.

We may picture the mechanism of the magnetization process on this part of the curve by discarding the idealized distribution of stresses given in Fig. 3.7, where we were,

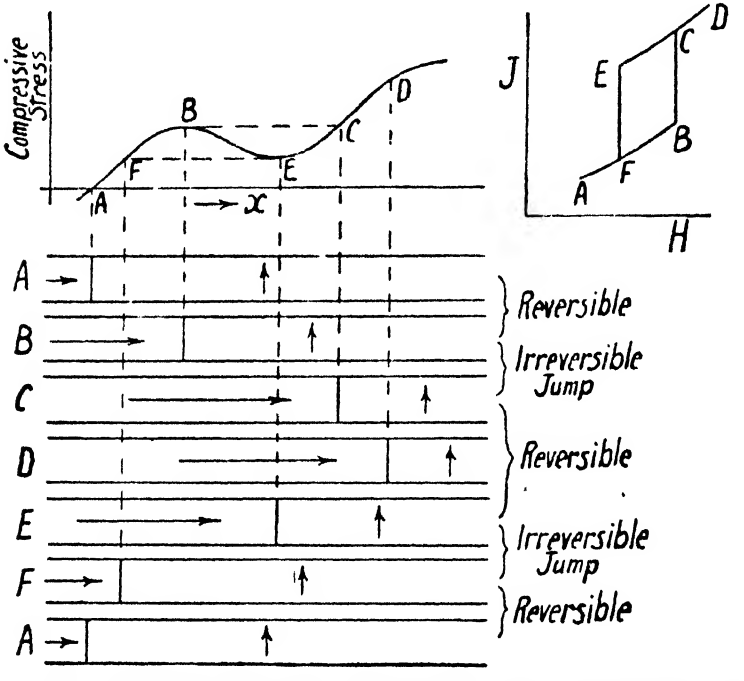

FIG. 3.8.—Domain Boundary Movements with Hysteresis Loss

in any case, concerned only with the stresses near the zero points of the wave, and by considering a stress variation in which successive amplitudes are unequal, as indeed we may expect to be the case in any actual crystal. Suppose, for example, that the stress variation along a strip of the single crystal, in an easy direction of magnetization, is as shown in Fig. 3.8. With no applied field the boundary between two domains would be at the position of zero

stress as shown at *A*. On increasing the field along the strip the boundary would move, reversibly, to the right up to the position *B* as shown. At this point, however, the boundary would have reached an unstable position and, without further increase in the field, could run forward to *C*. This is a Barkhausen jump and with it is associated hysteresis loss. On the reversible portion *AB* of the stress curve the increase in the elastic stored energy, which is associated with a magnetostrictive extension against the internal compressive stress, in the manner already described in Section 3.5, is derived from the corresponding fall of the potential energy of the spontaneous magnetization in the field, as it turns into the field direction. In the jump of the boundary from *B* to *C* there is a similar decrease in the potential energy, but, since the stress curve falls below *BC* only a portion of this energy is elastically stored in the crystal. The difference is dissipated as hysteresis loss and the amount of the loss in this one jump is proportional to the area *BCE* of the stress curve. The way in which this energy is converted to heat in the crystal will be, in part at least, by the eddy currents induced in the crystal by the local change of magnetization due to the sudden jump of the boundary. There is, however, evidence which indicates that there must be some other mechanism besides that of eddy currents for transferring this energy.

On reducing the field a similar discontinuity will occur between *E* and *F* and the elemental hysteresis loop for these movements of a single boundary will be of the form shown in the figure. The complete hysteresis loop of any specimen will, of course, comprise a very large number of such elementary loops.

So far only boundaries between domains having their respective spontaneous magnetizations at right angles have been considered. We may, however, have neighbouring domains in which the angle is not 90° but 180°. On the theory given above a boundary between two such domains

should move under the action of an applied field without any constraint, since a reversal of the direction of magnetization in the material swept out by the advancing boundary involves no magnetostrictive change of length and hence no change in the elastic energy. It has, however, been shown by Bloch [11] that the width of the boundaries between domains will be large on the atomic scale though still small compared with the domain size. In this boundary region, which may be of the order of 10^2 or 10^3 atom diameters in thickness, a gradual transition of the directions of the electron spins which are responsible for the magnetic moment of the atoms, from one direction to the other, will occur in passing across the boundary layer. It may be shown that a change in energy occurs when such a boundary moves through a region of non-uniform stress in which there is magnetostriction. Kondorski [12] has shown that this boundary layer between two oppositely directed domains would, in the absence of an applied field, be in equilibrium at a position of zero stress gradient. Under the action of an applied field it would advance reversibly until a point of maximum stress gradient was reached when instability and a Barkhausen jump would occur.

The relative amounts of the two types of domain boundary in a particular specimen at any point on its magnetization curve will not, in general, be known. A possible source of information, however, is the magnetostrictive behaviour of the specimen since a larger magnetostriction will occur with a 90° than with a 180° boundary movement, and some attempts to analyse which particular type of boundary movement is occurring have been made [13].

3.7. MAGNETIZATION AT HIGH FIELD STRENGTHS

It will be seen from the magnetization curves in Figs. 3.2, 3.3, and 3.4 that, for the easy direction, saturation is reached

for a relatively small applied field. In this case the only mechanism involved is one of domain boundary movements, both smooth and discontinuous, the magnetization process being impeded by the internal stresses of the crystal. We may suppose that in a perfect crystal free from any internal lattice distortion saturation could be achieved in a vanishingly small applied field, the theoretical relation between J and H then being represented by a vertical and a horizontal straight line as shown in Fig. 3.2. The work done to produce saturation in this ideal case will be zero, but for an actual crystal the work done and energy stored in the crystal, neglecting the small hysteresis loss, is given by $\int_0^{J_s} H dJ$, represented by the area between the ordinate axis and the magnetization curve.

Similarly for the more difficult directions of the crystal a relatively small field, only a few gauss, is sufficient to magnetize it up to the knee of the curve, but to take the magnetization from its value at this point up to saturation requires a field strength of a higher order of magnitude, several hundred gauss, this part of the curve also being very nearly reversible. This introduces a different mechanism of magnetization from that already described.

Following Akulov [14] we may describe this process and correlate the magnetization curves in different crystallographic directions theoretically in terms of observed constants of the material. For in any domain with low internal strains and no externally applied field the spontaneous saturation magnetization will lie along an easy crystallographic direction of magnetization. This therefore represents a condition of minimum stored energy for the domain. If the magnetization vector is turned out of this position, as it may be by the application of a field at a suitable angle, work is done against the crystalline forces which endeavour to hold the parallel, electron-spin axes in the easy direction, and additional energy is stored in the domain. In a crystal with cubic symmetry it may be

shown, mathematically, that the relation between this domain energy and the position of the magnetization vector is given by an expression of the form

$$E = K_0 + K_1(S_1^2S_2^2 + S_2^2S_3^2 + S_3^2S_1^2) + K_2(S_1S_2S_3)^2 + \ldots . \quad (3.6)$$

In this K_0, K_1, and K_2 are constants while S_1, S_2, and S_3 are the direction cosines of the direction of J_s in the domain relative to the cube edges as rectangular co-ordinate axes, the terms given being the only ones which need to be considered.

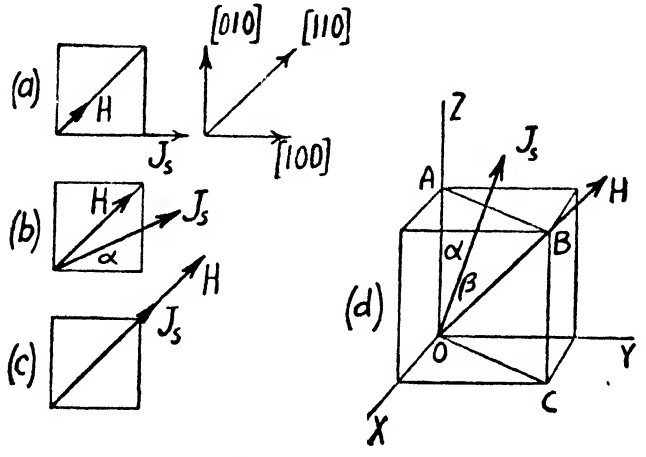

FIG. 3.9.—Rotational Magnetization Process at High Field Strengths

By the use of this equation we may readily deduce expressions for the magnetization curves above the knee for the principal crystallographic directions.

Let us consider, for example, the magnetization curve for the [110] direction of iron. A comparatively small field in the [110] direction causes all, or very nearly all, the domains to have their spontaneous saturation J_s directed along the nearest cube-edge direction to that of H. This condition is represented diagrammatically in Fig. 3.9(*a*) for one domain. Clearly the value of J in

the direction of H, which is the observed value, is equal $\frac{J_s}{\sqrt{2}}$, corresponding to the knee of the magnetization curve. If now H is further increased the vector J_s is turned thereby, in the plane of the cube face or (001) plane, out of its cube-edge direction, as indicated at (*b*). This rotation of the magnetization vector is resisted by those crystalline forces which are the cause of the magnetic anisotropy of the crystal, forces whose precise origin is not well understood but which we may nevertheless determine theoretically in terms of the anisotropy constants of equation 3.6. For rotation of J_s in a (001) plane we may, referring to Fig. 3.9(*b*), write the following values: $S_1 = \cos\alpha$, $S_2 = \sin\alpha$ and $S_3 = 0$, whence by substituting in equation 3.6, the variation of the stored energy of the domain with the position of the vector J_s is given by

$$E = K_0 + \frac{K_1}{8}(1 - \cos 4\alpha)$$

The restoring torque on J_s is clearly given by L_c where

$$L_c = \frac{dE}{d\alpha} = \frac{K_1}{2}.\sin 4\alpha \quad . \quad . \quad (3.7)$$

whilst the torque L_H in the opposite direction due to the field H is given by

$$L_H = HJ_s \sin\left(\frac{\pi}{4} - \alpha\right) \quad . \quad . \quad (3.8)$$

Therefore from equations 3.7 and 3.8 we have

$$HJ_s \sin\left(\frac{\pi}{4} - \alpha\right) = \frac{K_1}{2} \sin 4\alpha \quad . \quad . \quad (3.9)$$

Now the magnetization J in the direction of H is also given by

$$J = J_s \cos\left(\frac{\pi}{4} - \alpha\right) \quad . \quad . \quad (3.10)$$

What we have said for the domain under consideration applies to every domain in the crystal and therefore, by

eliminating α between equations 3.9 and 3.10, we have a relation between J and H which is the equation of the magnetization curve for the [110] direction. This equation is as follows:

$$H = \frac{2K_1}{J_s} \cdot \frac{J}{J_s} \cdot \left\{ 2\left(\frac{J}{J_s}\right)^2 - 1 \right\} \quad . \quad . \quad (3.11)$$

We see that this theoretical magnetization curve starts at the point where $H = 0$, $J = \frac{J_s}{\sqrt{2}}$, and that saturation is reached when $H = \frac{2K_1}{J_s}$.

In a similar way we may deduce an equation for the magnetization curve in the [111] direction. For with H along this direction the knee of the magnetization curve is reached when J_s in each domain lies along a cube-edge direction nearest to the direction of H. The observed magnetization J in the direction of H is then $\frac{J_s}{\sqrt{3}}$. As H is further increased a smooth rotation of J_s for each domain from the cube-edge direction, such as OZ in Fig. 3.9(*d*), towards the field direction then occurs. This rotation will be in the diagonal plane, such as $OABC$ in the figure, and where J_s is rotated through the angle α from OZ, we may obtain an expression for the energy of the domain in terms of α by substituting the values $S_3 = \cos\alpha$ and $S_1 = S_2 = \frac{\sin\alpha}{\sqrt{2}}$ in equation 3.6. The torque L_c, due to the crystalline forces, acting in a direction to restore J_s to a cube-edge direction, is then obtained as before by differentiating. This restoring torque in the diagonal plane, $(1\bar{1}0)$ in the figure, is given by

$$L_c = \left(\frac{K_1}{4} + \frac{K_2}{64}\right) \sin 2\alpha + \left(\frac{3K_1}{8} + \frac{K_2}{16}\right) \sin 4\alpha - \frac{3K_2}{64} \sin 6\alpha \quad . \quad (3.12)$$

The equal and opposite torque L_H due to the action of the field H on J_s is given by

$$L_H = HJ_s \sin(\beta - \alpha)$$

where $\cos\beta = \frac{1}{\sqrt{3}}$. The intensity of magnetization J in the [111] direction is clearly given by

$$J = J_s \cos(\beta - \alpha)$$

Eliminating α from these expressions, as before, we obtain the following rather lengthy expression for the magnetization curve in the [111] direction

$$HJ_s = K_1\frac{\sqrt{2}}{3}\sqrt{1-a^2}(4a^2-1) + K_1\frac{a}{3}(7a^2-3) - K_2\frac{\sqrt{2}}{18}\sqrt{1-a^2}(10a^4-9a^2+1) + K_2\frac{a}{18}(23a^4-16a^2+1) \quad . \quad (3.13)$$

where $a = \frac{J}{J_s}$.

These equations for the magnetization curves involve the anisotropy constants K_1 and K_2 which may be evaluated from the experimental results. The energy stored in the crystal when it is saturated in the [100] direction is proportional to the area between the ordinate axis and the magnetization curve for this direction, and is given by $\int_0^{J_s} HdJ$ as already mentioned. Let us call this energy E_{100}. It is, however, also derivable from equation 3.6, in which we put $S_1 = 1$ and $S_2 = S_3 = 0$. Therefore we have

$$E_{100} = K_0$$

Similarly, for the [110] direction, E_{110} is the stored energy for saturation in that direction, again given by the area between the observed [110] magnetization curve and

the ordinate axis. We may calculate E_{110} from equation 3.6 by putting $S_1 = S_2 = \frac{1}{\sqrt{2}}$ and $S_3 = 0$. Therefore

$$E_{110} = K_0 + \frac{K_1}{4}$$

Similarly, for [111] we obtain

$$E_{111} = K_0 + \frac{K_1}{3} + \frac{K_2}{27}$$

We thus obtain the following values for K_0, K_1, and K_2

$$K_0 = E_{100}$$
$$K_1 = 4(E_{110} - E_{100})$$
$$K_2 = 27(E_{111} - E_{100}) - 36(E_{110} - E_{100})$$

These constants may thus be determined from the magnetization curves.

An alternative method of evaluating K_1 and K_2 which does not involve observation of the magnetization curves is given in Section 3.8.

Magnetization curves calculated from equations 3.11 and 3.13 using the constants for iron $K_1 = 4{\cdot}5 \times 10^5$, $K_2 = 2{\cdot}25 \times 10^5$ ergs per c.c., and $J_s = 1{,}717$, are shown by the broken lines in Fig. 3.2, and these are seen to be in reasonably good agreement with Honda and Kaya's observed results.

The magnetization curves above have been calculated, by way of example, for the case of iron, but the same procedure may be followed for nickel or, indeed, for any ferromagnetic cubic crystal. The fact that the order of ease of magnetization in the principal crystal directions is reversed for nickel is taken care of by the magnitude and sign of K_1 and K_2, K_1 being negative for nickel.

With cobalt the energy equation takes a different form, since at temperatures below 477° C. cobalt has a hexagonal crystal structure as shown in Fig. 3.1. The equation in this case becomes

$$E = K_0 + K_1 S_1^2 + \ldots$$

In this S_1 is the direction cosine of J_s relative to the

principal axis of the crystal. The terms given are found to be sufficient to give agreement with the observed data, and this implies that the magnetic properties are the same for any direction perpendicular to the principal axis.

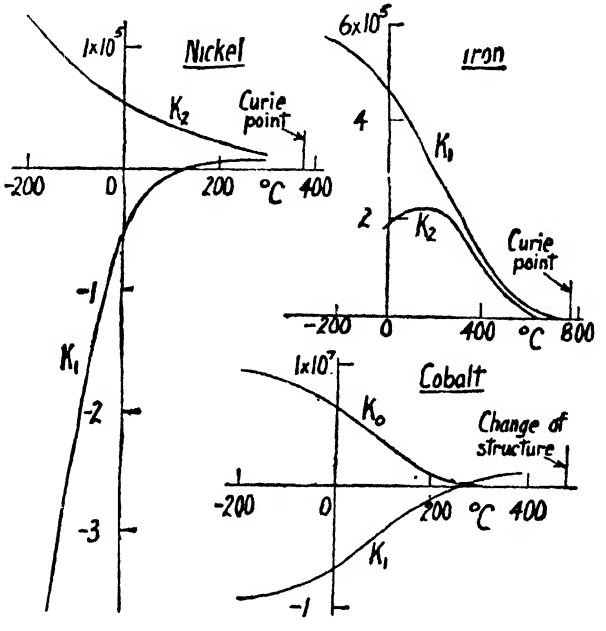

FIG. 3.10.—Magnetic Anistropy Constants of Iron, Nickel, and Cobalt in relation to Temperature

The values of the anistropy constants for iron, nickel and cobalt over a range of temperatures are given in Fig. 3.10. Some further data are given in later chapters.

3.8. TORQUE CURVES

If a specimen is cut from a single crystal in the form of a thin disc, or better, in the form of a thin ellipsoid of revolution, and this is rotated in a strong, saturating field about an axis perpendicular both to the field direction and to the central plane of the specimen, then, due to the magnetic anisotropy of the crystal a varying torque will be found to act.

The origin and magnitude of this torque will be clear from what has been said in Section 3.7. For suppose the sample is cut in the plane of a cube face, or (100) plane, of a single crystal of iron. Then, the field being very high, the saturation magnetization vector J_s for the disc or ellipsoid will always be held in line with the direction

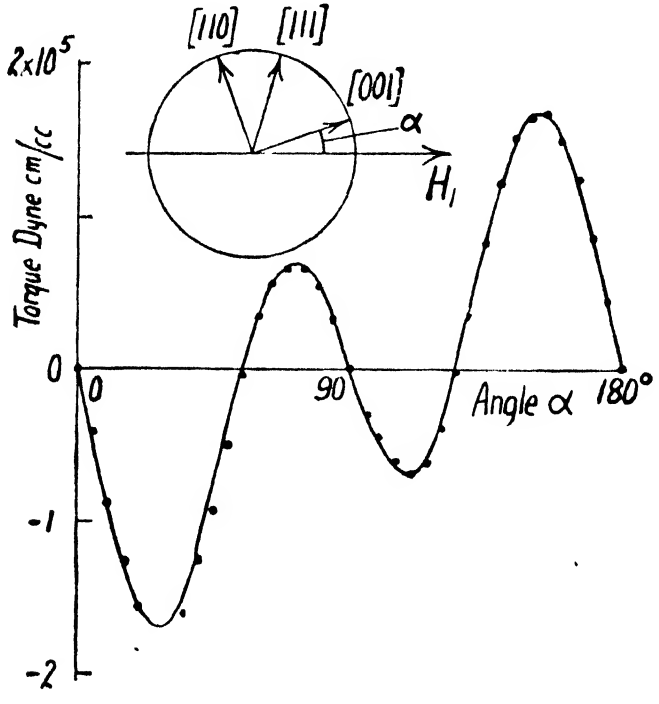

FIG. 3.11.—Torque Curve for Single Crystal Disc of 3·85% Silicon-Iron (Williams)

of the applied field as the sample is rotated. If a cube-edge direction of the crystal is turned by an angle α from the field direction, the torque acting in a direction to reduce this angle to zero is clearly given by equation 3.7, which, if we adopt the convention for signs that the torque L is positive for the direction of increasing α, becomes

$$L = -\frac{K_1}{2} \sin 4\alpha \quad . \quad . \quad . \quad (3.14)$$

Similarly, for a specimen cut from the diagonal plane, we see from equation 3.12 that the torque becomes

$$L = -\left(\frac{K_1}{4} + \frac{K_2}{64}\right)\sin 2\alpha - \left(\frac{3K_1}{8} + \frac{K_2}{16}\right)\sin 4\alpha + \frac{3K_2}{64}\sin 6\alpha \quad . \quad (3.15)$$

Excellent agreement between the observed and calculated forms of torque curves for single crystals is obtained in practice. It will be clear that the values of the constants K_1 and K_2 may be experimentally obtained in this way. Fig. 3.11, due to Williams, shows the agreement between theory and observation for a single crystal cut in the (110) plane of 3·85 per cent silicon-iron, in which $K_1 = 2{\cdot}87 \times 10^5$ and $K_2 = 1{\cdot}00 \times 10^5$ ergs per c.c.

This torque curve technique has also been applied to polycrystalline materials, as will be described later.

REFERENCES

1. K. Honda and S. Kaya, *Sci. Rep. Toh. Imp. Univ.*, 1926, Series 1, **15**, 721 ; S. Kaya, *Sci. Rep. Toh. Imp. Univ.*, 1928, Series 1, **17**, 639 and 1157.
2. H. J. Williams, *Phys. Rev.*, 1937, **52**, 747.
3. W. L. Webster, *Proc. Roy. Soc., A*, 1925, **109**, 570.
4. Y. Masiyama, *Sci. Rep. Toh. Imp. Univ.*, 1928, Series 1, **17**, 945.
5. Z. Nishiyama, *Sci. Rep. Toh. Imp. Univ.*, 1929, Series 1, **18**, 341.
6. F. Bitter, *Phys. Rev.*, 1932, **41**, 507 : *Introduction to Ferromagnetism* (New York, 1937).
7. R. Becker, *Zeits. f. Phys.*, 1930, **62**, 253 ; *Phys. Zeits.*, 1932, **33**, 905.
8. M. Kersten, *Zeits. f. Phys.*, 1931, **71**, 562 ; *Zeits. f. tech. Phys.*, 1938, **19**, 546 ; *Elektrotech. Zeits.*, 1939, **60**, 498.
9. P. P. Cioffi, *Phys. Rev.*, 1934, **45**, 742.
10. J. A. Ewing, *Magnetic Induction in Iron and Other Metals* (London, 1900), p. 124.
11. F. Bloch, *Zeits. f. Phys.*, 1932, **74**, 295.

12. E. Kondorski, *Phys. Zeits. der Sowjetunion*, 1937, **11**, 597.
13. F. Brailsford and R. G. Martindale, *Journ. I.E.E.*, 1942, **89**, Part 1, 225.
14. N. S. Akulov, *Zeits. f. Phys.*, 1929, **57**, 249; 1931, **67**, 794; 1931, **69**, 78.
15. L. Néel, *Journal de Physique et Radium*, 1944, **5**, 241 and 265; H. J. Williams, R. M. Bozorth and W. Shockley, *Phys. Rev.*, 1949, **75**, 155; H. J. Williams and W. Shockley, *Phys. Rev.*, 1949, **75**, 178.

CHAPTER 4

SOME FACTORS AFFECTING MAGNETIC PROPERTIES

4.1. TENSILE AND COMPRESSIVE STRESSES

DEFORMATION of the crystal lattice by applied stresses can have a profound effect on the magnetic properties of a ferromagnetic, the effect being also closely related to the magnetostriction characteristics of the metal. This

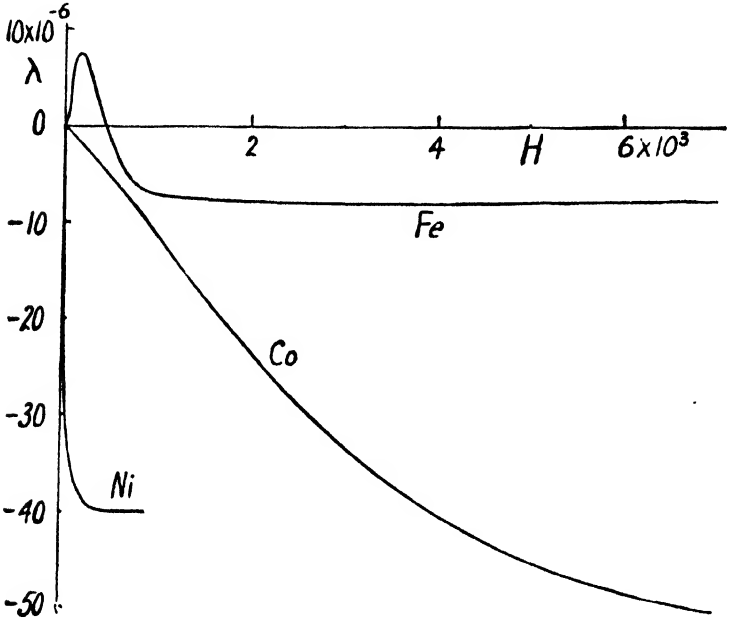

FIG. 4.1.—Magnetostriction of Polycrystalline Iron (Kornetzki), Nickel (Masiyama), and Cobalt (Nishiyama)

has already been referred to in the discussion of single crystals. The longitudinal magnetostriction λ of polycrystalline iron [1], nickel [2], and cobalt [3] in relation to the field strength H is shown in Fig. 4.1. The results

may be regarded as typical for these elements as to the form of the curves, although the observed values reported by different investigators vary fairly considerably, a fact which is not surprising when, apart from the question of purity and heat-treatment of the specimen, it is also remembered that the specimens are made up of crystals with directional properties. For the resultant magnetostriction will be influenced by any departure from a random arrangement of the constituent crystal axes. It will also

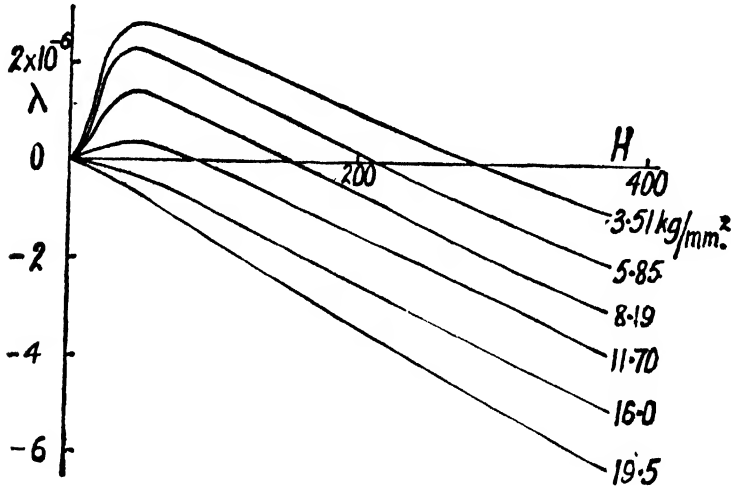

FIG. 4.2.—Magnetostriction of a sample of Iron when magnetized with various amounts of applied Tensile Stress (Bidwell)

clearly depend on whether, in the initial, demagnetized condition of the sample, the distribution of the domain magnetization vectors is a random one or not.

Magnetostriction is also affected by applied stresses and Fig. 4.2 shows the effect of different amounts of tension on the magnetostriction of a sample of iron [4]. Large variations in the magnetostrictive characteristics of thin specimens are also observed, depending apparently on conditions in the surface layers.

Fig. 4.3(*a*) shows the effect on the form of the hysteresis loop, the upper half only being shown, of a tensile stress

applied to an annealed nickel wire [5], while at (*b*) the effect of a compressive stress on the magnetization curve of hard nickel is shown [6]. Nickel contracts in the direction of the applied field when magnetized, and it is seen that in this case an externally applied compression raises the permeability, whilst a tensile load reduces it over the whole course of the magnetization curve. A further example, due to Buckley and McKeehan [7], is given in

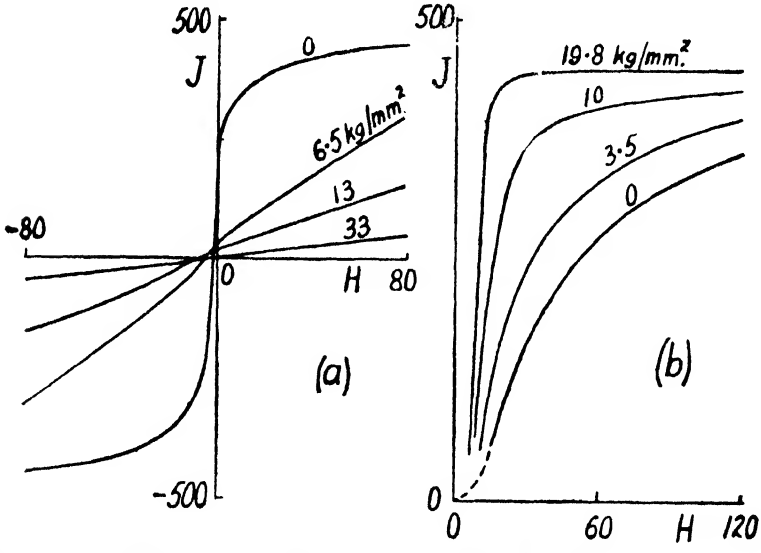

FIG. 4.3.—Effect of applied Stress on Magnetization of Nickel. (*a*) Tension applied to annealed Nickel Wire showing half Hysteresis Loops (Becker and Kersten). (*b*) Compressive Stress applied to Hard Nickel (Ewing)

Fig. 4.4 for two nickel-iron alloys. The magnetostriction of these alloys depends upon the nickel content as shown in Fig. 6.6. The curves in Fig. 4.4(*a*) are for an alloy with 84 per cent nickel and remainder iron the magnetostriction of which is negative, like that for nickel itself. A tensile stress is seen to reduce the permeability. At (*b*) the alloy has 65 per cent nickel and its magnetostriction is positive. In this case tension improves the permeability. The general rule, therefore, is that materials which extend

on magnetizing have their permeability raised by tension and lowered by compression, and vice versa for those in which magnetostriction is negative. In the case of iron the observed effects are not so clear-cut, for it has complicated magnetostriction characteristics. The general effect appears to be that tension improves the permeability at low inductions and reduces it at high values.

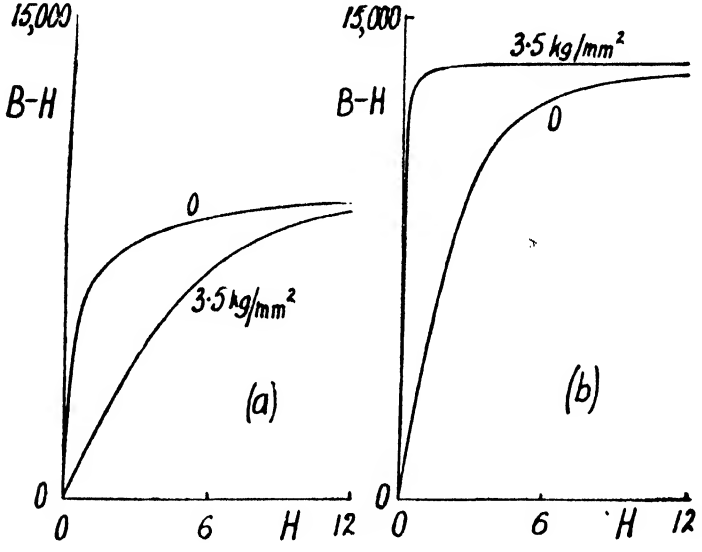

FIG. 4.4.—Effect of Tension on two Nickel-Iron Alloys (Buckley and McKeehan). (*a*) 84% Ni, 16% Fe, magnetostriction negative: (*b*) 65% Ni, 35% Fe, magnetostriction positive

The process of magnetization by Barkhausen jumps has been discussed in the previous chapters and an elemental hysteresis loop due to the movements of a single domain boundary is shown in Fig. 3.8. The distribution of the domain magnetization vectors according to the nature and direction of the internal strains has also been referred to, and we might expect that a large, externally applied stress, sufficient to swamp the internal stresses, would lead to large domains with their magnetization vectors directed either parallel or perpendicular to the direction of the

applied stress depending on its sign and on that of the saturation magnetostriction. Large Barkhausen jumps produced in this way have been observed by Forrer [8], Preisach [9], and others. Sixtus and Tonks [10] found that for hard-drawn nickel-iron wires, 0·038 cm. in diameter and with a nickel content between 10 and 20 per cent, it was possible with a high tensile strain to convert the whole wire, in effect, into a single domain with its saturation

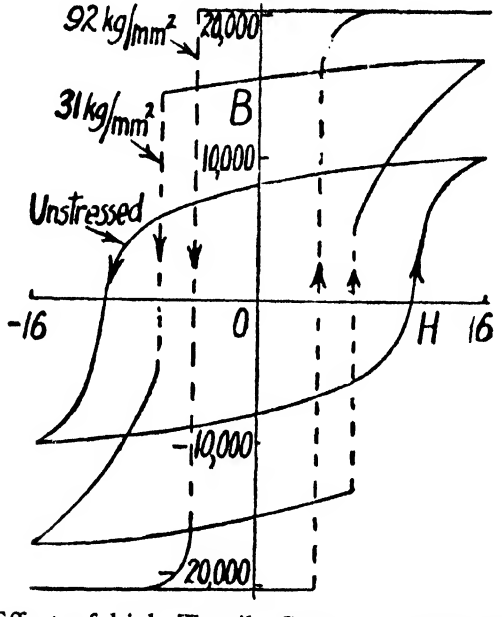

FIG. 4.5.—Effect of high Tensile Stress on Hysteresis Loop of 15% Nickel-Iron hard-drawn Wire (Sixtus and Tonks)

magnetization directed longitudinally. Under these conditions a normal type of hysteresis loop was converted to the rectangular form shown in Fig. 4.5, in which, for the highest tensions, the magnetization in the wire changed from saturation in one direction nearly to saturation in the reverse direction in a single jump, as shown by the broken lines. This reversal occurred by the movement, from one end of the wire to the other, of the domain boundary existing between oppositely directed magnetization vectors,

and it could be initiated by a local magnetizing coil at one end of the specimen. The speed of travel of the boundary was observed and depended on the magnitude of the coercive field applied at the time. The investigators reached some conclusions as to the shape of the advancing boundary surface and they also concluded that the hysteresis loss involved could not be wholly accounted for by the eddy currents induced in the neighbourhood of the moving boundary.

4.2. VIBRATION

It has long been known that magnetism may be induced in iron by vibration. Gilbert showed that an iron bar,

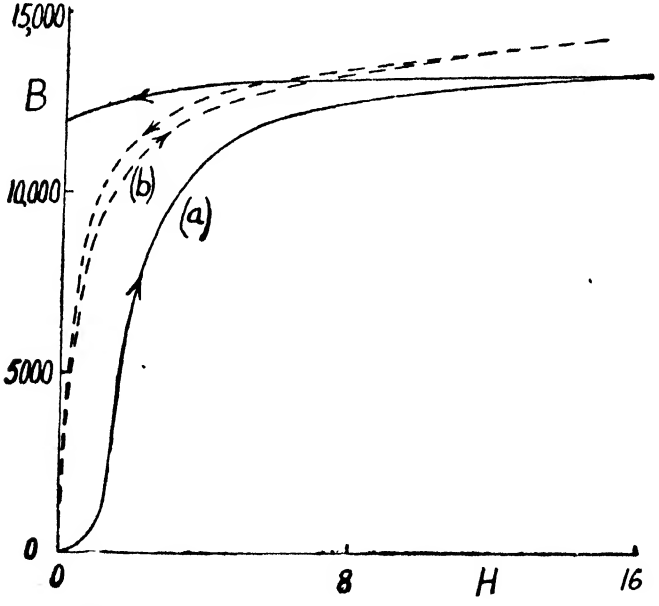

FIG. 4.6.—Effect of Vibration on Soft Annealed Iron Wire: (*a*) Without Vibration, (*b*) With Vigorous Tapping (Ewing)

hammered in the earth's field, became magnetized, and the fact that magnetism is induced during construction in the hull of a steel ship is also familiar. Fig. 4.6 shows

how, according to Ewing [11], the magnetization curve and upper part of the hysteresis loop of a sample of very soft, annealed iron wire are changed by vigorously tapping the specimen. It will be seen that vibration in this case has raised the permeability enormously at low inductions

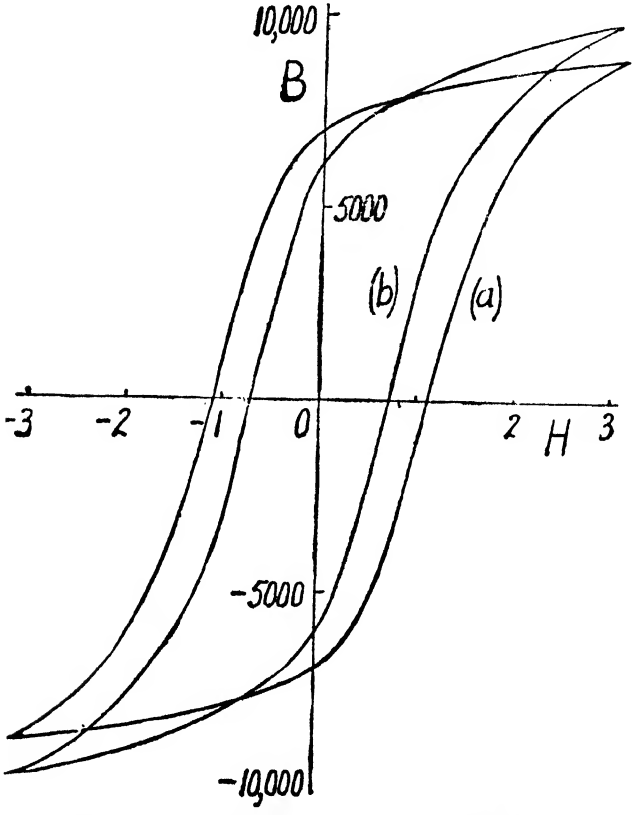

FIG. 4.7.—Effect of a Longitudinal Alternating Current on the Hysteresis Loop of a Sample of Dynamo Sheet Steel: (*a*) No Current, (*b*) 41·6 amperes per sq. cm. at 50 cycles per second

and to a lesser extent at higher values. The remanence is reduced to a very small amount and the hysteresis loop is also only a small fraction of the size of the normal loop. This result and the effects of vibration generally on magnetic properties may be readily understood in terms of the domain theory as already outlined. For magnetiza-

tion below the knee of the $B - H$ curve occurs by the movement of the domain boundaries under a changing field. The boundaries have to pass over regions of peak stress to give the Barkhausen jumps. We may suppose that the varying internal stresses induced by vibration, added to the internal stresses already existing, produce momentary reductions in the peak stresses sufficient to enable the boundaries, with a given applied field, to slip past these barriers, thus leading to increased permeability and reduced hysteresis loss.

A similar result can be achieved by passing an alternating current through the sample. The effect of this is to superimpose on the applied steady field an alternating component, so that the field in some direction periodically reaches values higher than the steady value. These peak fields may be sufficient to push the boundaries over the stress maxima which would otherwise constrain the movement, leading again to higher permeability and a smaller hysteresis loop. Fig. 4.7 shows the observed change in the hysteresis loop of a sample of dynamo sheet when an alternating current with a frequency of 50 cycles per second was passed through the specimen in the same direction as the applied field. A similar change was observed in this specimen with a transverse current.

4.3. COLD WORK

The effects mentioned in the preceding sections were produced by externally applied stresses, but internally produced strains also have remarkable effects on magnetic properties. Theoretical relations between permeability and internal strains have already been given in Chapter 3 and it is clear that on theoretical grounds the higher the stress peaks in the material the poorer will the magnetic properties be. One source of such strains is that due to ' cold work ', which includes bending, stretching, rolling, machining operations, and the like, in which the elastic

limit of the material is exceeded and plastic deformation of the constituent crystals occurs. In this case the crystals become broken up and severe distortion of the regular atomic lattice pattern occurs. This is accompanied by a marked deterioration of magnetic properties. Fig. 4.8 shows, for example, the effect on the magnetization curve,

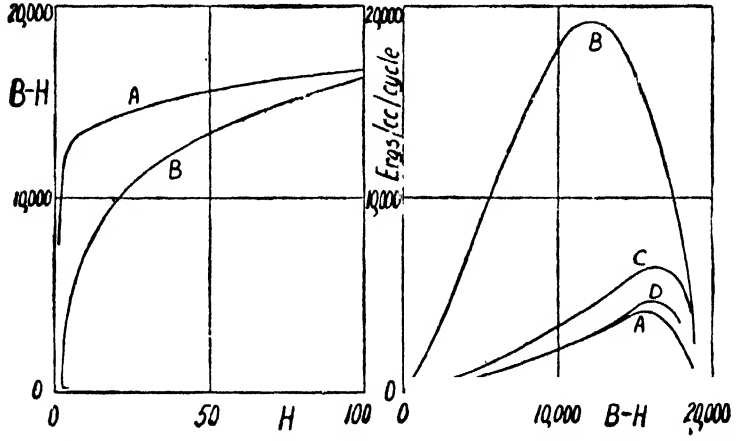

FIG. 4.8.—Effect of Severe Cold Work on 4% Silicon Steel
A—Original annealed Material, 0·65 mm. thick
B—Cold Rolled to 0·3 mm. thickness
C—Annealed at 630° C. for 2 hours
D—Annealed at 1100° C. for 4 hours

and on the rotational hysteresis loss, obtained by cold-rolling a sample of 4 per cent silicon steel in a series of passes from 0·65 to 0·3 mm. thickness [12]. Recrystallizing the strained material by heating to a sufficiently high temperature relieves the strains and restores the magnetic properties. This is shown in the figure in which the rotational hysteresis loss is seen to be restored almost to its original value by heat-treatment.

4.4. IMPURITIES

Perhaps the most important source of internal strains in the higher grade soft magnetic materials is that due to

the presence of impurities held in solution in the metal. These may be classified into two groups, ' substitutional ' and ' interstitial '. Atoms of the former substitute themselves in place of atoms of the parent metal in the crystal lattice and, because of the dissimilarity between the atoms

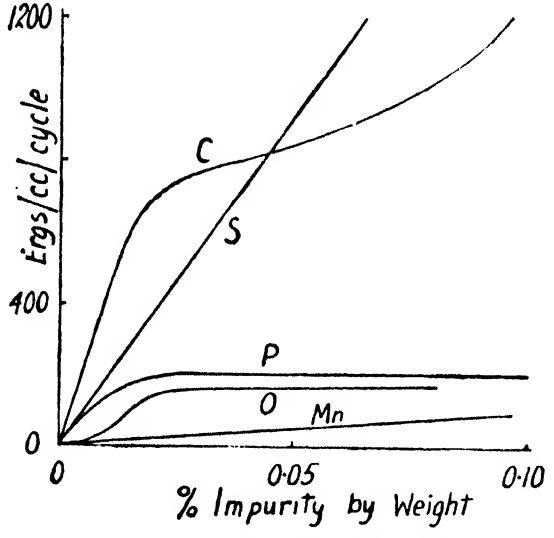

FIG. 4.9.—Effect of Impurities on the Alternating Hysteresis Loss of Iron at $B_{max.}$ = 10,000 gauss (Yensen)

of the two elements, produce some local distortion. Silicon and manganese in iron are examples. The former element, however, although it may be expected to have some harmful effect on account of its own contribution to the lattice distortion, has beneficial effects which outweigh this and make it a very desirable addition for some steels, as will be described in the next chapter. In general the substitutional elements are not as harmful to magnetic properties as the interstitial impurities. The latter squeeze themselves in between the regular planes of atoms without ejecting a parent atom, and thus create a greater local disturbance of the lattice than the substitutional kind. Carbon and sulphur in iron are important offenders. The impurities may, depending on their nature and amount,

be present not only as atoms in solution, but also in molecular form in the form of aggregates, and the imperfections they introduce into the metal crystals cannot be wholly eliminated even in laboratory specimens.

Yensen [13] has made an exhaustive study of the effect of impurities on the magnetic properties of iron and silicon-iron and, in spite of the difficulty of separating out the losses due to different impurities and to other causes, has given quantitative results for the more common impurities. Fig. 4.9 shows Yensen's results for the hysteresis loss attributable to various impurities in iron, and these curves at least show the relative importance of different elements, carbon appearing as the impurity most detrimental.

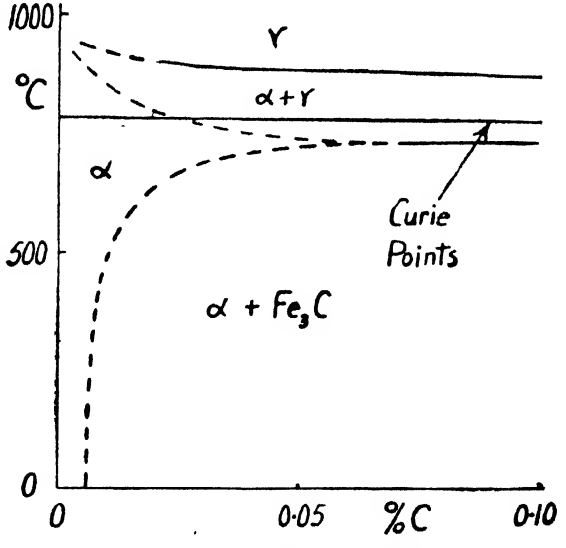

FIG. 4.10.—The Iron-Carbon Diagram for Low Values of Carbon

Fig. 4.10 shows the form of the equilibrium diagram of the iron-carbon system for low percentages of carbon. The probable state of the carbon is indicated by the broken lines, according to which, at room temperature, carbon below about 0·006 per cent is held in solid solution, but

to the right of the line precipitates as Fe_3C or cementite. Fig. 4.11 shows curves, also due to Yensen, relating coercivity and maximum permeability with the carbon content in iron and these, together with that for carbon in Fig. 4.9, indicate that small percentages of carbon corresponding to the solubility limit in the equilibrium diagram are most detrimental to magnetic properties.

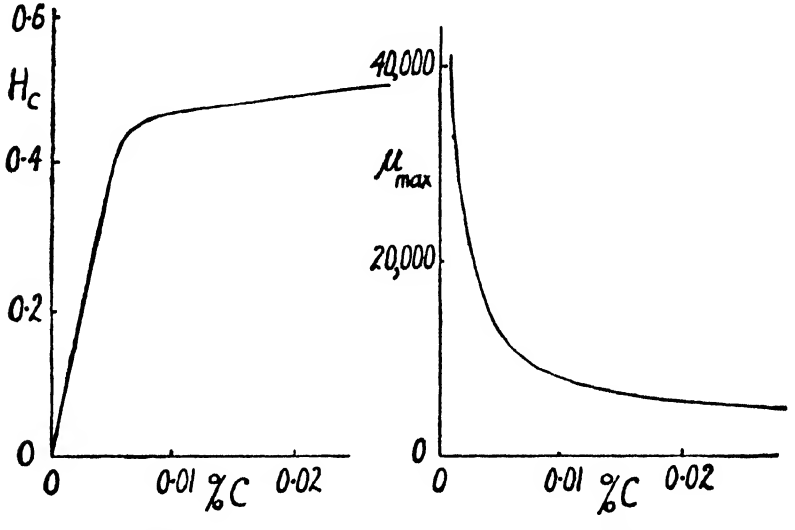

FIG. 4.11.—Effect of Carbon on the Coercivity and Maximum Permeability of Iron (Yensen)

In the early days of the electrical industry overheating of electrical apparatus, particularly transformers, often occurred as a result of a gradual, though frequently very large, increase of hysteresis loss in the iron or mild steel used for magnetic purposes at that time. This phenomenon, known as 'magnetic ageing', occurs to only a small degree in present-day commercial magnetic materials. Its cause is attributed to slow metallurgical changes in the material occurring at normal operating temperatures. In the case of carbon it will be seen from the equilibrium diagram that this element is soluble in the iron in much greater quantities at temperatures in the

region of, say, 700° to 800° C. than at room temperature and thus, on cooling from a high temperature, carbon may remain in a supersaturated solid solution in excess of the equilibrium solubility limit. Subsequently the excess carbon is slowly precipitated, at first, according to Yensen, as aggregates of colloidal size. These later coagulate into larger inclusions. It is suggested that the effect on magnetic properties is greatest while the process is passing through the colloidal stage and that some improvement in properties follows afterwards as the larger inclusions form. What has been said of carbon is true also of oxygen and nitrogen as impurities, since their behaviour in regard to solubility in iron is similar to that of carbon. Magnetic ageing in unalloyed iron is thus attributed to the precipitation of these three impurities in the form of iron carbide, oxide, or nitride respectively. The early troubles with ageing arose from the high percentage of impurities present, the materials being put into service with comparatively large amounts still held in supersaturated solution. In present-day materials the impurities are relatively low in amount and a metallurgically stable state can also be produced by appropriate heat-treatment, so that ageing is small in the commercial unalloyed iron produced for electrical purposes, whilst in the silicon steels to be described in the next chapter it is almost entirely absent.

The impurities in iron can be reduced to relatively low amounts by suitable treatment. There are a number of refining processes including chemical methods, electrodeposition, melting or annealing in a vacuum, and high temperature annealing in a hydrogen atmosphere. From the point of view of magnetic properties the latter has been found to be the most effective process.

Cioffi [14] heat-treated small ring specimens of iron of varying thicknesses in hydrogen. In his earlier experiments he used moist hydrogen but later pure hydrogen. A typical treatment was to maintain the specimen for 18 hours at 1,475° C., then to cool in one hour to 880° C.,

and to maintain at this temperature for a further 12 hours, followed by slow cooling to room temperature. He found that the interstitial impurities, oxygen, carbon, nitrogen, and sulphur, could be reduced by this treatment to a few thousandths of a per cent each (see Table 5.1) without greatly affecting the metallic impurities. Fig. 4.12 illus-

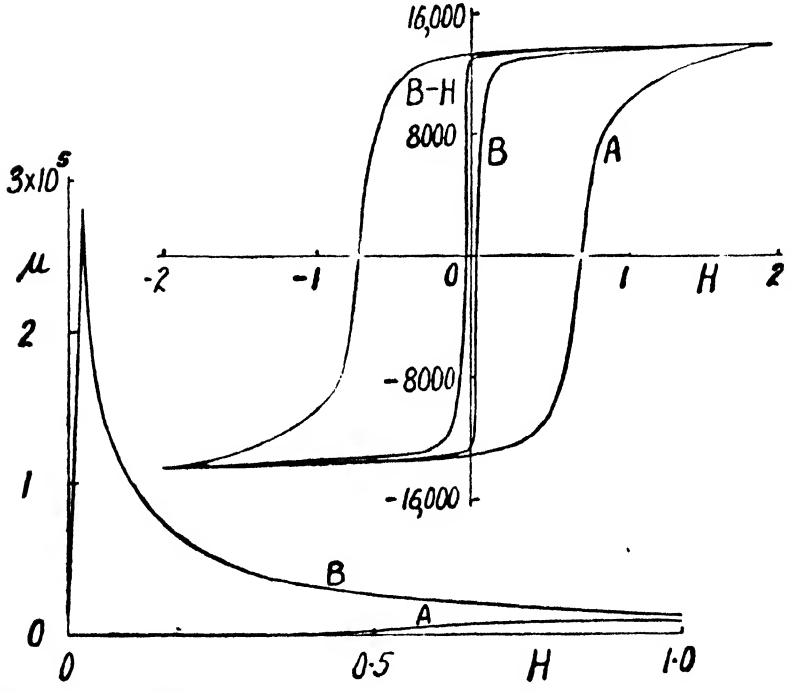

FIG. 4.12.—Effect of High Temperature Hydrogen Annealing on the Hysteresis Loop and Permeability of Iron:

A—In the annealed condition before Hydrogen Treatment
B—After Hydrogen Annealing (Cioffi)

trates the improvement in hysteresis loss and permeability obtained by this treatment in pure hydrogen. The initial permeability for this sample is 14,000 and the maximum permeability 280,000, while the hysteresis loss, corresponding to about 190 ergs per c.c. per cycle for the loop shown, is only about one-twentieth of that for a commercial unalloyed iron sheet. The reintroduction of nitrogen or

sulphur into the hydrogen-treated iron impaired the magnetic properties which, however, could be restored by further hydrogen annealing.

Polycrystalline iron of greater purity than Cioffi's has been produced by Cleaves and Hiegel [15], who, however, even after careful high temperature heat-treatment in hydrogen, found the maximum permeability in the best specimen to be 88,400, that is, a lower value than that obtained by Cioffi. This serves to confirm that other

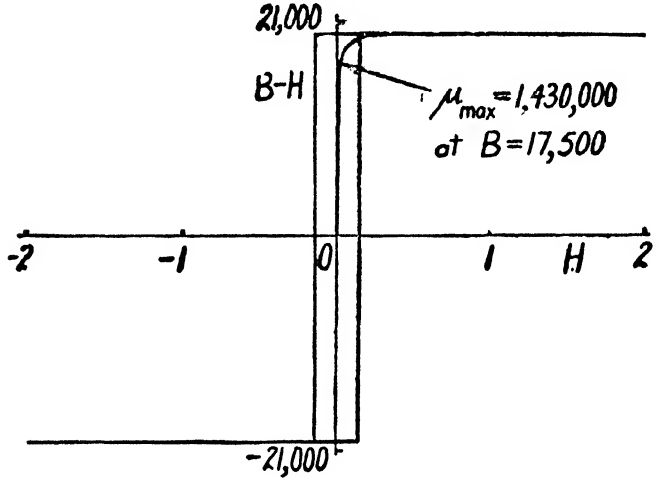

FIG. 4.13.—Magnetization Curve and Hysteresis Loop of Hydrogen-treated Single Crystal of Iron in [100] Direction (Cioffi, Williams, and Bozorth)

strains affecting magnetic properties may be present besides those due to impurities, and this is referred to in the next section.

It may be mentioned here that the highest maximum permeability so far reported was obtained by Cioffi, Williams, and Bozorth [16], who prepared a single crystal of iron of the purity given in Table 5.1, by maintaining the metal at 1,500° C. for 28 hours in pure hydrogen, cooling to 880° C. and by then holding this temperature for a further 24 hours. From this was cut a single crystal

' picture frame ' specimen having its four sides parallel to a [100] direction, and this was again annealed after cutting for 18 hours at 880° C. This single crystal of iron was found to have a maximum permeability of 1,430,000 at $B = 17{,}500$ gauss. This high value is clearly the result, not only of the purification and careful annealing but also of selecting the [100], or easy crystallographic direction of magnetization in the crystal. Its coercive force was 0·15 gauss, a value which was, however, unexpectedly high for such a pure, high permeability specimen. The magnetization curve and hysteresis loop are shown in Fig. 4.13.

4.5. GRAIN BOUNDARIES AND SURFACE EFFECTS

A further source of lattice distortion is that due to the grain boundaries, that is the surfaces where the constituent crystals of the metal meet. Since neighbouring grains will in general have differing crystallographic orientations, a distortion of the regular lattice pattern will occur in the region of the junctions between them. Thus high local strains will occur at the grain boundaries with a local deterioration of the magnetic properties. We might thus expect that the greater the proportion of this strained boundary material, that is the smaller the grain size, the poorer also the magnetic properties. Since there are so many possible causes of internal strain and it is also impossible to change the grain size in a particular sample without also altering other conditions of internal strain, there is some doubt of the quantitative effect of grain boundaries. Yensen [13] has proposed the formula

$$W_h = 100\sqrt{N}$$

or the alternating hysteresis loss in iron with low impurities, due to grain size alone, where W_h is in ergs per c.c. per cycle at $B_{max.} = 10{,}000$ gauss and N is the number of

grains per sq. mm. For a 4 per cent silicon transformer steel Richer [17] has given the corresponding formula

$$W_h = 18\sqrt{N} + 3{\cdot}6N$$

Ruder [18], however, has produced experimental evidence which indicates that such expressions can be regarded as only of very limited application because of the involved interrelated effects on hysteresis not only of purity, mechanical condition, and heat-treatments, but also of the thickness of the specimen.

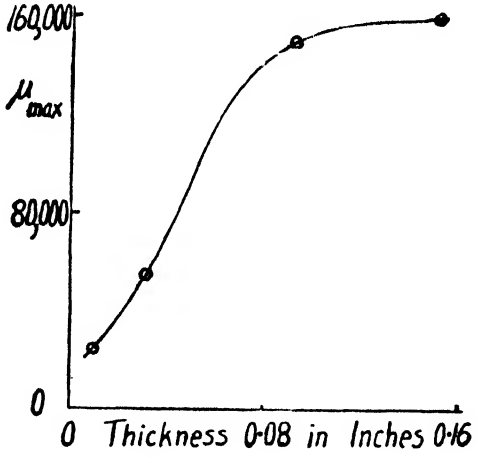

FIG. 4.14.—Variation of Maximum Permeability with Thickness of Hydrogen-treated Samples of Iron (Cioffi)

At the surface of a metal the regular crystal lattice pattern is interrupted and deformation of the lattice will occur in the surface material. The material affected may constitute only a very thin layer and the effect on magnetic properties might be expected to be small. There is, however, some evidence to indicate that a substantial surface effect exists in magnetic materials, although what its precise cause may be is not known. For example, Ruder found a 16 per cent increase in hysteresis loss after annealing in a 5 per cent silicon steel which had been rolled down from 2 mm. thickness to 1 mm. Almost the same increase was found

for this material when the thickness was reduced the same amount by cutting instead of rolling, there being no change in the grain size or grain shape after the annealing. Cioffi also found, in his experiments on hydrogen annealing of iron, that the exceptionally good magnetic quality could not be obtained on thin specimens. Some results obtained with varying thickness of specimen are shown in Fig. 4.14. It may be mentioned in this connection that the pure iron of Cleaves and Hiegel mentioned in the previous section and having a maximum permeability of 88,400 had a thickness of 0·062 inch.

4.6. EFFECT OF TEMPERATURE

The effect of temperature on the saturation value of a ferromagnetic has been discussed in Chapter 2 and the effect on the anisotropy constants in Chapter 3. Fig. 4.15 shows the relation between the permeability and temperature, at $H = 0{\cdot}3$, of a sample of iron according to Hopkin-

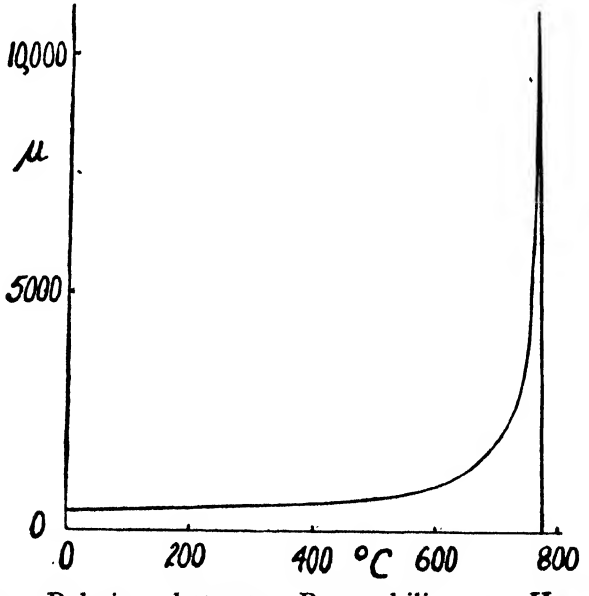

FIG. 4.15.—Relation between Permeability at $H = 0{\cdot}3$ and Temperature for Iron (Hopkinson)

son [19]. This indicates a remarkable increase just below the Curie temperature, followed by a sudden fall at the change point. The relation between permeability and applied field at different temperatures for a sample of soft iron, due to Kuhlewein and Neumann [20], are shown in Fig. 4.16. Similar effects are observed with other ferromagnetics. An increase of temperature therefore facilitates the magnetization process at the lower field strengths but

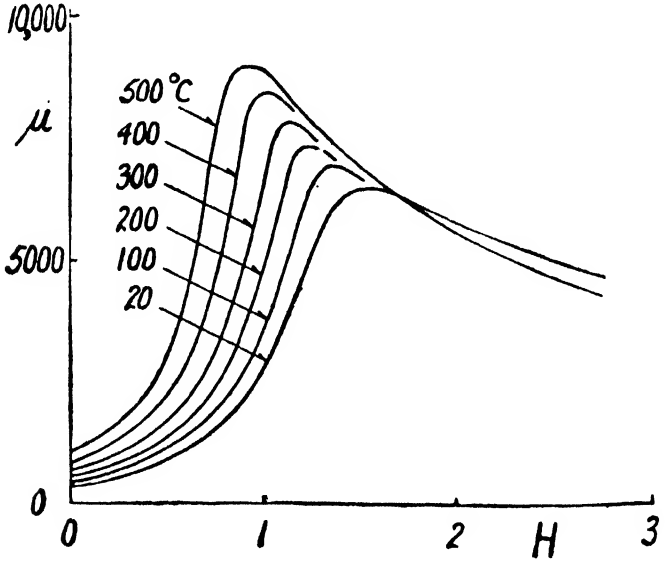

FIG. 4.16.—Effect of Temperature on the Permeability of Soft Iron (Kuhlewein and Neumann)

reduces the saturation magnetization. The improved permeability is consistent with a reduction of internal strains with rise of temperature, and the observed reduction of the anisotropy factors K_1 and K_2 at elevated temperature would, as suggested by Bozorth [21], also contribute to an increase of permeability, since when these factors become zero the directional effects disappear and every crystal direction becomes an equally easy direction of magnetization.

4.7. MAGNETIC ANNEALING

At temperatures above the Curie point there is no ferromagnetism and therefore the domains do not exist. However, on cooling below this point, the spinning electrons, responsible for the magnetic moment of the atoms, are pulled into nearly parallel alignment by the forces of exchange, as described in Chapter 2, and the self-saturated domains are formed. If the metal has positive magnetostriction in its easy crystallographic direction of

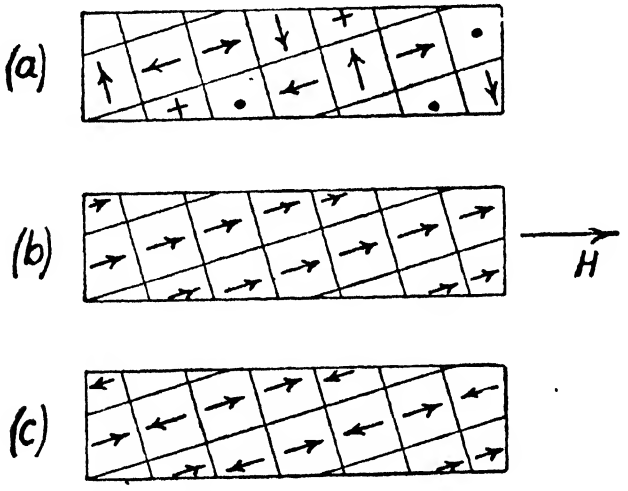

FIG. 4.17.—Effect of Magnetic Field applied during cooling on Distribution of Domains

magnetization, each domain, in forming, will extend magnetostrictively, as far as neighbouring restraints allow, in the direction of its saturation magnetization; or alternatively, if the metal is characterized by negative magnetostriction, the domain will contract in this direction. In general the domains will form with their magnetization vectors directed at random in the various easy crystallographic directions. This condition is represented diagrammatically for part of a single crystal in Fig. 4.17(*a*). If, however, during cooling through the Curie point, a

magnetic field is applied, for example to a sample of iron, and this is sufficient to pull the domain vectors into the nearest cube-edge direction to that of the field, then the condition represented at (*b*) will be obtained. If, in the latter condition, the temperature is sufficiently high to permit strain relief in the specimen, then, on further cooling, we may expect the domains to ' freeze in ' in these positions. Thus if the sample were demagnetized after cooling the positions of the domain vectors would be as shown at (*c*), that is the lateral domains have been eliminated. A tensile stress applied during cooling might have a similar effect. Now in the material (*c*) domain boundaries between oppositely directed domain vectors predominate, in contrast with the untreated material (*a*) in which there are 90° boundaries. 180° and 90° boundary movements have already been discussed in Chapter 3. Movements of the former involve no magnetostrictive change in length, although some energy change is entailed, and therefore they should occur more easily than in the case of 90° boundaries. We may thus expect the material in the condition represented by (*c*) to have higher permeability than in condition (*a*), for that direction in the specimen in which the field was applied during cooling. Laterally the permeability would be poorer.

The explanation given above may serve in a qualitative way to account for the remarkable improvements in permeability which have been observed in some alloys by heat-treating in a magnetic field, although it is evidently not a complete explanation of all the phenomena observed. Fig. 4.18 shows the effect of magnetic annealing on a sample of nickel-iron alloy with 65 per cent nickel according to Dillinger and Bozorth [22]. Curve (*a*) shows the permeability in relation to the applied field for the material after annealing in hydrogen at 1,400° C., while curve (*b*) shows the effect of a further treatment consisting of holding the specimen for a few minutes at 650° C. in a field of 10 gauss. This additional treatment has raised the maxi-

mum permeability from 20,000 to 600,000. A similar result was obtained by Cioffi, Williams, and Bozorth, who prepared a single crystal ' picture frame ' specimen, cut for [100] crystal directions, of a nickel-iron with 66 per cent

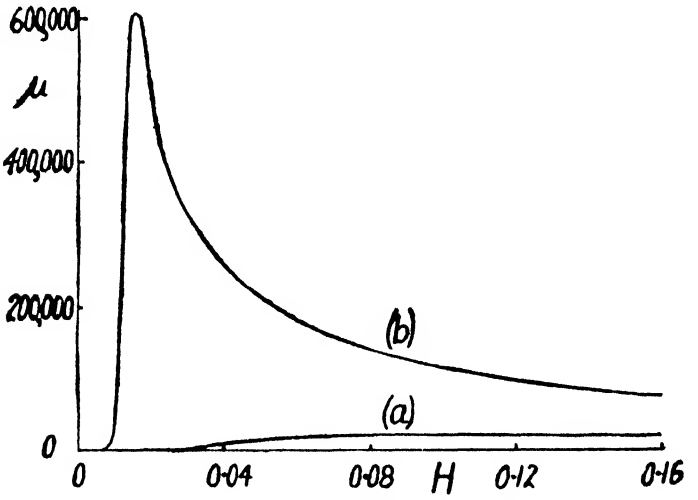

FIG. 4.18.—Effect of Magnetic Annealing on a Sample of Nickel-Iron Alloy with 65% Nickel. (*a*) Annealed in Hydrogen at 1,400° C. (*b*) Reannealed at 650° C. in a field of 10 gauss (Dillinger and Bozorth)

nickel. After annealing at 1,360° C. for 18 hours in pure hydrogen this had a maximum permeability of 18,000, but after further treatment with an applied field of 10 gauss the maximum permeability rose to the high value of 1,330,000. Fig. 4.19, also due to Dillinger and Bozorth, shows the effect of various treatments on a range of nickel-iron alloys. Comparing curves (*a*) and (*b*) it will be seen that the permeability of these alloys is dependent upon the rate of cooling, rapid cooling leading to a higher permeability than slow. A great increase is, however, produced by slow cooling in a magnetic field as shown by curve (*c*). The improvement is greatest for about 65 to 70 per cent of nickel, for which composition the Curie temperature of the alloys is also greatest. This is con-

sistent with what has been said already about strain relief and the freezing in of the domains which may be expected to occur during treatment in a magnetic field if the Curie point is sufficiently high.

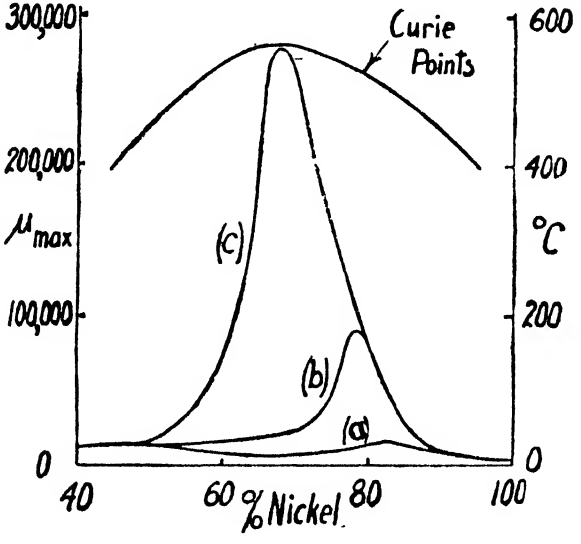

FIG. 4.19.—Showing Effect of Rate of Cooling and of Magnetic Annealing on the Nickel-Iron Alloys. (*a*) Alloys slowly cooled, (*b*) Alloys cooled rapidly, (*c*) Slow Cooling in a Magnetic Field (Dillinger and Bozorth)

Improvements have been obtained also by magnetic annealing of commercial iron and silicon-iron materials, but these are relatively small. Iron has a high Curie point (770° C.), but its magnetostriction characteristics are complicated as may be seen from Fig. 3.5, which may account for the present lack of success. Williams [23], however, with the 3·85 per cent silicon-iron single crystal cut for [100] was able to raise the maximum permeability of the specimen which, after annealing at 1,300° C. in hydrogen, had a value of 1,180,000 to 1,380,000 by means of a further anneal at 600° C. for 3 hours, in a magnetic field of 10 gauss, followed by etching.

REFERENCES

1. M. Kornetzki, *Zeits. f. Phys.*, 1933, **87**, 560.
2. Y. Masiyama, *Sci. Rep. Toh. Imp. Univ.*, 1931, Series **1**, **20**, 544.
3. Z. Nishiyama, *Sci. Rep. Toh. Imp. Univ.*, 1929, Series 1, **18**, 341.
4. S. Bidwell, *Proc. Roy. Soc.*, 1890, **47**, 469.
5. R. Becker and M. Kersten, *Zeits. f. Phys.*, 1930, **64**, 660.
6. J. A. Ewing, *Magnetic Induction in Iron and Other Metals* (London, 1900), p. 204.
7. O. E. Buckley and L. W. McKeehan, *Phys. Rev.*, 1925, **26**, 261.
8. R. Forrer, *Journ. Phys. Radium*, 1926, (6), **7**, 109.
9. F. Preisach, *Ann. Phys.*, 1929, **3**, 737.
10. K. J. Sixtus and L. Tonks, *Phys. Rev.*, 1931, **37**, 930.
11. See Reference 6 above, p. 116.
12. F. Brailsford, *Journ. I.E.E.*, 1943, **90**, Part 2, 307.
13. T. D. Yensen, *Trans. Amer. I.E.E.*, 1924, **43**, 145; T. D. Yensen and N. A. Ziegler, *Trans. Amer. Soc. Metals*, 1935, **23**, 556; 1936, **24**, 337.
14. P. P. Cioffi, *Phys. Rev.*, 1932, **39**, 363; 1934, **45**, 742; *Bell Lab. Record*, 1932, **10**, 159. W. C. Ellis and E. E. Schumacher, *Metals and Alloys*, 1934, **5**, 269.
15. H. E. Cleaves and J. M. Hiegel, *Journ. Res. Nat. Bur. Stds.*, 1942, **28**, 643.
16. P. P. Cioffi, H. J. Williams, and R. M. Bozorth, *Phys. Rev.*, 1937, **51**, 1009; R. M. Bozorth, *Journ. App. Phys.*, 1937, **8**, 575.
17. G. C. Richer, *Journ. Iron and Steel Inst.*, 1937, **136**, 323.
18. W. E. Ruder, *Trans. Amer. Soc. Metals*, 1934, **22**, 1120.
19. J. Hopkinson, *Phil. Trans.*, 1889, **180**, 443.
20. H. Kuhlewein and H. Neumann, *Phys. Zeits.*, 1931, **32**, 427.
21. R. M. Bozorth, *Journ. App. Phys.*, 1937, **8**, 575.
22. J. F. Dillinger and R. M. Bozorth, *Physics*, 1935, **6**, 279.
23. H. J. Williams, *Phys. Rev.*, 1937, **51**, 1009.

CHAPTER 5

IRON AND SILICON-IRON ALLOYS

5.1. 'PURE' IRON

A GENERAL requirement for the magnetically soft materials is that, apart from alloying constituents deliberately added for a particular purpose, the metal shall be as pure as is economically possible. Table 5.1 gives an indication of the relative purity of iron prepared by different investigators and by different methods.

Cleaves and Hiegel [1] prepared 19 1-lb. ingots by a chemical method from ferric nitrate, and some of these had a total for the impurities given in the table of less than 0·008 per cent. Some of the properties of this iron are as follows:

Density at 20° C. . . .	7·874 ± 0·001 g./c.c.
Freezing-point	1,539 ± 1° C.
Electrical resistivity at 20° C. .	9·71 ± 0·01 microhm cm.
Magnetic saturation ($4\pi J$) . .	21·58 ± 0·01 kilogauss.
Highest value of $\mu_{max.}$ . . .	88,400

The maximum permeability of the iron was found to be lower than that obtained by Cioffi, whose iron was actually less pure, as already mentioned.

Electrolytic iron is seen to be relatively pure but specimens suffer from porosity, irregularities, and brittleness, while carbonyl iron, which is produced chemically in the form of powder, has a rather poorer chemical analysis.

5.2. EFFECTS OF ALLOYING

The harmful effect of small quantities of foreign elements, particularly the interstitial impurities, on magnetic properties has already been discussed. Large changes in the properties of the pure metal, beneficial for particular

TABLE 5.1

COMPARATIVE ANALYSIS OF HIGH-PURITY IRON (PER CENT BY WEIGHT)

	C	S	P	Mn	Si	Cu	Al	Be	N_2	O_2	H_2	Approx. Total of Impurities Listed
National Bureau of Standards (Cleaves & Hiegel)	<0·001 to 0·001	0·001 to 0·004	<0·0005		nil to 0·002	<0·002	<0·001	<0·001	0·000	0·000 to 0·004	0·000	<0·013
Hydrogen treated iron (Cioffi, Williams & Bozorth)	0·008	0·001		<0·001	0·002	<0·005				<0·001		<0·02
Hydrogen treated iron (Cioffi)	0·005	0·003	0·004	0·028	0·0012				0·0001			0·04
Average electrolytic iron deposits	0·005 to 0·007	0·002 to 0·005	0·002 to 0·005	0·002 to 0·005	0·002 to 0·01	0·002 to 0·02						0·015 to 0·05
Swedish charcoal iron	0·02 to 0·06	0·005 to 0·01	0·04 to 0·07	<0·1	0·02 to 0·04							0·1 to 0·3
Carbonyl iron powder	0·02 to 0·1	0·005 to 0·007	0·005 to 0·007	0·08 to 0·1	0·04 to 0·05				0·005	0·1 to 0·6		0·2 to 0·8
Good quality electrical sheet	0·03	0·02	0·02	0·15	0·15							0·4

applications, can, however, be brought about by the deliberate addition of certain alloying constituents. The nickel-iron alloys and the permanent magnet materials will be dealt with in the following chapters. Where high permeability and low hysteresis are required it has been pointed out by Kussman and Scharnow [2] that the alloys must be single phase. This immediately limits the scope for development by alloying, for the amount of the added constituent must not exceed that which is soluble in the

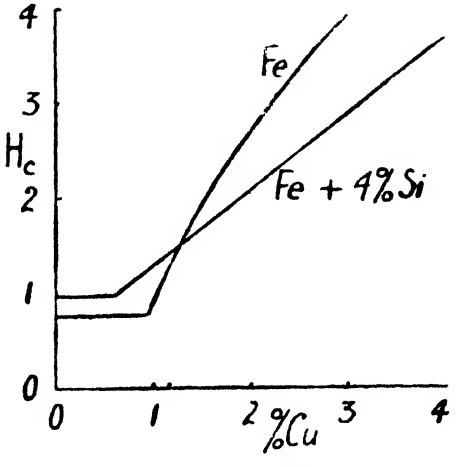

FIG. 5.1.—Showing the Variation of Coercivity with Percentage of Copper in Iron and in 4% Silicon Steel (Kussmann, Scharnow, and Messkin)

parent metal. In this case the crystals comprising the alloy are all of the same kind, but if the limit of solid solubility is passed a second phase consisting of crystals of different composition and characteristics is formed. This entails increased internal strains and poorer magnetic properties. The results in Fig. 5.1 due to Kussman, Scharnow, and Messkin [3] show, for example, the sharp rise of coercivity which occurs as the amount of copper added to iron and to a 4 per cent silicon-iron is increased, although it may be noted that some investigators place the limit of solubility of copper in iron for room temperature

rather lower than that indicated in the figure. However, the soft magnetic materials are invariably single phase alloys.

Fig. 5.2 shows the effect of various alloying constituents on the saturation value of iron. Most added elements reduce the value to a marked degree, but cobalt is an exception and there is also a small increase with low percentages of nickel. Fallot [4] has also reported that a marked rise of saturation value occurs for platinum added to iron,

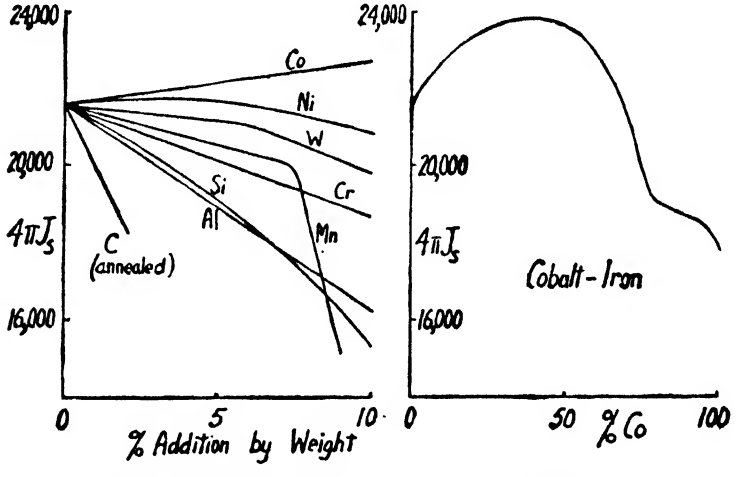

FIG. 5.2.—Effect of Alloying Constituents on the Saturation Value of Iron

12½ per cent of platinum raising the saturation value by 10 per cent. The complete curve for iron and cobalt in all proportions is also shown, the maximum increase of the saturation value over that for iron being about 10 or 11 per cent. Such high saturation alloys would be useful in technology but for the relatively high cost of cobalt and the fact that to make the alloy workable other alloying constituents such as vanadium have to be added which, by again lowering the saturation value, counteract the benefit of the cobalt.

The effect of various elements on the electrical resistivity

of iron is given in Fig. 5.3. Silicon and aluminium, which behave similarly in several respects when added to iron, are noteworthy on account of the large increase in resistivity obtainable with relatively small percentages added. High

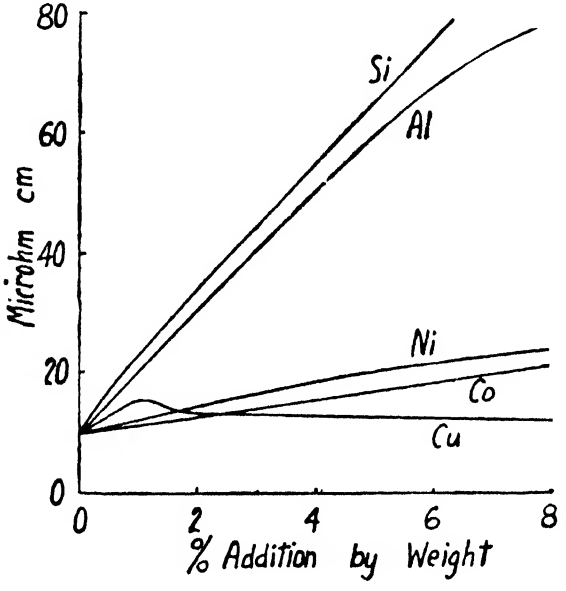

FIG. 5.3.—Effect of Alloying on Electrical Resistivity of Iron

electrical resistivity is a desirable characteristic in many practical applications, as already mentioned in Chapter 1, as it reduces the Foucault currents and energy losses in materials subjected to alternating or changing induction.

5.3. THE SILICON STEELS

The improvement in magnetic properties obtainable by alloying iron with silicon was discovered during a joint systematic research, started about 1890, on a number of binary and ternary alloys by Barrett, Brown, and Hadfield [5]. It was found that the addition of silicon raised the maximum permeability, reduced the area of the hysteresis loop, eliminated ageing troubles and substantially

raised the electrical resistivity. At the same time, however, it depressed the saturation value and introduced difficulties with the mechanical properties but, nevertheless, the usefulness of the alloy for electrical equipment, and particularly for the magnetic cores of transformers, was quickly recognized. Silicon steels soon came into universal use and they still have no competitor as transformer steels at normal power frequencies, while they are also

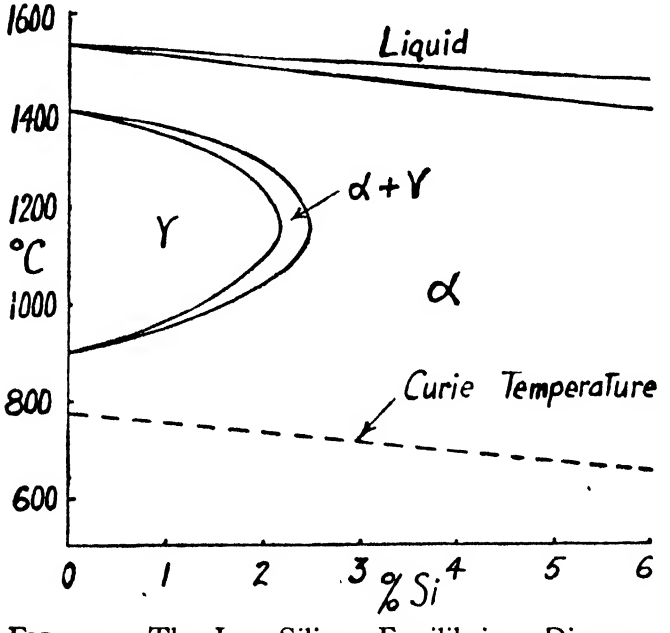

FIG. 5.4.—The Iron-Silicon Equilibrium Diagram

extensively used in large alternators and in high frequency rotating machines. Transformer sheets normally have $3\frac{1}{2}$ to $4\frac{1}{2}$ per cent silicon and a standard thickness of 0·014 inch. Lower silicon contents and unalloyed sheets are used in motors and generators with a standard thickness of 0·016 inch.

The equilibrium diagram of the iron-silicon system up to 6 per cent of silicon is shown in Fig. 5.4. This, it will be seen, has a closed gamma loop and the A_1 transformation, shown in Fig. 4.10 for the iron-carbon system at

about 730° C., is absent. Thus with more than about 2 or 2½ per cent silicon present the alloy may be annealed at a high temperature without a change of crystal structure occurring during cooling, although the width of the gamma loop is, according to Yensen [6], somewhat dependent on the amount of carbon present in the alloy.

The commercial steels are produced by a hot-rolling process from slabs which, after preliminary reduction in thickness in the rolls, are doubled and twice redoubled with intermediate reheats and further reduction, the final rolling being thus done on a pack of eight sheets. In a later development which will be discussed in Section 5.6, a cold-rolling process is employed. The magnetic characteristics of the sheets produced by these two methods are rather different and both types of steel are now being made and used.

5.4. EFFECTS OF SILICON

The variation of some physical properties with the percentage of silicon in iron is shown in Fig. 5.5, in which d is the density of the alloy according to several investiga-

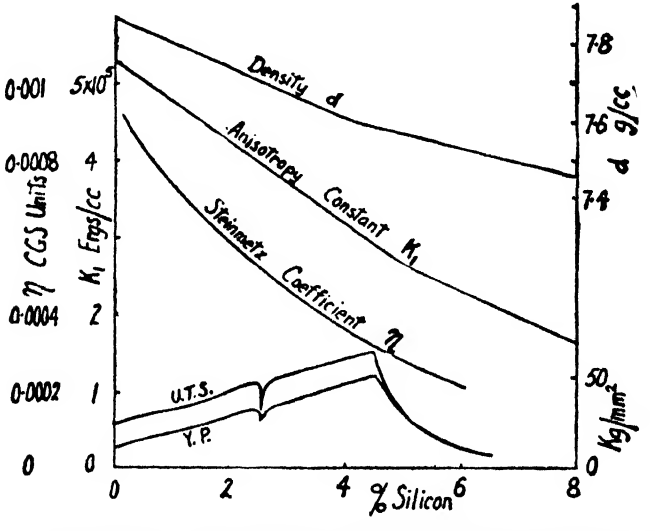

FIG. 5.5.—Variation of Properties with Content of Silicon in Iron

tors. The magnetic anisotropy constant K_1, referred to in Chapter 3, falls as shown with increasing silicon, which means that the higher the silicon the lower is the applied field required to produce saturation. The curve given is due to Tarasov [7], who showed how the magnitude of the field applied and the form of the specimen may introduce errors in determinations of this constant. The curve given for the Steinmetz hysteresis coefficient η is indicative of the rather remarkable way in which increasing silicon reduces the hysteresis loss. The values represented by the curve may be taken as typical of moderately good fully annealed commercial hot-rolled sheet materials, though considerable variation may occur for different samples since, as already described, there are other factors besides the silicon content affecting hysteresis. Table 5.2 gives some typical values of the hysteresis constants of sheet materials of varying silicon contents [8], these values being applicable in equations 1.1 and 1.2 in Chapter 1.

Fig. 5.5 also shows the ultimate tensile strength and yield point of the alloys according to Yensen [9]. These curves in conjunction with the elongation and reduction-of-area figures obtained on tensile specimens show the deterioration of the mechanical properties when the silicon content reaches about $4\frac{1}{2}$ per cent.

TABLE 5.2

TYPICAL HYSTERESIS CONSTANTS OF SILICON STEELS

Steel	Silicon Content %	$\eta \times 10^4$	n	b	c
Hot-rolled	0·13	9·1	1·6	1·39	11,260
Hot-rolled	1·9	5·9	1·65	1·96	12,050
Hot-rolled	3·7	3·4	1·65	0·77	10,370
Cold-rolled	3·1	0·86	1·8	0·59	12,370

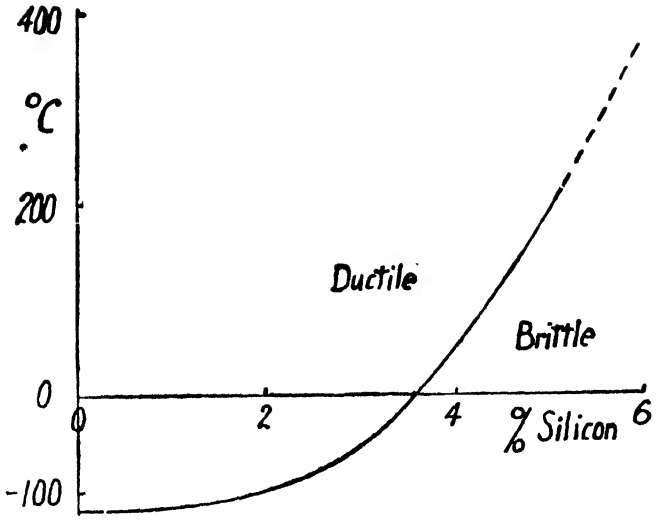

FIG. 5.6.—Approximate Boundary between Brittleness and Ductility for Silicon Alloys (Pilling)

Above this percentage the material becomes exceedingly brittle at room temperature but ductility returns at higher temperatures. Fig. 5.6, due to Pilling [10], shows the

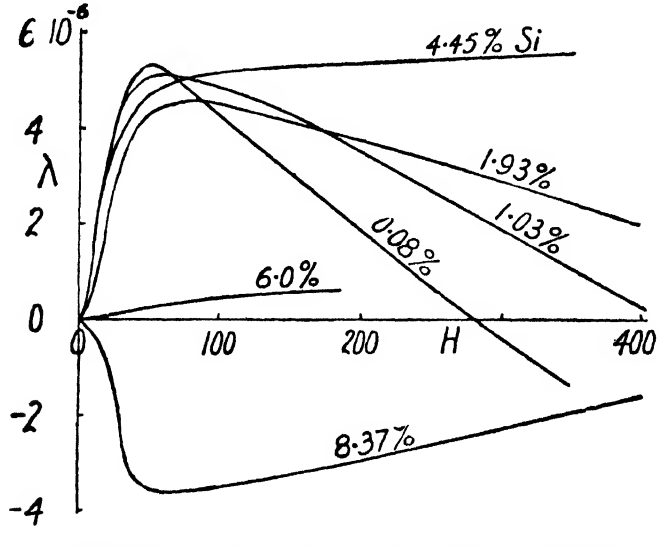

FIG. 5.7.—Magnetostriction of the Iron-Silicon Alloys (Schulze)

approximate boundary between ductility and brittleness in relation to the silicon content and the temperature.

Silicon in iron also has a considerable effect on the magnetostriction. This is illustrated by the curves in Fig. 5.7 which are due, except that for 6 per cent silicon, to Schulze [11]. It will be seen that with about 7 per cent silicon the magnetostriction becomes relatively small and has in fact a substantial negative value with 8·37 per cent silicon. No satisfactory explanation of these effects appears to have been given.

5.5. THE PROPERTIES OF COMMERCIAL SHEETS

The curves in Fig. 5.8 are typical magnetization curves for good quality commercial hot-rolled silicon steel sheet materials as used in electrical equipment. These, however, also include 6 per cent silicon steel, which is not

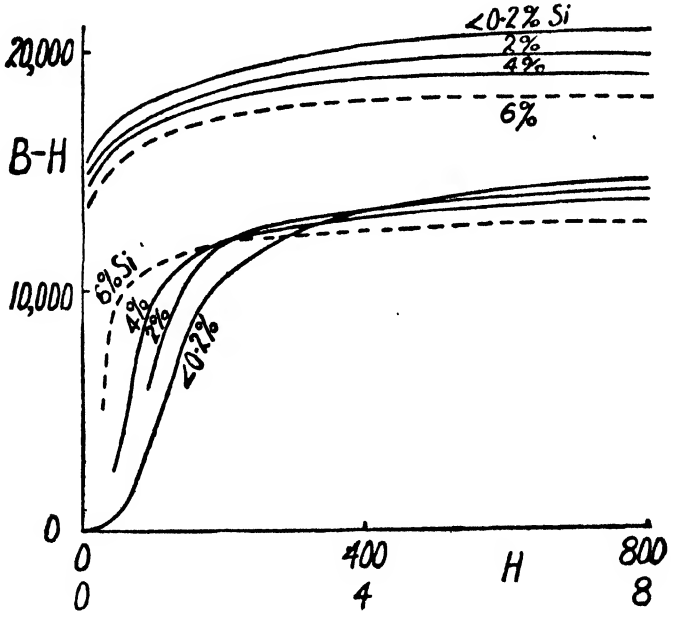

FIG. 5.8.—Typical Magnetization Curves of Good Quality Silicon Steel Sheet Materials

suitable for general use because of its inferior mechanical properties. They show very clearly the general effect of silicon in improving the permeability at inductions below about 12,000 gauss and in depressing the curves at high inductions.

The alternating [8] and rotational [12] hysteresis loss for a sample of 3·7 per cent silicon transformer steel and for a sample of ordinary unalloyed dynamo sheet are shown

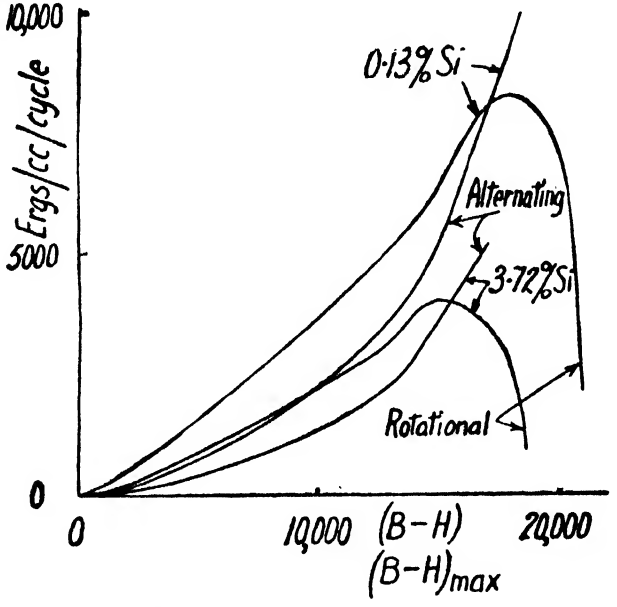

FIG. 5.9.—Alternating and Rotational Hysteresis Loss in Samples of Dynamo Sheet and Transformer Sheet Steel (Brailsford)

in Fig. 5.9, which shows both the form of these loss curves and the effect of the added silicon.

Fig. 5.10 similarly shows the total iron loss to alternating magnetization at a frequency of 50 cycles per second, indicating again the general effect of silicon. The curves are intended to give only the order of magnitude of the iron losses for the materials whose magnetic properties vary to a fairly considerable extent depending on their origin and treatment.

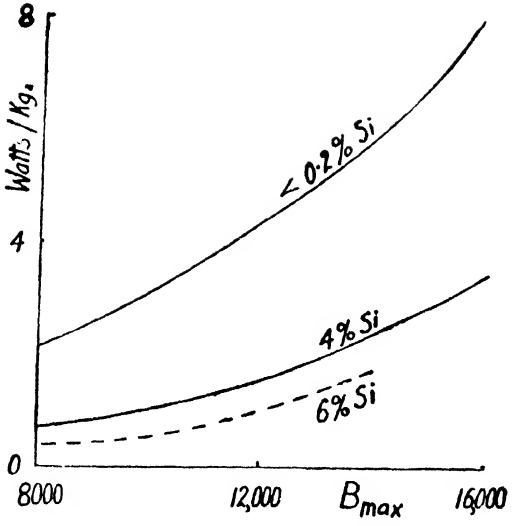

FIG. 5.10.—Total Iron Loss at 50 c.p.s. for Silicon Steel Sheet Materials

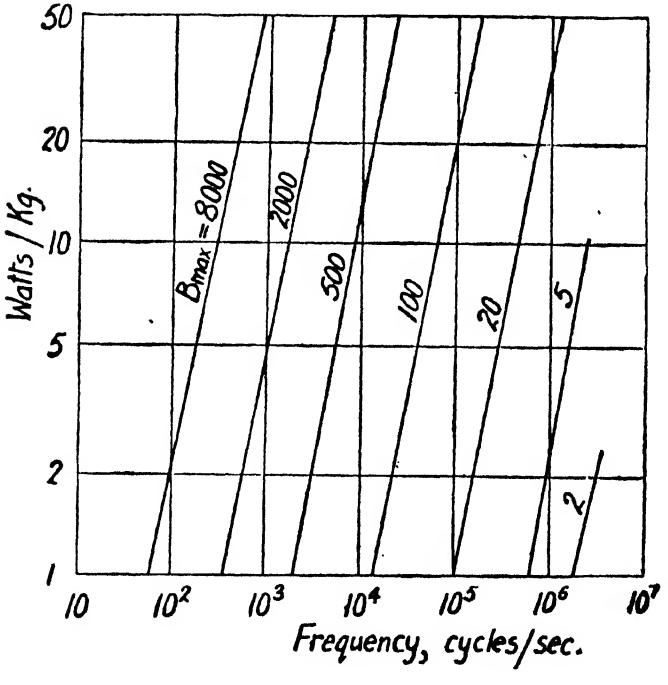

FIG. 5.11.—Total Iron Loss in 4% Silicon Transformer Sheet Steel 0·014" thick at High Frequencies (Dannatt)

Dannatt [13] has given data for the iron losses in silicon steel at frequencies up to over one megacycle per second and those for a sample of 4 per cent silicon transformer steel are shown in Fig. 5.11. It will be clear that at high frequencies a low induction only can be employed because of the great heat loss in the steel.

In some practical applications the magnetic circuit carries a steady flux in addition to the alternating one and,

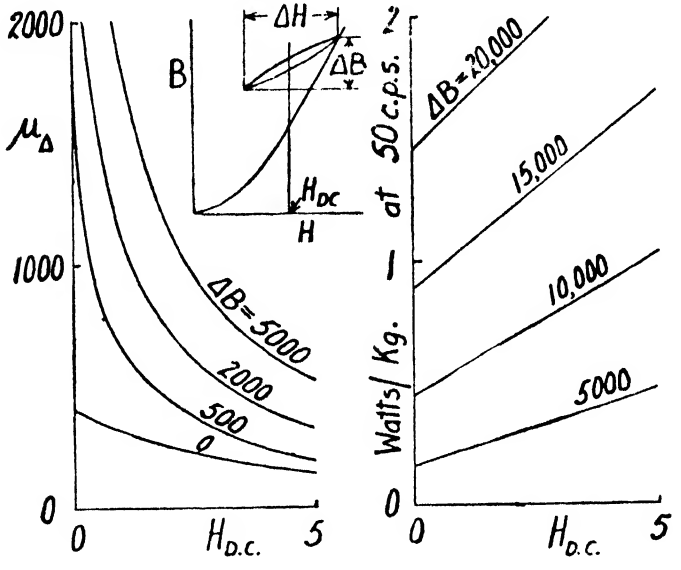

FIG. 5.12.—Incremental Permeability and Iron Losses with Superimposed Alternating and Steady Fields for a Sample of 4% Silicon Sheet Steel. (From Sims and Clay)

as already mentioned in Chapter 1, this may lead to a substantial fall in the alternating or incremental permeability and an increase in the hysteresis loss with a given alternating flux swing. Little data on this subject appear to have been published but that given in Fig. 5.12 for a sample of 4 per cent silicon steel is due to Sims and Clay [14]. The incremental permeability is there defined as the ratio $\frac{\Delta B}{\Delta H}$ where ΔB and ΔH are the total flux and

applied field variations, a steady field of $H_{D.C}$ being applied to the specimen. It will be seen that the incremental permeability for a given alternating flux falls rapidly as the steady field applied to the steel is increased. Similarly the total iron loss for a given alternating flux is also considerably increased as the applied field is raised, an effect which is due to increased hysteresis loss.

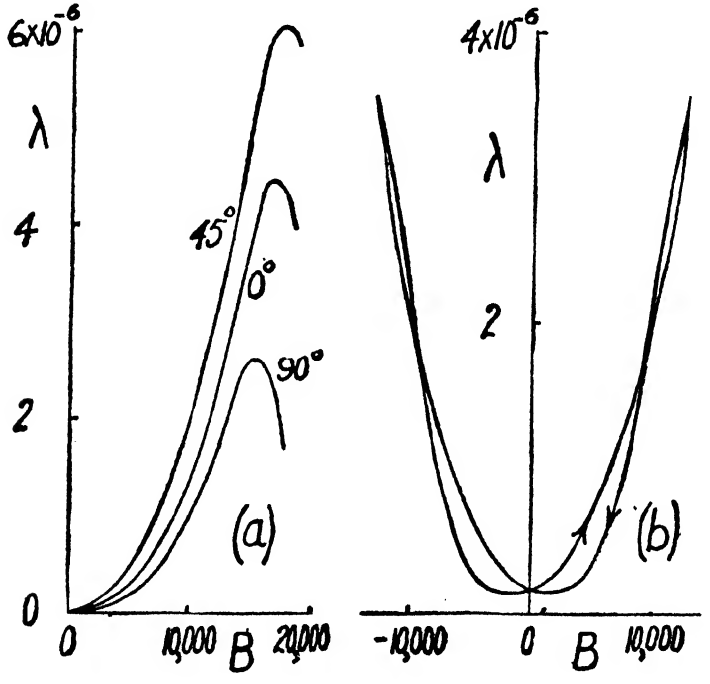

FIG. 5.13.—Magnetostriction for a Sample of 1·88% Silicon Sheet Steel showing (*a*) Variation with different Directions relative to the Rolling Direction, and (*b*) Magnetostriction for a Hysteresis Loop (Brailsford and Martindale)

On account of the phenomenon of magnetostriction a magnetic material changes its dimensions during magnetization as already mentioned. Thus a transformer core subjected to an alternating magnetization will change its dimensions periodically with double the frequency of the supply to the core. This effect is considered by some

authorities to be the initiating cause of the noise emitted by transformers which, depending on the location of the transformer, does in fact in many cases set a limit to the working induction in the cores. Apart from its general interest to the theory of ferromagnetism the magnetostriction of sheet materials is thus of some practical importance. Measurements made on single strips [15] cut in different directions from the sheet reveal that the magnetostriction varies with direction in the sheet, which is, however, not surprising since the permeability and hysteresis loss are also found to be somewhat directional in character, a fact which will be referred to in the next section. Fig. 5.13 shows the observed variation of magnetostriction with direction in a sample of 1·88 per cent silicon steel. It is also found that in taking the steel through a cycle of magnetization a loop is obtained no matter whether the magnetostriction is plotted against B or against H as abscissae. An example of such a loop is shown in the figure.

5.6. COLD-ROLLED SILICON STEEL

In the design of transformers at normal supply frequencies the amplitude of the working flux density in the laminated steel core is limited to a value near the knee of the magnetization curve, about 13,000 to 14,000 gauss for a 4 per cent silicon hot-rolled steel, because if the induction is increased much beyond this the magnetizing current becomes excessive and undesirable harmonics also appear in the output voltage wave-form. We have, however, seen in Chapter 3 that ferromagnetic single crystals have highly directional magnetic properties and that for iron and silicon-iron the cube-edge direction is a direction of high permeability. The magnetization curve for this direction has a knee only a little below the saturation value of the metal. If transformer steels could be made with a magnetization curve similar in form to this one for the

single crystal it would be an advantage to the transformer designer, who could, provided other limiting factors such as noise or iron losses did not become of greater importance, work the cores at a higher flux density and hence reduce the size and weight of transformers of a given power.

Now it has been found possible to produce silicon steels, with silicon in the range of about 2·5 to 3·5 per cent, with an improved shape of the magnetization curve in which the position of the knee has been substantially raised. It is true that this material has highly directional properties and the improvement relates chiefly to one direction in the sheet, but this is not a great disadvantage where transformers are concerned, since the alternating core flux is, in this case, confined to one direction in the transformer core. The same is not, of course, true of the armature of a rotating machine, in which the flux may be required to rotate through all directions in the plane of the laminations.

This steel is produced, in contrast to the ordinary hot-rolled steels, by a cold-rolling process. The material is subjected to severe reduction in the cold state with, according to one published process [16], one intermediate anneal. It is finally annealed in hydrogen at a temperature of about 1,100° C. The severity of the cold reduction limits the process to steels with less than about 3·5 per cent silicon because of the inferior mechanical properties already referred to, and hence the difficulty in the cold-working of higher silicon steels.

It is found that by this process silicon steels may be produced in which a large percentage of the constituent crystals fall into approximately parallel alignment. This 'preferred orientation' of the grains is with a [001] direction in the direction of rolling and with [110] perpendicular to it in the plane of the sheet. This gives a [111] crystallographic axis in the plane of the sheet at an angle of arc tan $\sqrt{2}$ with the rolling direction. Thus, referring back to Fig. 3.4, the high permeability axis of the crystals lies in the rolling direction of the sheet and the least per-

meable axis of the crystal is at 54·7° to the direction of rolling. That this preferred orientation exists has been proved by X-ray examination of the sheets, a method which is capable of giving detailed information, for example of the spread of the crystal directions about particular directions in the sheet. There is, however, a magnetic method which while it cannot give the precise information of the X-ray method may be employed quickly to determine the approximate average amount of preferred orientation in a sample, particularly where a high degree of preferred orientation exists [12].

The magnetic method referred to consists in taking a disc sample of the sheet material and by means of a suitable instrument, frequently called a torque magnetometer, in measuring the torque required to rotate the specimen in a steady magnetic field which is strong enough to saturate the material. The disc is rotated about an axis normal to the plane of the disc and to the direction of the field in the same manner as that described in Chapter 3 for single crystal discs. A torque curve thus obtained for a typical sample of cold-rolled silicon steel is shown in Fig. 5.14. This curve may be compared with that given in Fig. 3.11 for a disc cut from a (110) plane of a silicon-iron single crystal and it will be seen that the curves, though differing in amplitude, are almost identical in form. If the preferred orientation in the polycrystalline sample is of the kind mentioned in the preceding paragraph this similarity in form is, indeed, what would be expected. If all the grains were perfectly aligned, with their (110) planes in the plane of the disc and a cube-edge in the rolling direction, then knowing the anisotropy constants K_1 and K_2 appropriate to the silicon content the corresponding torque curve may be calculated by use of equation 3.15, since this should be precisely the same as that for a single crystal of the same composition. This theoretical curve is drawn in Fig. 5.14. By comparing the amplitudes of the observed and calculated curves we may deduce the

approximate percentage of the constituent crystals of the disc which exhibit the preferred orientation. For the example in the figure this amounts to about 62 per cent, the remaining crystals being supposed to be, on the average, randomly arranged. It is of some interest to note that torque curves may also be observed in samples of the ordinary hot-rolled steels, but these curves are of relatively

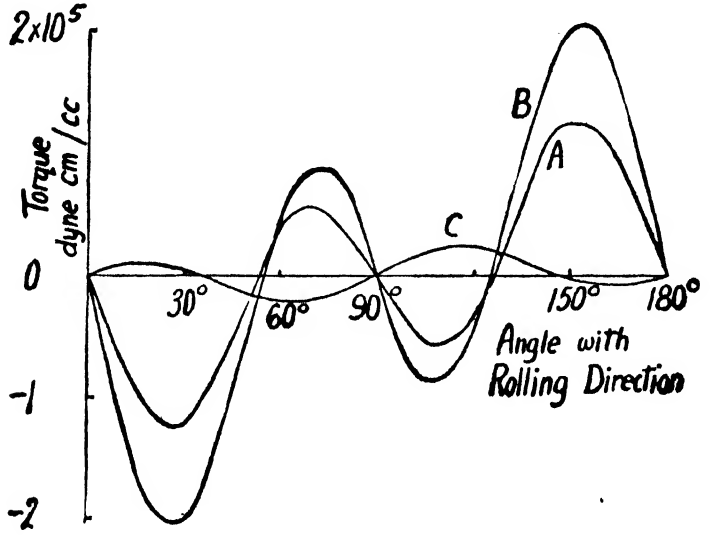

FIG. 5.14.—Torque Curves for Polycrystalline Sheet Steel
A—Observed for a Sample of 3% Silicon Cold-Rolled Steel
B—Theoretical Curve for 100% Preferred Orientation, assuming $K_1 = 3{\cdot}5 \times 10^5$ and $K_2 = 1{\cdot}75 \times 10^5$ ergs/cc.
C—Observed for a Sample of 4% Silicon Hot-Rolled Steel

small amplitude and different in form from those for the cold-rolled materials. A typical curve for a sample of hot-rolled transformer steel is shown in the figure, and it is clear from this that even in the hot-rolled steels the grains are not disposed entirely at random.

Since the single crystals of silicon-iron are magnetically anisotropic and these cold-rolled silicon steels have such marked preferred orientation of the kind already described

the steels have, as may be expected, highly directional magnetic properties. The magnetization curves for a sample of cold-rolled steel with 3 per cent silicon and a preferred orientation of about 60 per cent for three directions in the sheet, that is, in the rolling direction, perpendicular to it and at an angle of 54·7°, are shown in Fig. 5.15. The similarity between this set of curves and

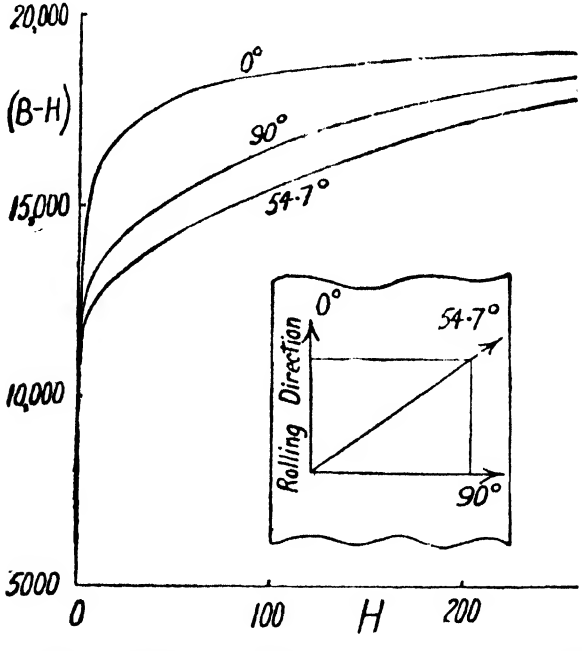

FIG. 5.15.—Magnetization Curves for 3% Silicon Cold-Rolled Steel showing Directional Properties

those in Fig. 3.4 for a single crystal will be noted, and we should expect the resemblance to become closer the higher the degree and perfection of the preferred orientation became.

Measurements of the static hysteresis loss for different directions in the sheet for this same material [8] are shown in Fig. 5.16, which shows that the direction of rolling of the sheet, which is also the direction of highest permea-

bility, is the direction of lowest hysteresis. It was inferred from these results on the polycrystalline material that the [100] direction of the single crystal would be the direction of lowest hysteresis loss and this has since been confirmed by Wilson [17], who has deduced the hysteresis loss from measurements made by a thermal method, over a range of frequencies, on a 2·1 per cent silicon-iron single crystals. The similarity between these two sets of curves, shown in Fig. 5.16, for the polycrystalline material and for the

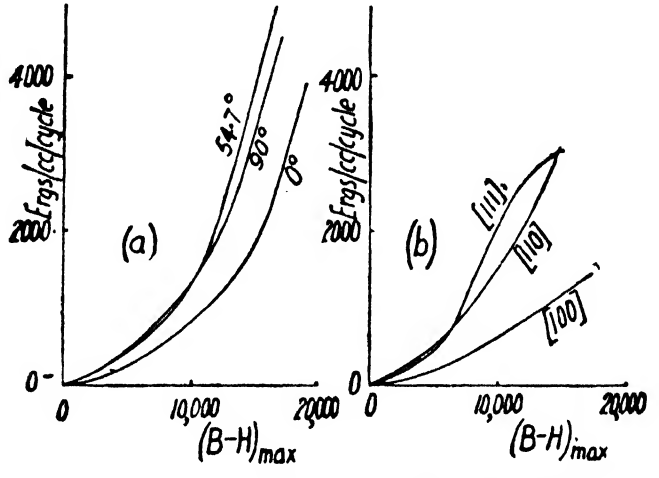

FIG. 5.16.—Comparison of Alternating Hysteresis Loss and Directional Properties of (*a*) 3% Silicon Cold-Rolled Steel Polycrystalline Sheet (Brailsford), (*b*) 2·1% Silicon-Iron Single Crystal (Wilson)

single crystal is noteworthy. The polar diagram, Fig. 5.17, shows clearly the variation of hysteresis loss with direction in the sheet for a typical cold-rolled steel. The corresponding values for a 3·7 per cent silicon transformer steel are shown for comparison and in this material the directional effect, as will be seen, is not nearly so marked.

Fig. 5.18(*a*) shows the observed longitudinal magnetostriction for three directions in the sheet for a sample of cold-rolled 3 per cent silicon steel [15]. At (*b*) is shown, for the rolling direction, the relation between the magneto-

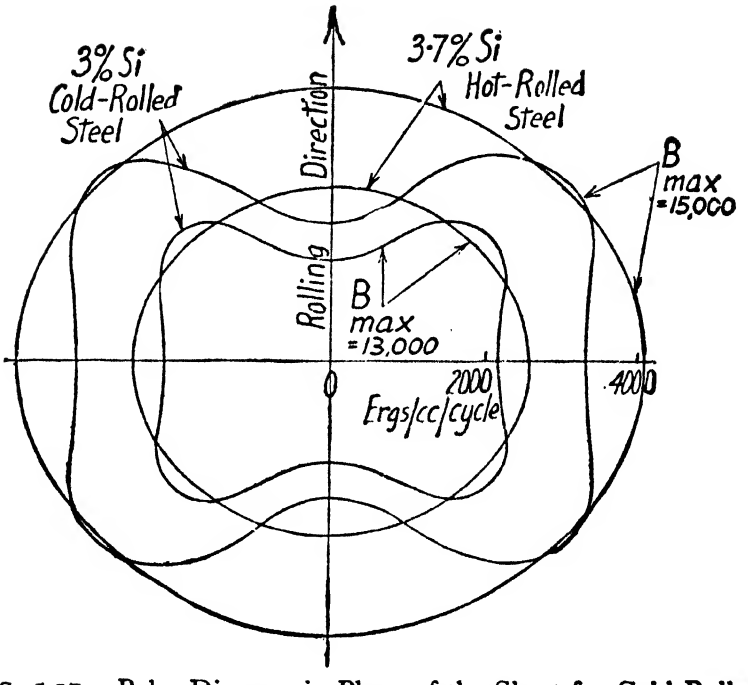

FIG. 5.17.—Polar Diagram in Plane of the Sheet for Cold-Rolled and Hot-Rolled Silicon Steels showing how Alternating Hysteresis Loss varies with Direction

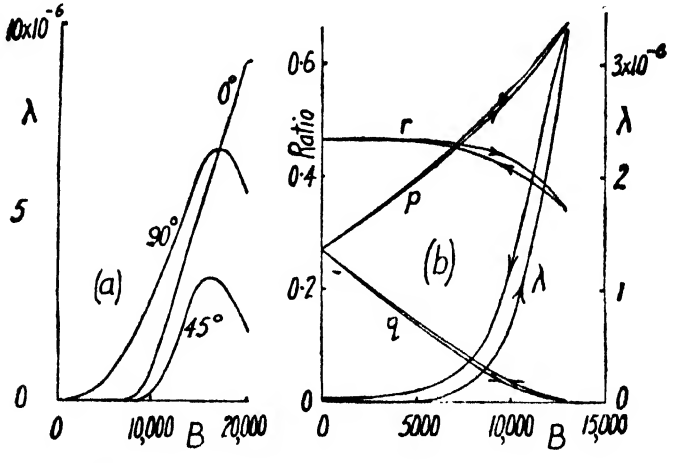

Fig. 5.18.—Magnetostriction of Cold-Rolled 3% Silicon Steel Sheet. (*a*) Directional Variation with Angle relative to Rolling Direction, (*b*) Magnetostriction Loop for Rolling Direction and Curves giving an Estimate of the Domain Distribution

striction and the induction corresponding to one side of a hysteresis loop. The shape of this loop and the direction of traversal are seen to differ from those for the typical hot-rolled material already shown in Fig. 5.13. It will be seen that both for the initial magnetization curve and for the hysteresis loop, corresponding to the rolling direction, there is at first no change in length as the induction increases from zero. If we suppose that a spontaneously saturated domain for this material has its saturation magnetostriction in the cube-edge crystallographic direction, as in the case of iron, and remember the preferred orientation of the crystals in this material, then it would appear that the magnetization in the rolling direction increases at first entirely by 180° reversals of the domain magnetization vectors. For in this case an increase in the observed magnetization may occur without any change in length of the domains along the axis of the applied field. Then as the magnetization is further increased and extension of the material occurs we may infer that 90° turns of the domain vectors are occurring. Thus it appears that, for a single crystal, and also, perhaps, for materials like the cold-rolled silicon steels having a high degree of preferred orientation, some information of the internal process of magnetization and of the distribution of the domain vectors might be obtained by a careful analysis of the magnetostriction curves. Some, perhaps rather qualitative, attempts in this direction have already been made, and the curves labelled *p*, *q*, and *r* in Fig. 5.18(*b*), and applying to the hysteresis loop in the figure, give the estimated fractions of the material in which the domain vectors are directed along the rolling direction, in the reverse direction and at 90° to the rolling direction, respectively. The curves indicate that over a range of induction $B = \pm 4{,}000$ gauss, approximately, the induction changes, on the average, by 180° reversals and that later a contribution is made by the laterally directed domains turning into the field direction. Clearly, when $B = 0$, *r* would be equal

$\frac{2}{3}$ if the domain vectors were then randomly distributed. The curves, however, indicate that, in fact, r is substantially less than this, which means that, in addition to a preferred orientation of the constituent crystals, there may also be a preferred orientation of domains. Such a departure from random conditions initially might be due to the method of

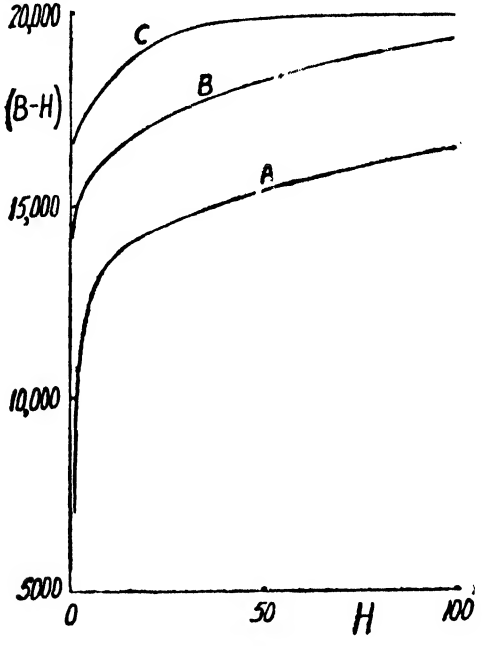

FIG. 5.19.—Comparison of Magnetization Curves

A—Average 4% Silicon Hot-Rolled Transformer Steel
B—Good 2·4% Silicon Cold-Rolled Steel in the Direction of Rolling
C—Williams's 3·85% Silicon-Iron Single Crystal for the [100] Direction

demagnetization, or to the prior magnetic history of the sample, or again to the presence of some directional residual strains in the material.

The development of silicon steels with a high degree of parallel alignment of the constituent crystals represents one method of improving these materials, at least for those applications where full use can be made, as in transformers,

of their high-permeability low-loss direction. It is not known why the particular method of rolling, combined with the subsequent annealing, leads to the type of preferred orientation which is obtained and which, luckily, aligns the cube-edge directions of the crystals along the rolling direction. It may be noted that, after the cold reduction, the arrangement of the crystals is generally quite different from that which is obtained after the final anneal, with its accompanying complete recrystallization of the metal. Before annealing this arrangement is not of a useful kind. That this is the case is readily shown by taking torque curves. It appears that further improvement of these materials may occur by increasing the degree and perfection of the preferred orientation, the limit, of course, being reached when all the constituent crystals come into parallel alignment. Fig. 5.19 shows the magnetization curve of a good sample of 2·4 per cent silicon cold-rolled steel, which may be compared with the curve for an average sample of 4 per cent silicon hot-rolled transformer steel. The magnetization curve of Williams's 3·85 per cent silicon-iron single crystal for [100] is also shown. Although these samples are not all of the same silicon content, they do serve to give some guide to the improvement in the shape of the magnetization curve which has been achieved by the cold-rolling process, and indicate the extent of the further improvement which is theoretically possible.

REFERENCES

1. H. E. Cleaves and J. M. Hiegel, *Journ. Res. Nat. Bur. Stds.*, 1942, **28**, 643.
2. A. Kussmann and B. Scharnow, *Zeits. f. Phys.*, 1929, **54**, 1.
3. A. Kussmann, B. Scharnow, and W. S. Messkin, *Stahl u. Eisen*, 1930, **50**, 1194.
4. M. Fallot, *Comptes Rendus*, 1934, **199**, 128.
5. W. F. Barrett, W. Brown, and R. A. Hadfield, *Sci. Trans. Roy. Dublin Soc.*, 1900, **7**, (2), 67 : *Journ. I.E.E.*, 1902, **31**, 674.

6. T. D. Yensen, *Journ. Iron Steel Inst.*, 1929, **120**, 187.
7. L. P. Tarasov, *Phys. Rev.*, 1939, **56**, 1231.
8. F. Brailsford, *Journ. I.E.E.*, 1939, **84**, 399.
9. T. D. Yensen, *Trans. Amer. I.E.E.*, 1915, **34**, 2601 ; *Trans. Amer. Inst. Min. Eng.*, 1915, **53**, 274.
10. N. B. Pilling, *Trans. Amer. Min. Met. Eng.*, 1923, **69**, 780.
11. A. Schulze, *Zeits. f. Phys.*, 1928, **50**, 448.
12. F. Brailsford, *Journ. I.E.E.*, 1938, **83**, 566.
13. C. Dannatt, *Journ. I.E.E.*, 1936, **79**, 667.
14. L. G. A. Sims and D. L. Clay, *Wireless Eng.*, 1935, **12**, 238 and 312.
15. F. Brailsford and R. G. Martindale, *Journ. I.E.E.*, 1942, **89**, Part 1, 225.
16. N. P. Goss, *Trans. Amer. Soc. Metals*, 1935, **23**, 511 ; Brit. Pat. 442,211.
17. A. J. C. Wilson, *Proc. Phys. Soc.*, 1946, **58**, 21.

CHAPTER 6

NICKEL-IRON AND OTHER ALLOYS

6.1. HISTORY AND APPLICATIONS

THE improvement in the magnetic properties of iron which is obtainable by the addition of silicon has already been described and, as previously stated, was first discovered by Barrett, Brown, and Hadfield [1] in the course of their comprehensive investigations into the magnetic and electrical properties of a wide variety of binary and ternary alloys. It is worth noting that these investigators also examined a number of nickel-iron alloys and observed some of the special features of these materials. In particular it was found that an annealed nickel-iron sample with 31·4 per cent nickel had a higher permeability at low magnetizing fields than the best iron.

Later investigations were carried out by Yensen [2], who examined the complete range of nickel-iron compositions in an effort to find an alloy with a saturation value higher than that of iron, and by Arnold and Elmen [3]. The latter found that with 75 to 80 per cent nickel exceptionally high initial and maximum permeabilities were obtainable and also that the magnetic properties were very sensitive to variations, not only in the composition, but also in the heat-treatment of the alloys. Subsequent developments were aimed at improving the materials in the latter respect in order to facilitate control of the processes of manufacture. These developments took the form of adding a third element which also had the desirable effect of increasing the electrical resistivity. The alloys soon became known by their various trade names, Mumetal, Permalloy, and Megaperm, and subsequently a number of other alloys in the nickel-iron range were produced with other names and with various applications in view.

The principal initial usefulness of the alloys was for the inductive loading of submarine telegraph cables. In this application a ductile magnetic material is required having high permeability in weak fields with low hysteresis and high electrical resistivity, requirements which may readily be met on a commercial scale with these materials. It should be noted, on the other hand, that to produce magnetic properties in iron approaching those of the high permeability nickel-iron alloys requires extreme care in the elimination of impurities and in heat-treatment which can, for the most part, only be given under laboratory conditions. Other applications of the alloys are for the cores of precision instrument transformers and of transformers and reactors operating at audio frequencies, for magnetic screens used to protect cathode ray tubes, galvanometers, or other apparatus from stray magnetic fields, and for special applications in communication engineering and sound reproduction.

6.2. THE EQUILIBRIUM DIAGRAM OF THE NICKEL-IRON SYSTEM

The equilibrium diagram, showing also the Curie temperatures, for the nickel-iron system is given in Fig. 6.1. At the iron-rich end, except at high temperatures, the alloys are single phase with a body-centred cubic lattice. At the nickel-rich end they are again single phase with a face-centred cubic lattice. There is, however, also a two-phase region in which both the α body-centred phase and the γ face-centred phase exist together. The phase boundaries, according to Hoselitz and Sucksmith [4], are as shown. It appears to be practically impossible, as the investigators just mentioned have pointed out, to complete this phase diagram for temperatures below about 365° C. because of the extreme length of time then taken for diffusion in the alloys to take place and thus for equilibrium conditions to be reached. The curve for the magnetic

change points is noteworthy, and it will be seen that for alloys with about 27 per cent nickel the Curie point is below room temperature, that is to say these alloys may

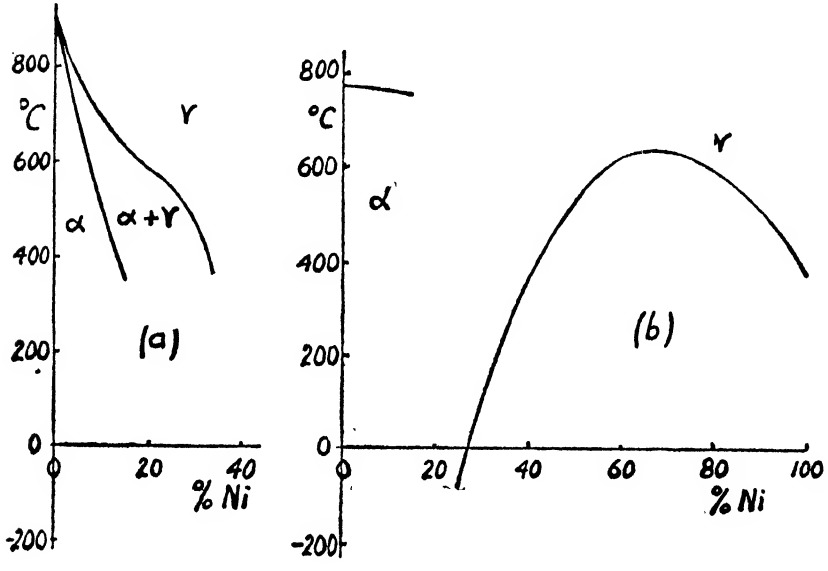

FIG. 6.1.—(*a*) Equilibrium Diagram (Hoselitz and Sucksmith)
(*b*) Curie Temperatures of Nickel-Iron System

be non-ferromagnetic at room temperature, although made up of two elements which, separately, are highly ferromagnetic.

6.3. SATURATION VALUE OF NICKEL-IRON ALLOYS

The effect on the magnetic saturation value of adding various elements as alloying constituents to nickel has been experimentally determined [5] and Stoner [6], to whose original work the reader is referred, has shown that there is an interesting correlation between observation and theory for a number of the alloys. The average distribution of the orbital electrons for nickel in the metallic state has already been discussed in Chapter 2, and by reference to Table 2.2 it will be seen that, on the average, there are

approximately 0·6 uncompensated electron spins per nickel atom, that is, the saturation value of pure nickel amounts to 0·6 Bohr magnetons per atom. This results from the fact that the $3d$ sub-shell of the atom, which would require 10 electrons to fill it, is incomplete, having 5 electrons with a positive spin and an average of 4·4 with a negative spin. There is therefore in this sub-shell a vacancy or hole corresponding to 0·6 electron. This deficiency is the cause of the magnetic moment of the atom, for if the hole were filled the magnetic moment would be reduced to zero. The observed reduction in saturation value of nickel with foreign elements added is in fact accounted for by the partial filling up of the $3d$ sub-shell.

Consider, for example, the addition of copper to nickel. Copper is next to nickel in the periodic table, having one more electron per atom. Each copper atom slips into the crystal lattice in place of a nickel atom and adds one additional electron to the common stock. If there are a total of t atoms including c copper atoms there will be $0{\cdot}6t$ vacant places in the $3d$ sub-shell with an additional c electrons to fill them. If these electrons pass into the $3d$ sub-shell then, clearly, the number of uncompensated electron spins per atom of the alloy, that is the saturation value in Bohr magnetons per atom, b, is given by

$$b = \frac{0{\cdot}6t - c}{t}$$

or

$$b = 0{\cdot}6 - \frac{p}{100}$$

where p is the atomic percentage of the alloying element. This expression gives the straight line shown in Fig. 6.2, which is seen to be in excellent agreement with the experimentally observed values.

Zinc, which follows copper in the periodic table, when added to nickel, contributes two extra electrons per added atom, and should be twice as effective as copper in reducing the saturation value of the alloy. The relation between

the saturation value b and the atomic percentage p of the added zinc becomes

$$b = 0{\cdot}6 - \frac{2p}{100}$$

Referring to Fig. 6.2, theory and experiment are again seen to be in quite good agreement.

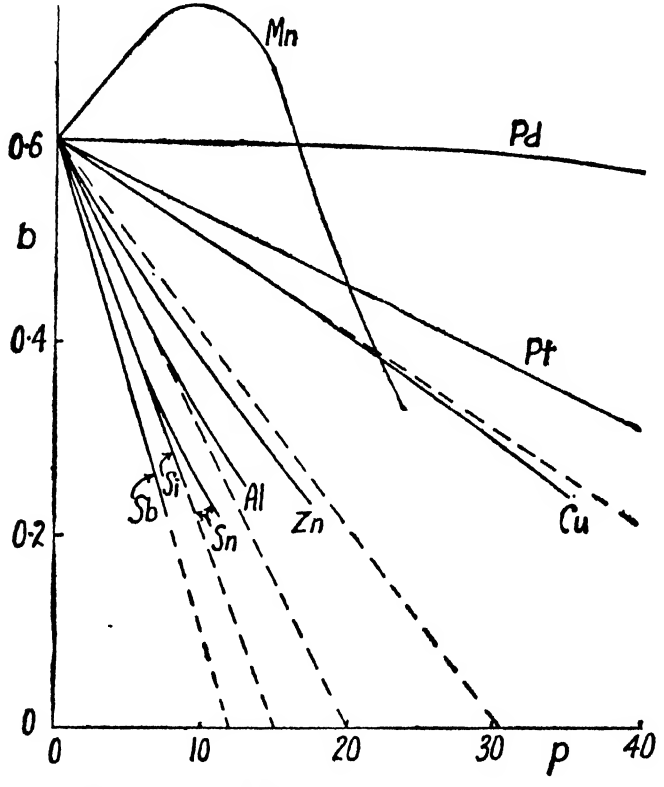

FIG. 6.2.—Effect of Alloying Constituents on the Saturation Value of Nickel. Full lines are observed values (Marian, Sadron) and broken Lines are theoretical (Stoner) : b is the Saturation Value in Bohr Magnetons per Atom and p the Atomic Percentage of the Added Element

Aluminium and silicon have, respectively, 3 and 4 electrons in their incompleted third shells. If, on adding either of these elements to nickel, these electrons become

available for the same purpose as in the case of copper and zinc, then we have for aluminium

$$b = 0{\cdot}6 - \frac{3p}{100}$$

and for silicon

$$b = 0{\cdot}6 - \frac{4p}{100}$$

Tin also has four electrons in its incomplete (fifth) shell and gives the same formula as silicon. Here again theory

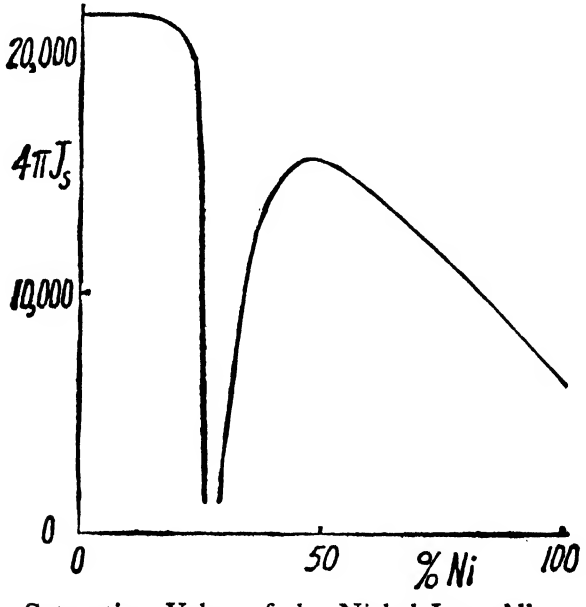

FIG. 6.3.—Saturation Value of the Nickel-Iron Alloys (Yensen)

and experiment agree, as indeed they do also for antimony, with five available electrons, and the formula

$$b = 0{\cdot}6 - \frac{5p}{100}$$

Platinum, however, which might be expected to behave as if it had two available electrons per atom, behaves anomalously as though the number was $\frac{3}{4}$. Palladium has only a minor effect on the saturation value and this would be consistent with this element having no free conductivity electrons.

In general, then, non-ferromagnetic alloying additions to nickel reduce the saturation value, but manganese is an exception. It will be seen from the figure that a substantial increase in saturation value occurs with up to about 8 per cent manganese.

Fig. 6.3 shows the saturation values for the complete range of the nickel-iron alloys. As already mentioned in Section 6.2 the alloys with about 27 per cent nickel are non-ferromagnetic at room temperature, and there is also an optimum saturation value with about 50 per cent nickel.

6.4. ELECTRICAL RESISTIVITY AND OTHER PROPERTIES OF THE NICKEL-IRON ALLOYS

Fig. 6.4 shows the electrical resistivity ρ of the complete range of nickel-iron alloys. The high resistivity of the alloys with about 30 to 35 per cent nickel will be noted.

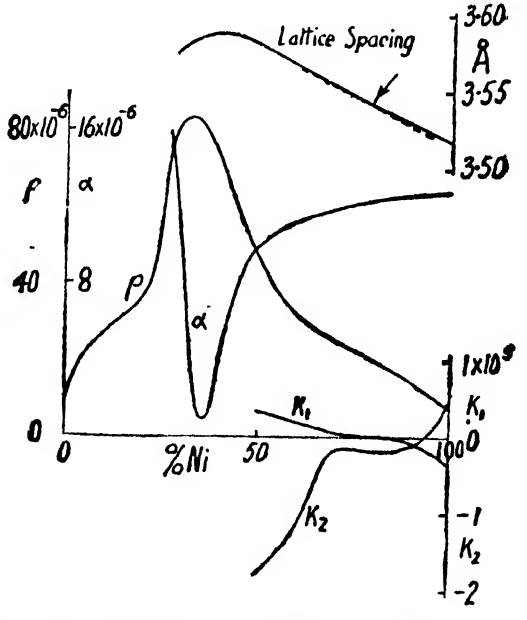

FIG. 6.4.—Electrical Resistivity ρ, Magnetic Anisotropy Constants K_1 and K_2, Linear Coefficient of Expansion α and Lattice Spacing of Nickel-Iron Alloys

The anisotropy constants K_1 and K_2, also shown in the figure, are seen to be small in value in the high permeability region already referred to in Section 6.1 and which will be discussed further in the next section. In this region, too, Bradley, Jay, and Taylor [7] have observed a slight discontinuity in the curve relating the lattice spacing and the percentage of nickel, as shown in the figure.

As a matter of interest a curve for the temperature coefficient of expansion α of the alloys corresponding to room temperature is also included. An alloy with 36 per cent nickel (Invar) is seen to have a very low coefficient and has practical applications on that account.

6.5. MAGNETOSTRICTION AND PERMEABILITY OF NICKEL-IRON ALLOYS

The longitudinal magnetostriction for a series of nickel-iron alloys, according to Masiyama [8], is shown in Fig. 6.5. It will be observed from the curves that the magnetostriction changes from positive to negative as the nickel content increases beyond about 82 per cent.

The nickel-iron alloys became of great commercial importance as magnetic materials following the discovery by Arnold and Elmen [3] that, by suitable heat-treatment, alloys in a limited range of composition could be produced with exceptionally high initial and maximum permeabilities. It was found that to obtain the best magnetic properties rapid cooling was necessary, this treatment being effective over the range of nickel contents from about 50 to 90 per cent. The greatest effect and highest permeability were obtained for a composition having 78·5 per cent nickel. These high permeability alloys were given the general name 'Permalloys'. Fig. 6.6 gives some of Elmen's results. Curve (*a*) shows the initial permeability of the alloys which had been annealed between 900 and 1,000° C. for 1 hour and then slow cooled (in 10 hours) to room temperature. Curve (*b*) shows the improvement

resulting from reheating the annealed alloys to 600° C. and 'air-quenching' by cooling the samples on a cold copper plate in air, the rate of cooling being about 20° C. per second. Similar curves showing maximum permeability are given in Fig. 4.19, which also indicate how the permeability can further be raised by cooling in a magnetic field.

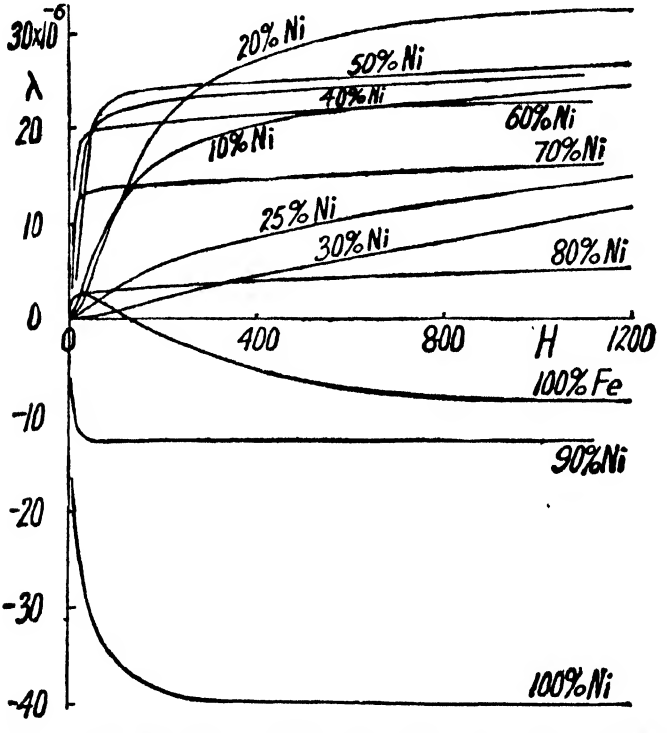

FIG. 6.5.—Longitudinal Magnetostriction of the Nickel-Iron Alloys (Masiyama)

The reasons why high permeabilities are obtainable in the Permalloy region have been the subject of much discussion. McKeehan [9] linked the high permeability with the disappearance of magnetostriction in this region of composition. The relation between initial permeability and magnetostriction has been discussed fully in Chapter 3, and equation 3.5 gives a relation between initial permea-

bility, saturation magnetization, saturation magnetostriction, and Young's Modulus. The curve relating the saturation magnetostriction with composition is given in Fig. 6.6 and this, as already stated, indicates that magnetostriction is zero at about 82 per cent nickel, while at 78·5 per cent nickel the magnetostriction has a fairly sub-

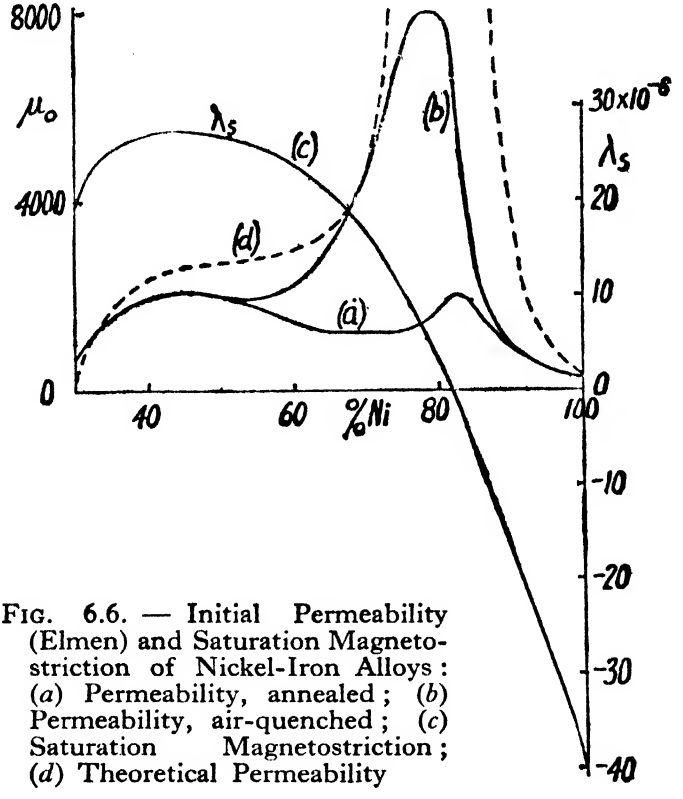

FIG. 6.6. — Initial Permeability (Elmen) and Saturation Magnetostriction of Nickel-Iron Alloys: (*a*) Permeability, annealed; (*b*) Permeability, air-quenched; (*c*) Saturation Magnetostriction; (*d*) Theoretical Permeability

stantial value. It is therefore not clear why the best magnetic properties are obtained at the lower composition, although it has been suggested, among other things, that the small internal strains set up by the magnetostriction may be balanced in some way against the internal strains from other causes, when the right rate of cooling is used, to give a minimum of strain at this composition. How-

ever, it is of interest to calculate from equation 3.5, using the saturation values of magnetization and magnetostriction in Figs. 6.3 and 6.6, the theoretical initial permeability. This equation, it will be remembered, was based on the assumption that the only internal strains present are those occurring as a result of the magnetostrictive strains set up on cooling the metal from above the Curie point. The result of this calculation, assuming a Young's Modulus throughout of 20×10^{11} dynes per sq. cm., is shown by the broken line in Fig. 6.6. It will be seen that there is a striking similarity between the theoretical curve and that for alloys which have been air-quenched.

Further confirmation of the close connexion between low magnetostriction and high permeability has been provided by von Auwers and Neumann [10], who investigated the iron-nickel-copper ternary alloys. Fig. 6.7 shows the initial permeability of these alloys, the contours being lines of constant initial permeability. These results are for alloys air-quenched from 625° C. after annealing for 1 hour at 900° C. The broken line indicates the compositions of the alloys with zero magnetostriction, and it will be observed that the ridge of high permeability in the diagram follows this line fairly closely. It was found that when the alloys were annealed at 1,100° C. and slowly cooled, the line of zero magnetostriction was unchanged, but the ridge of optimum permeability moved downwards to the right but still, however, along the zero magnetostriction line.

The explanations given of the behaviour of these alloys are not entirely satisfactory, and an alternative idea that the high permeability might be associated with the formation of a crystallographic superlattice in the alloys has been investigated. A composition having 76 per cent of nickel by weight, which is near the observed 78·5 per cent for Permalloy, corresponds to 75 per cent of nickel as an atomic percentage, i.e. to the composition Ni_3Fe. In this case with a superlattice, or ordered arrangement of atoms, the alloy, which is of face-centred cubic structure, would

have iron atoms at the cube corners and nickel at the centres of the cube faces. Leech and Sykes [11] have shown that a superlattice is produced in this alloy when

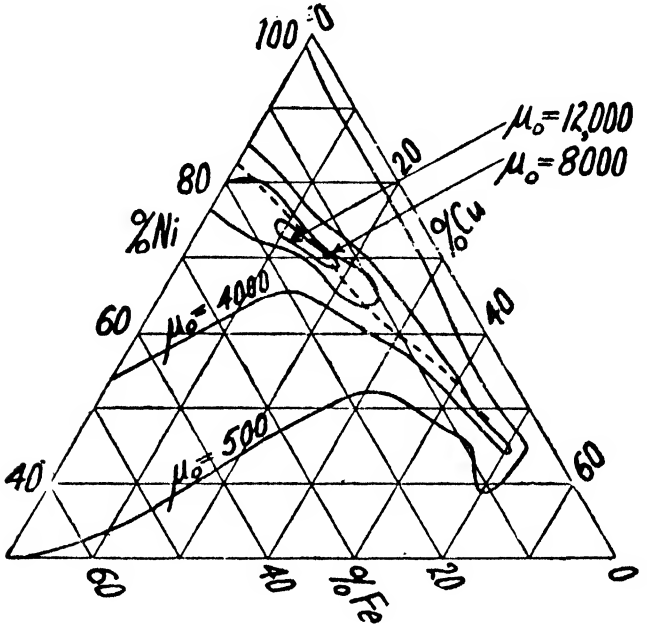

FIG. 6.7.—Contours showing the initial Permeability of Iron-Nickel-Copper Alloys after Air-Quenching. The broken line shows the Compositions of the Alloys having zero Magnetostriction (Von Auwers and Neumann)

slowly cooled, but this heat-treatment is not that which produces high permeability. On the other hand, the rapid cooling necessary to develop the best magnetic properties does not result in any great ordering of the atoms.

6.6. MATERIALS WITH CONSTANT PERMEABILITY

It was shown by Elmen [12] that alloys containing nickel, cobalt, and iron could be produced having almost constant permeability for an applied field from zero up to about 2 gauss. Such an alloy has possible applications for the magnetic cores of inductances which are required to main-

tain a constant inductance value independently of variations of the magnetizing current. The most noteworthy alloy, containing about 30 per cent iron, 45 per cent nickel, and 25 per cent cobalt has been given the name Perminvar. This, after suitable heat-treatment, has the curious characteristics shown in Fig. 6.8. It will be seen that for low

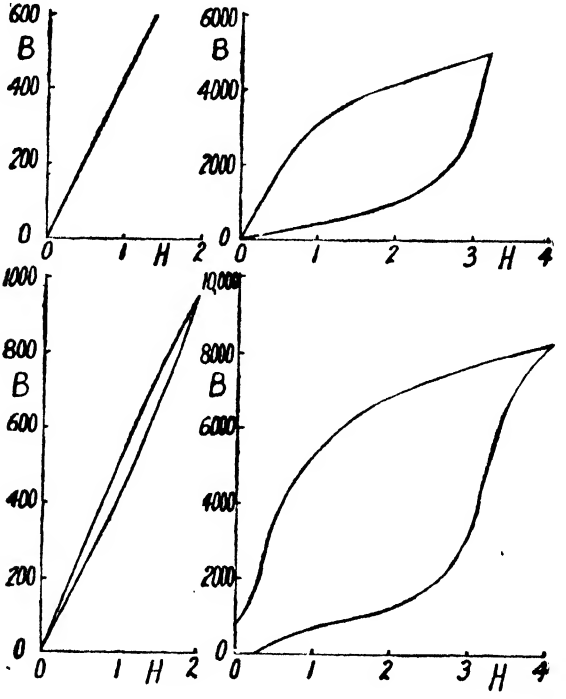

FIG. 6.8.—Hysteresis Loops of Perminvar for different Amplitudes of the applied Field (Elmen)

inductions the hysteresis effect is very small, and even for a flux variation up to B = 5,000 gauss the loop still has zero remanence and therefore zero coercive force also. When the magnetization is pushed still higher, however, some remanence and coercive force reappear in the loops. The explanation of this behaviour seems to be that magnetization first occurs, in this case, by a swing of the domain vectors from the lateral into the field direction, the residual strains being such as to pull the domain vec-

tors back into the lateral position on removal of the field, thus leaving no remanent induction.

Other materials, called Isoperms, have been developed in Germany having somewhat similar characteristics. In one class of the Isoperms, having an approximate composition of 40 to 45 per cent nickel, 45 to 50 per cent iron, and 5 to 15 per cent copper, the material, after being severely cold-worked, is quenched from a high temperature, and this is followed by further cold-rolling and a final heat-treatment. This treatment produces precipitation of the copper atoms from the solid solution probably along the slip planes in the material which are present because of the cold-working, and this in turn is believed to give preferred orientations to the domain vectors in the finished sheet. With such preferred orientations determined by the internal strains, a plausible explanation of the absence of remanence can be given as in the preceding paragraph. These materials are said to have a constant permeability of the order of 50 for applied field strengths up to about 100 gauss.

Materials of constant permeability may also be made up, employing the magnetic material in the form of small insulated particles bonded together under pressure with a suitable binder. The constancy of permeability is then the result of the magnetic path being partly through the magnetic particles and partly through the non-magnetic insulation between them. According to Kersten [14] the permeability of such a magnetic core, if the individual particles are of high permeability and the permeability of the insulation is unity, is given simply by $\mu = \frac{3}{a}$ where a is the fraction of the volume of the core material occupied by insulation. If, for example, a is made as low as 2 per cent, this would give μ a maximum value of 150. Since the fine subdivision of the material confines the eddy currents set up in an alternating field to within the particles, the iron losses from this cause are greatly reduced, and the material becomes suitable for use at high frequencies.

Typical applications of these dust or powder cores are in telephone loading coils and in tuning coils at radio frequencies. Iron powder with a particle size of 1 to 40 microns may be made by blowing iron oxide through a hydrogen furnace, and a permeability up to 50 is obtainable for the cores [15]. Alternatively, Permalloy may be powdered mechanically and used in place of iron, giving permeabilities up to about 125. In Germany a chemical process of producing relatively pure iron in the form of fine particles has been perfected. This involves heating liquid iron carbonyl, the iron being then precipitated from the vapour as fine spherical particles of varying size from 1 to 10 microns diameter. By selecting suitable grades of dust cores high efficiency inductances may be made for use at frequencies up to 40 megacycles per second or even higher with, however, permeabilities falling as low as 2. Non-metallic magnetic materials known as ferrites have also recently been developed for use at high frequencies [19], although these are not materials of constant permeability.

6.7. PROPERTIES OF COMMERCIAL MATERIALS

The trade names, compositions, and magnetic and electrical properties of a number of British, American, and German nickel-iron sheet materials are given in Table 6.1. This is intended to be a representative selection of these high permeability, low loss steels and is by no means a complete list. There is also a series of Japanese alloys known as 'Furukawa alloys', which are similarly based on nickel and iron and have much the same properties as for those given in the table. The figures given for resistivity, permeability, saturation value, and hysteresis loss are typical values, but will all vary with different samples of nominally the same material due to variations in the precise chemical compositions, the presence of impurities, and the unavoidable differences in the rolling and heat-treatments occurring during manufacture. This is particularly the case with permeability, the comparative

TABLE 6.1

Alloy	Chemical Analysis % by Weight					ρ	μ_0	$\mu_{max.}$	$(B-H)_{sat.}$	w_h
	Ni	Fe	Cu	Cr	Mo					
Permalloy A	78·5	21·5				20	12,000	90,000	11,000	50
Cr-Permalloy	78·5	17·7		3·8		65	12,000	60,000	8,000	
Mo-Permalloy	78·5	17·7			3·8	55	20,000	75,000	8,500	
Permalloy C						60	16,000	75,000	8,000	50
Mumetal	75	16	5		4	62	20,000	80,000	8,500	45
'1040'	72	11	14		3	56	40,000	100,000	6,000	
Megaperm						97	3,300	68,000	9,300	
Hipernick	50	50				46	3,000	70,000	15,500	
45 Permalloy	45	55				45	2,700	23,000	16,000	
Radio Metal	50	50				45	2,500	35,000	16,000	300
Permalloy B						45	2,000	15,000	16,000	300
* Rhometal	36	64				90	250–2,000	1,200–8,000	9,000	450
† Supermalloy [18]	79	15			5	65	50,000 –150,000	600,000 –1,200,000	7,900	< 5
4% Silicon Steel		96				55	450	8,000	19,500	400
Dynamo Sheet		→ 100				14	250	5,000	21,200	700

ρ = resistivity in microhm cm.
w_h = hysteresis loss at $B_{max.}$ = 5,000 gauss in ergs/c.c./cycle.

* Properties depend on different heat-treatments deliberately given.
† Contains 0·5% Mn. also.

values of which may vary in commercial samples by three to one or more.

Comparison of the alloys of differing compositions with each other and with the ordinary hot-rolled transformer and dynamo steels, which have been included for reference, brings out clearly the features of the nickel-iron system and the effects of a third alloying constituent, which have already been mentioned. It will be seen that

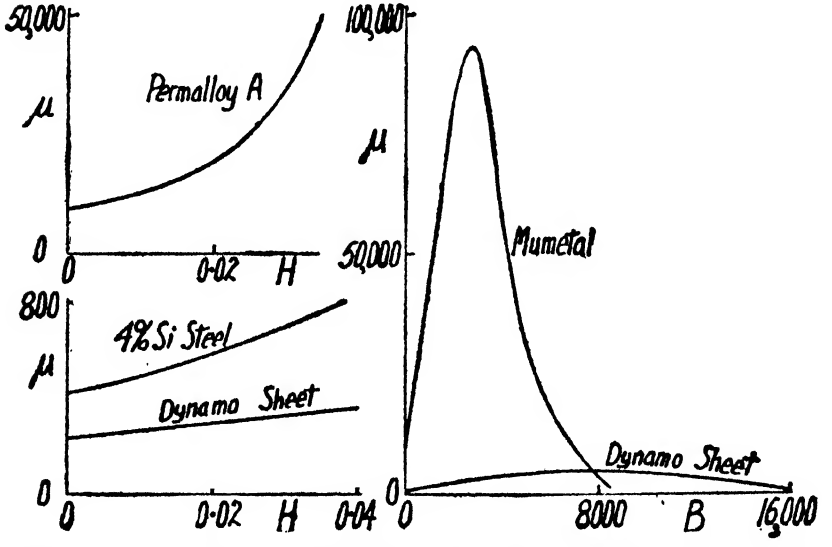

FIG. 6.9.—Curves illustrating the high Permeability at low Inductions of Permalloy A and Mumetal compared with Dynamo Sheet and 4% Silicon Steel

all the alloys, except Rhometal whose nickel content is relatively low, have very high permeability, and particularly initial permeability, when compared with the iron and silicon-iron materials, and they also have exceedingly low hysteresis loss. In all cases, however, the saturation value is much lower than for iron, the best alloys in this respect having 45 to 50 per cent nickel. The addition of a third element to the simple nickel-iron alloy with 78·5 per cent nickel, 21·5 per cent iron gives a greatly increased electrical resistivity but, on the other hand, depresses the

saturation value substantially. It will be seen that the high resistivity of Rhometal is to be expected since its composition is near that which gives the maximum value on the resistivity curve shown in Fig. 6.4.

Fig. 6.9 shows the great superiority in permeability, at low field strengths and at inductions below about 8,000 gauss, of Permalloy and Mumetal when compared with the commercial iron or silicon-iron dynamo and trans-

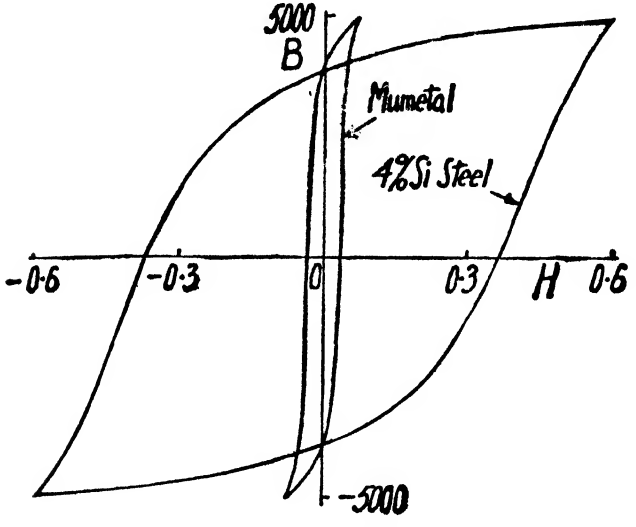

FIG. 6.10.—Typical Hysteresis Loops for Mumetal (0·015″ thickness) and 4% Silicon Transformer Sheet Steel (0·014″ thickness)

former sheet materials. Hysteresis loops for Mumetal and for a sample of 4 per cent silicon transformer steel for a maximum flux density of 5,000 gauss are also shown in Fig. 6.10, illustrating the relatively low hysteresis loss of the nickel-iron alloy. These alloys therefore have wide application in light current work, as previously mentioned, but because of their higher cost and low saturation value they do not compete with iron and silicon-iron alloys for heavy electrical plant in which the magnetic properties at low inductions are generally of little importance. The

magnetization curves for some nickel-iron sheet materials, compared with ordinary dynamo sheet and with a 2·4 per cent silicon cold-rolled transformer steel in the rolling direction, are given in Fig. 6.11. These curves, for which a logarithmic scale of H has been employed, serve further to emphasize what has already been said about the superiority of Mumetal and Permalloy at low field strengths and their relatively low saturation values.

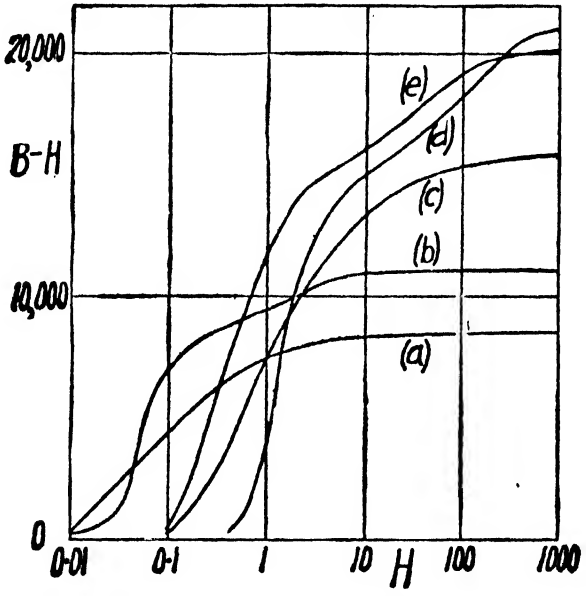

FIG. 6.11.—Magnetization Curves for Sheet Materials (0·012″ to 0·015″ thickness). (*a*) Mumetal, (*b*) Permalloy, (*c*) Radiometal, (*d*) Dynamo Sheet, (*e*) 2·4% Silicon Cold-Rolled Steel along the Rolling Direction

The directional effects obtainable in silicon steel by employing a cold-rolling process during manufacture have already been described. The method of obtaining high magnetic permeability in the direction of rolling by a controlled process of cold-rolling and annealing had, however, previously been employed on nickel-iron alloys, and the consequent magnetic anisotropy of the rolled sheets was known to be due to the resulting preferred orientation of

the constituent crystals [16]. The curves in Fig. 6.12, due to Randall [17], show that the highest permeability for the rolling direction is obtainable in the case of Mumetal when the cold-reduction of the steel amounts to about 63 per cent. The magnetic anisotropy of a sample of the steel is illustrated by the permeability curves in the figure,

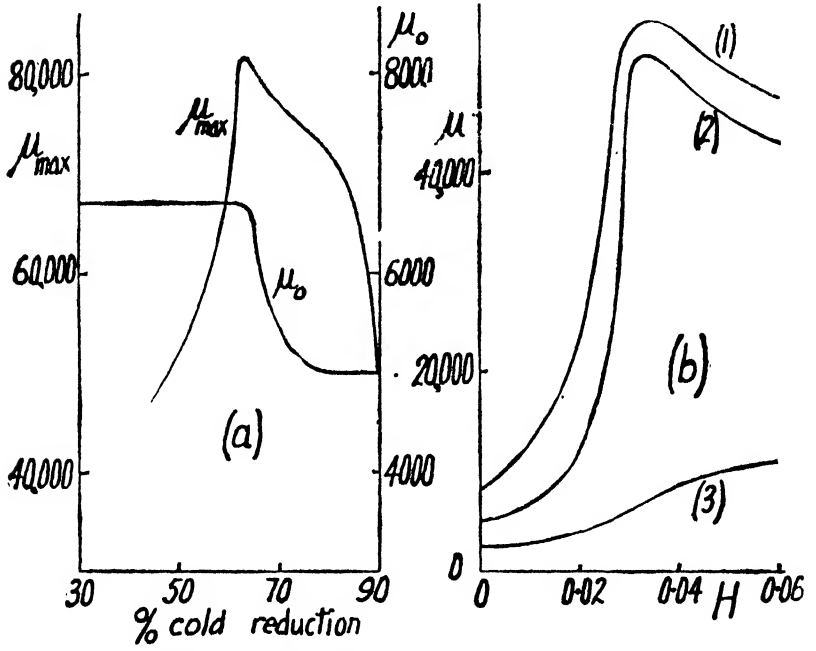

FIG. 6.12.—Magnetic Anisotropy of Mumetal Sheet (Randall). (*a*) Effect of Amount of Cold-Rolling on initial and Maximum Permeability in the Rolling Direction for the finished heat-treated Sheet. (*b*) Permeability for different Directions of the Sheet, 0·015″ thickness: (1) in the Rolling Direction, (2) at 45°, and (3) at 90° to the Rolling Direction

which indicate a maximum permeability in the rolling direction about five times greater than in the crosswise direction.

The performance of the nickel-iron alloys under conditions of alternating magnetization, in relation to that of the ordinary 4 per cent silicon hot-rolled transformer steels, is illustrated in Figs. 6.13 and 6.14 for samples of com-

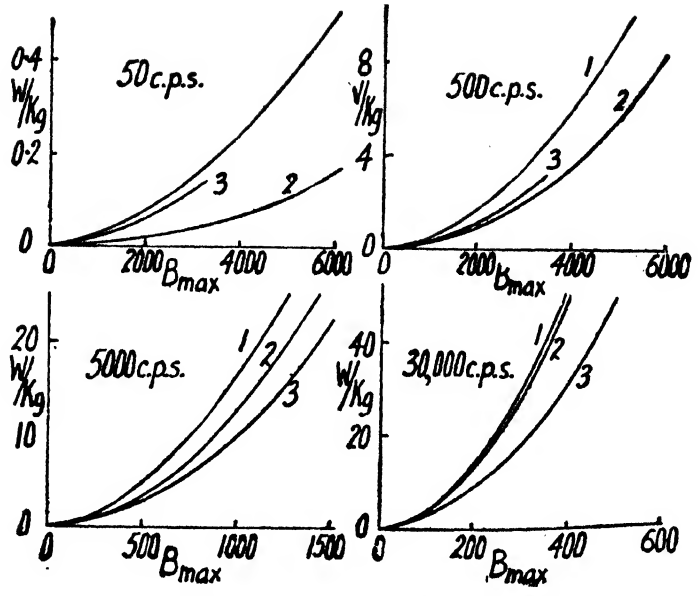

FIG. 6.13.—Iron losses at various frequencies for samples of Mumetal and Rhometal compared with 4% Silicon Steel of comparable thickness. (1) 4% Silicon Steel, 0·014″ thickness, (2) Mumetal, 0·015″ thickness, (3) Rhometal, 0·015″ thickness

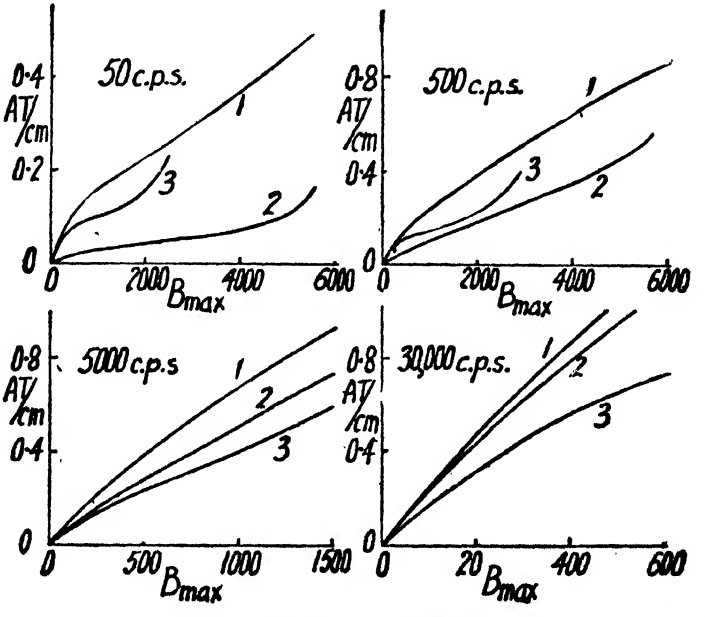

FIG. 6.14.—Total Magnetizing Current required at various frequencies for the same materials as those given in Fig. 6.13

parable thickness, at four frequencies of supply. These results relate to ring specimens and the flux thus passes through all directions of the material relative to its rolling direction without regard to the magnetic anisotropy which may exist. At low frequencies the low hysteresis loss of Mumetal gives this the lowest total loss for the three materials compared, and over the range of flux densities being considered, but the benefit of low hysteresis is largely lost at the higher frequencies, where the eddy current component of loss predominates and where a high electrical resistivity becomes desirable. Thus at the higher frequencies Rhometal, with a resistivity of about 90 microhm cm., is superior in total loss and magnetizing current to Mumetal or 4 per cent silicon steel, which have approximate resistivities of 45 and 55 microhm cm. respectively. A further important factor affecting the total iron losses at high frequencies is, of course, the thickness of the material, and the nickel-iron alloys have here an advantage over the silicon steels. The latter require a relatively high percentage of silicon to keep the resistivity high and in consequence have relatively poor mechanical properties, while the former may much more readily be rolled into very thin sheet or tape form.

The manner in which the effective or incremental permeability of silicon steel for a varying applied field is reduced when there is also an additional superimposed steady field, is shown in Fig. 5.12. This effect is even more marked in the higher permeability nickel-iron alloys as might, indeed, be expected, since these alloys may be brought near to saturation with relatively small applied fields. Fig. 6.15, due to Randall [17], shows how, in the case of Mumetal, the incremental permeability corresponding to a small applied field of 0·005 gauss, at a frequency of 50 cycles per second, varies as the steady field increases. A steady polarizing field of 0·5 gauss is sufficient to reduce this permeability by about four times. On account of this property of magnetic materials it is possible to design steel-

cored reactors whose reactance to an alternating current can be varied at will by varying a direct current in auxiliary windings on a core or pair of cores. Using this principle, the alternating current power supplied to a load can be controlled by the employment of a relatively much smaller direct current power, the arrangement acting as a kind of magnetic amplifier. The high permeability nickel-iron alloys have characteristics which make them particularly suitable for this application.

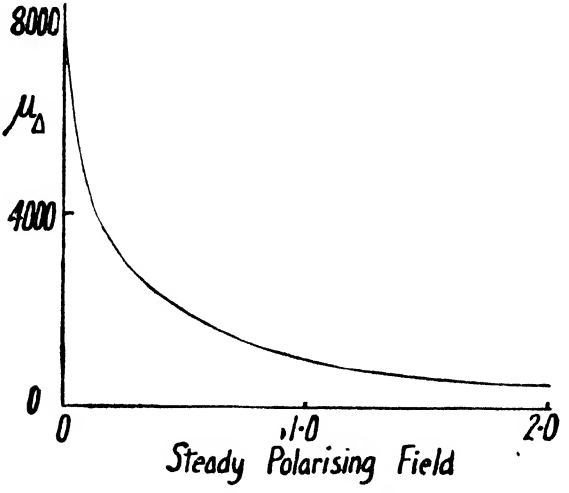

FIG. 6.15.—Incremental Permeability of Mumteal for an applied Alternating Field of 0·005 gauss at 50 c.p.s. (Randall)

The effect of remanent induction in a magnetic material is also to reduce the observed permeability, and this effect is quite marked in the high permeability nickel-iron alloys especially at low inductions. Care is therefore necessary in testing, particularly with ring specimens, to demagnetize the sample first and also to see that the material is free from tight wrappings of insulation or windings, since the strains imposed in this way can materially affect the properties.

A greatly improved alloy of the Permalloy type called Supermalloy has recently been described [18] and its properties are given in Table 6.1.

REFERENCES

1. W. F. Barrett, W. Brown, and R. A. Hadfield, *Sci. Trans. Roy. Dublin Soc.*, 1900, **7**, (2), 67 ; *Journ. I.E.E.*, 1902, **31**, 674.
2. T. D. Yensen, *Trans. Amer. I.E.E.*, 1920, **39**, 791.
3. H. D. Arnold and G. W. Elmen, *Journ. Franklin Inst.*, 1923, **195**, 621.
4. K. Hoselitz and W. Sucksmith, *Proc. Roy. Soc.*, 1943, **181**, 303.
5. C. Sadron, *Ann. d. Phys.*, 1932, **17**, 371 ; V. Marian, *Ann. d. Phys.*, 1937, **7**, 459.
6. E. C. Stoner, *Phil. Mag.*, 1933, **15**, 1018.
7. A. J. Bradley, A. H. Jay, and A. Taylor, *Phil. Mag.*, 1937, **23**, 545.
8. Y. Masiyama, *Sci. Rep. Toh. Imp. Univ.*, 1931, Series 1, **20**, 574.
9. L. W. McKeehan, *Phys. Rev.*, 1926, **28**, 158.
10. O. von Auwers and H. Neumann, *Wiss. Veroff. a.d. Siemens-Werk.*, 1935, **14**, (2), 93.
11. P. Leech and C. Sykes, *Phil. Mag.*, 1939, Series 7, **27**, 742.
12. G. W. Elmen, *Journ. Franklin Inst.*, 1928, **206**, 317 ; 1929, **207**, 582.
13. O. Dahl, J. Pfaffenberger, and H. Sprung, *Elek. Nach. Tech.*, 1933, **10**, 317.
14. M. Kersten, *Elektrotech. Zeits.*, 1937, **58**, 1335 and 1364.
15. A. Crossley, *Journ. App. Phys.*, 1943, **14**, 451.
16. W. S. Smith, H. J. Garnett, and W. F. Randall, Brit. Pat. 366,523, 1930.
17. W. F. Randall, *Journ. I.E.E.*, 1937, **80**, 647.
18. O. L. Boothby and R. M. Bozorth, *Journ. App. Phys.*, 1947, **18**, 173.
19. J. L. Snoek, *Phillips Tech. Rev.*, 1946, **8**, 353.

CHAPTER 7

PERMANENT MAGNET MATERIALS

7.1. TECHNICAL REQUIREMENTS

THE important requirements of the magnetic materials so far considered have been, in general, that they should have high permeability and low hysteresis loss. Such materials have a narrow hysteresis loop and the lowest attainable coercivity. Materials for use as permanent magnets should have, however, the opposite characteristics, namely, high coercivity with a high retentivity, in fact a hysteresis loop expanded to the greatest possible degree.

As already mentioned in Chapter 1, the characteristic upon which the quality of a permanent magnet material may be judged is the demagnetization curve, which is that portion of the hysteresis loop, obtained after taking the material to saturation, lying between the retentivity and coercivity points of the loop. The curve indicates the amount of the reverse field necessary to reduce or remove the remanent induction of the material and therefore is a criterion of its capabilities as a 'permanent' magnet.

A simple discussion of the demagnetization curve in relation to the elementary design of a magnet will serve to emphasize the more important features.

Let the demagnetization curve of a material be as shown in Fig. 7.1. This curve gives the induction B in a sample, for example a test-piece in ring form, in relation to an applied field H decreasing from a value high enough to bring the material to near saturation, and subsequently reversing in direction. Naturally, if the applied field is not taken to such a high initial value the resulting curve will lie somewhat lower than the true demagnetization curve. The simplest requirement in a practical case is that a certain total flux shall be produced in an air-gap

of a given length and cross-sectional area, using at the same time the minimum weight of magnet material.

Let it be required to produce a total flux ϕ in an air-gap whose reluctance is R, and, to do this, let l be the necessary length of the magnetic material, of uniform cross-section a. Such a magnet is shown diagrammatically in Fig. 7.1. If this magnet is magnetized to saturation, the air-gap being at first closed with some highly permeable material, such as soft iron, and the applied field is then

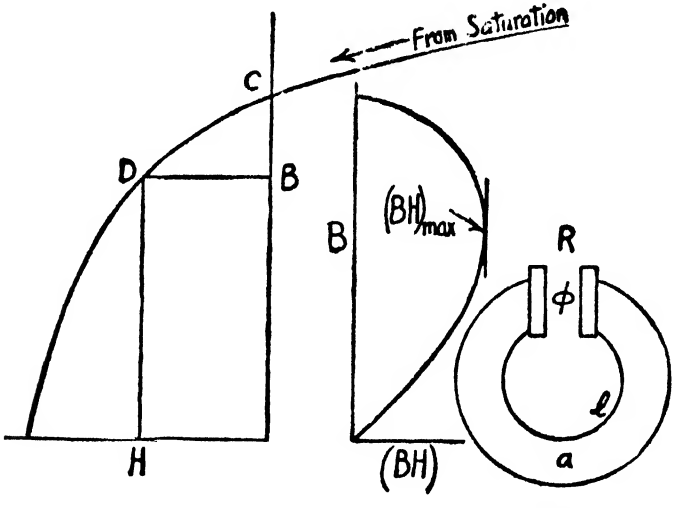

FIG. 7.1.—Calculation of a Permanent Magnet

removed, the flux density in the magnet material will have the value corresponding to point C, the retentivity. If the applied field is reversed the flux density will fall along the demagnetization curve, the abscissa of the curve indicating at any instant the magnitude of the applied reverse field. Alternatively, a reverse field will also act on the material if the permeable material in the air-gap is withdrawn. Suppose, when this is done, the flux density falls to the value B at the point D on the curve, the total flux in the air-gap being then ϕ, and H being the value of the abscissa at D. Clearly, the reverse magnetomotive force acting on

the magnet material is produced by the free poles at the air-gap and acts also across the air-gap itself.

Therefore $\text{m.m.f.} = \phi R = Hl$

whence $$l = \frac{\phi R}{H} \quad . \quad . \quad . \quad . \quad (7.1)$$

In any practical case, in addition to the useful flux ϕ in the useful air-gap of reluctance R, there will also be a distributed leakage flux, and hence a non-uniform flux density along the length of the magnet if this is, as assumed, of uniform cross-sectional area. We will, however, for present purposes, suppose that the leakage flux is all concentrated in the neighbourhood of the poles and that the flux density in the material, except near the poles, is therefore uniform.

We may define a leakage factor K as the ratio of the total flux produced by the magnet to the useful flux.

Therefore $$K = \frac{Ba}{\phi}$$

and $$a = \frac{K\phi}{B} \quad . \quad . \quad . \quad (7.2)$$

If it is decided at what point on the demagnetization curve it is proposed to work so that B and H are known, equation 7.1 at once gives the length of the magnet material required and equation 7.2 the cross-section, provided also in the latter case that a value can be assigned from experience or otherwise to the factor K.

However, it will also be clear from the two equations that the volume V of the magnet material is given by

$$V = al = \frac{KR\phi^2}{BH}$$

Hence the volume of the magnet will be a minimum when the product BH is a maximum. The form of the curve relating (BH) with B is also shown in Fig. 7.1 and the $(BH)_{max.}$ point of this curve gives the, theoretically, most economical working values of B and H for the material in question.

The $(BH)_{max.}$ value of a permanent magnet material is therefore an index of the quality of the material, but the coercivity and retentivity are also obviously important quantities. For example, a material might have a high $(BH)_{max.}$ value but a low retentivity. Clearly, in that case, the working B would be low and H high, and from equations 7.1 and 7.2 it will be clear that the active portion of the magnet would be short and of large cross-section. Alternatively, if the coercivity is low a long thin magnet would be the result. Thus the choice of a given material must depend also on space considerations and the shape of magnet required. For a fuller discussion of the design of permanent magnets the reader is referred to the literature [1], where information on the design of magnets subjected to a pulsating flux as well as the simpler case of constant conditions will be found.

7.2. MARTENSITIC STEELS

The general relation between magnetic properties and internal strains has already been discussed; to obtain high permeability and low magnetic hysteresis the internal strains should be as small as ever possible. For a permanent magnet material where the largest possible hysteresis loop is desired, clearly the opposite must hold and the atomic lattice must be put into the highest possible state of strain. It is known that the strains introduced by cold-working will increase the hysteresis and the coercivity to a certain degree, but in general such strains are quite insufficient to produce an effect of the magnitude desired in a permanent magnet material. For this the severest lattice distortion throughout the whole of the constituent crystals of the metal becomes necessary, and this can only be obtained by introducing strain centres on an atomic scale.

The earlier permanent magnets were of steel in which the high internal strains, accompanied by a high degree of mechanical and magnetic hardness, depended upon the

presence of carbon and the formation of a martensitic structure resulting from quenching of the metal from a high temperature in oil or water.

Prior to about 1910 permanent magnets were made from a simple carbon steel with carbon up to about 1·5 per cent, this being used in a glass-hard condition. The changes in, for example, a 1·2 per cent carbon steel, if it were slowly cooled from a temperature of, say, 1,000° C., may be followed by reference to the iron-carbon equilibrium diagram. At 1,000° C. such a steel would consist of iron in the face-centred, or γ condition, having iron carbide, Fe_3C, in solution, a structure known as austenite. On cooling below about 870° C., the iron carbide would begin to precipitate out of the solution into a second phase called cementite. On further cooling below about 690° C. the iron would recrystallize on to a body-centred lattice, as α iron or ferrite, and with this would be intimately mixed iron carbide to form a structure known as pearlite, having a total carbon content corresponding to the eutectoid composition of 0·89 per cent. The remaining carbon is then present in a second phase of iron carbide or cementite. For these changes to occur during cooling sufficient time must be allowed, and if the steel is rapidly cooled by quenching the movement of the iron carbide is partially arrested. Martensite is the structure corresponding to the condition immediately following the decomposition of austenite into pearlite. Its hardness and high internal strains are probably due to the iron carbide in a fine state of division throughout the lattice in process of separating out, the crystal structure also having just changed from the face-centred to the body-centred state. Steel in the austenitic or face-centred condition, it should be noted, is non-ferromagnetic. The observed relation between the coercivity and the carbon content for a series of plain carbon steels is shown [2] in Fig. 7.2.

It may readily be understood that such a structure obtained by quenching is not entirely stable, and, in fact,

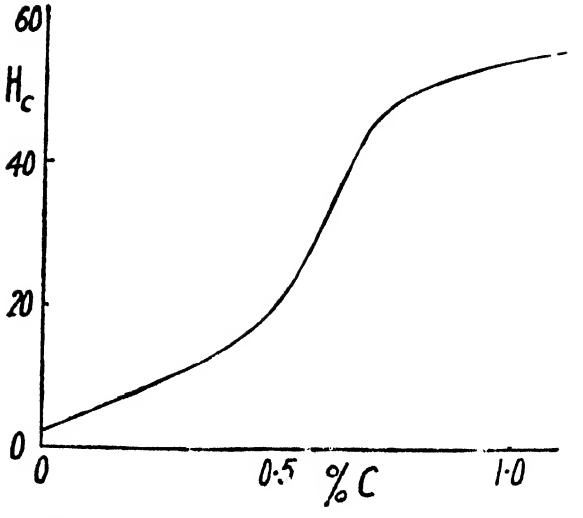

FIG. 7.2.—Coercivity of a quenched Carbon Steel relative to the amount of Carbon (Curie)

slow metallurgical changes, or 'ageing' of the material, continue at room temperature, the effect being accelerated if the temperature is raised. These simple carbon steels are also badly affected by vibration and mechanical shock.

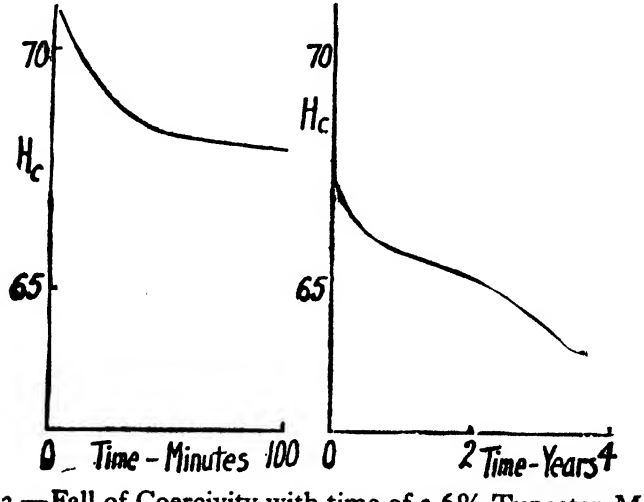

FIG. 7.3.—Fall of Coercivity with time of a 6% Tungsten Magnet Steel (Evershed)

Such changes are, of course, highly undesirable in a permanent magnet material which, in many applications, for example in precision electrical indicating instruments and in meters, is required to maintain a working flux over a period of many years to a high degree of constancy.

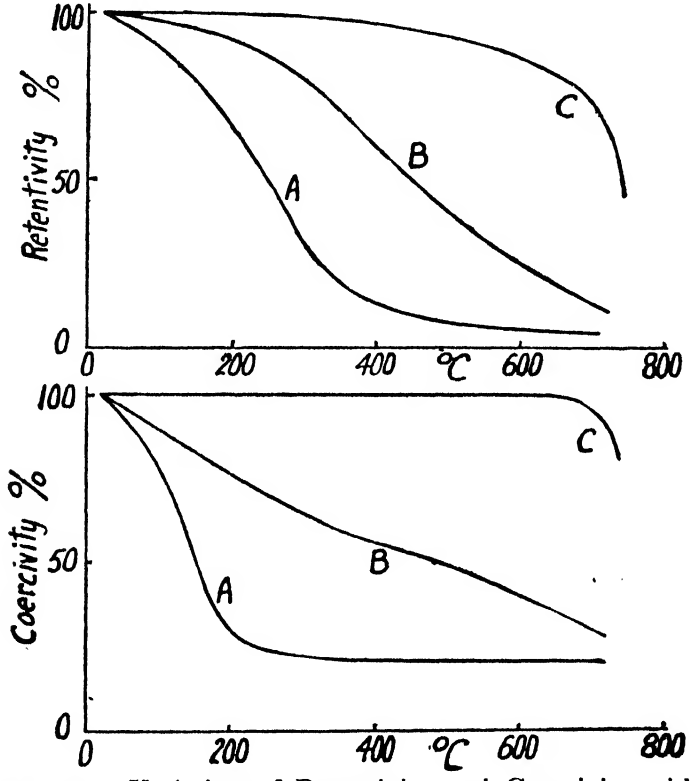

FIG. 7.4.—Variation of Retentivity and Coercivity with Temperature

A—Tungsten Steel
B—35% Cobalt Steel
C—Iron–Nickel–Aluminium Alloy (Kussmann)

The martensitic steels were subsequently improved by the addition of a third element, tungsten in the first instance and later chromium. These steels, however, are also subject to secular changes and Fig. 7.3 shows some results due to Evershed [3] for the fall in coercivity with time of a sample of tungsten magnet steel immediately

after hardening, and also after a period of several years. In 1920, Honda [4] described a greatly improved alloy containing 35 per cent cobalt, which also contained, in addition to carbon, either tungsten or molybdenum, and subsequently a complete range of cobalt steels came into use. The heat-treatment of these martensitic steels consists in oil- or air-quenching from temperatures in the

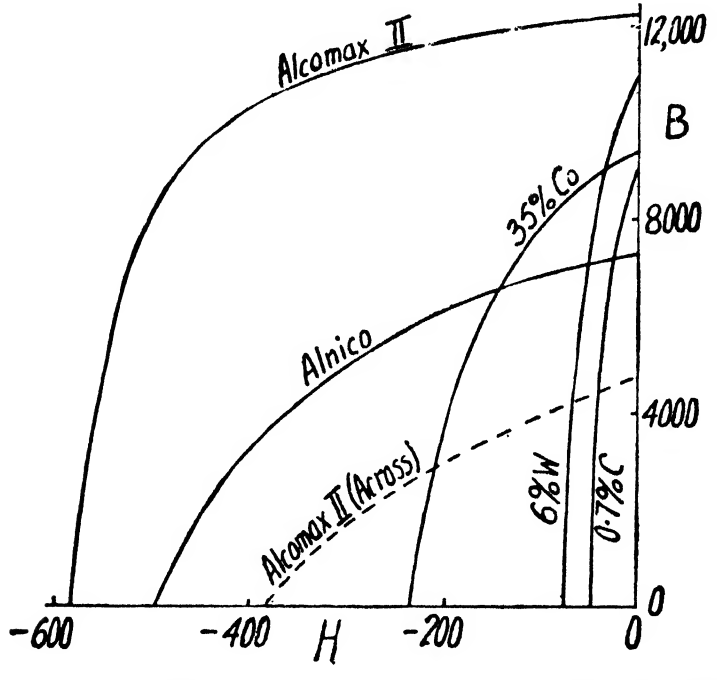

FIG. 7.5.—Demagnetization Curves of Commercial Permanent Magnet Materials

range 800 to 950° C., depending on the composition. Curves *A* and *B* in Fig. 7.4 show how tungsten steel and 35 per cent cobalt steel compare in the reduction of coercivity and retentivity with increasing temperature [5]. Table 7.1 gives the compositions and typical magnetic properties of some of these alloys, while Fig. 7.5 shows typical demagnetization curves.

It should be noted that the instability and ageing of the

TABLE 7.1

Material	Composition	Coercivity	Retentivity	$(BH)_{max.} \times 10^{-6}$
	Martensitic Steels			
Carbon Steel	1·2% C	60	8,000	0·18
Chrome Steel	6% Cr, 1% C	70	9,500	0·28
Tungsten Steel	6% W, 0·9% C	80	10,000	0·34
Cobalt-Chrome Steel	9% Co, 9% Cr	150	8,500	0·55
35% Cobalt Steel	35% Co, 3·5% Cr, 3% W, 1% C	240	9,600	0·94
	Dispersion-Hardened Alloys			
Iron-Nickel-Aluminium	29% Ni, 13·5% Al, 57·5% Fe	550	6,000	1·3
Iron-Cobalt-Tungsten	15% Co, 10–20% W, plus Fe	150	11,500	0·8
Iron-Cobalt-Molybdenum	15% Co, 10–20% Mo, plus Fe	300	10,000	1·25
Iron-Nickel-Copper	20% Ni, 62% Cu, 18% Fe	450	3,000	0·46
Nickel-Cobalt-Copper	21% Ni, 29% Co, 49% Cu, 0·75% Pb	740	3,600	0·9
'Alnico'	18% Ni, 10% Al, 12% Co, 6% Cu, 54% Fe	500	7,500	1·6
'Alnico V'	13·5% Ni, 8% Al, 24% Co, 3% Cu, 51·5% Fe	610	12,700	4·8

materials referred to above relates to slow metallurgical changes in the steels. Some weakening of a magnet can also be caused, however, independently of such changes, by mechanical effects. The permanent magnetism of a material may be attributed to the domain boundaries being held in position by barriers imposed by internal strains, in the general manner already discussed in connexion with Becker's theory. Some boundaries will be more lightly held than others, depending on the nature of the internal stress distribution, and a reverse field due to the free poles of the magnet is also always present, acting to move the boundaries in the direction which will reduce the remanent induction of the material. It is thus not difficult to see that if the internal distribution of stresses is disturbed by other stresses of a transient character introduced, for example, by an impact on the material, or by vibration, or by temperature changes, some of the internal barriers to domain boundary movement are momentarily removed or reduced and a fall in the induction in the material occurs. In practice it is customary to minimize this type of instability by suitable treatment following the magnetization of the magnet. This treatment is intended to eliminate those domains which are most lightly held in position by the internal stresses, and which are therefore most likely to reorient themselves and thus to reduce the magnet flux if the material is subjected to a mechanical shock or other disturbing influence. One method is deliberately to reduce the working flux by a few per cent by the application of an alternating field. This eliminates the more unstable domains and brings the working point of the magnet somewhat inside the characteristic demagnetization curve.

7.3. DISPERSION-HARDENED ALLOYS

The quench-hardened steels already described are still widely used, but more recently greatly improved alloys

have been produced. These newer alloys do not depend upon the presence of carbon for their high internal strains. They depend, however, upon the formation, in general, of two phases in the alloy, the phases being in an arrested state of separation out from one another. These materials are frequently referred to as ' dispersion-hardened ' alloys. Descriptions of them were first given in 1932, by Mishima [6] for alloys of iron, nickel, and aluminium, and by Seljesater and Rogers [7] and by Köster [8] for alloys of iron, tungsten, and cobalt, and of iron, molybdenum, and cobalt.

The composition of Mishima's alloy giving the best permanent magnet properties corresponds with about 29 per cent nickel, 13·5 per cent aluminium and the remainder iron. This approximates to the formula Fe_2NiAl. The best magnetic properties depend upon the rate of cooling of the alloy and are sensitive also to the precise composition. The structure of the alloy for different heat-treatments has been very thoroughly investigated by Bradley and Taylor [9]. At high temperatures the alloy is a single phase of body-centred cubic structure. If slowly cooled this breaks up into two body-centred cubic phases, one nearly pure iron and the other NiAl, these phases being only slightly different in lattice spacing. In this slow-cooled condition the internal strains are not sufficient to produce a good permanent magnet material, but if, however, an optimum rate of cooling from high temperature occurs, an incipient separation of the phases only takes place, separate crystals of the two phases not having time to grow. In this condition of arrested precipitation the whole lattice is thrown into a state of immense strain to which is attributed the high coercivity of the alloy.

A somewhat comparable magnetic performance is obtainable from the iron-tungsten-cobalt and iron-molybdenum-cobalt alloys mentioned above, with about 15 per cent cobalt and 10 to 20 per cent of tungsten or molybdenum.

The heat-treatment for these alloys consists of a quench from 1,300° C. followed by annealing at 700° C. On account of the almost simultaneous discovery of the iron-nickel-aluminium alloys, which are cheaper to produce, these alloys have not been commercially exploited.

Another interesting ternary alloy of the dispersion-hardening type is that containing iron, nickel, and copper [10]. The best composition is for about 20 per cent iron, 20 per cent nickel, and 60 per cent copper. The $(BH)_{max.}$ value of this alloy falls below those considered above (see Table 7.1), but an interesting feature is that the alloy can be readily cold-worked either before or after the hardening treatment, cold-working actually improving the magnetic properties. Similar claims [11] are made for an alloy containing iron, copper, and vanadium, and for [12] an alloy with the typical composition 21 per cent nickel, 29 per cent cobalt, 0·75 per cent lead, and 49 per cent copper.

The nickel-iron-aluminium alloy mentioned above was further improved in 1934 by Horsburgh and Tetley [13] by the further addition of cobalt and copper, the alloy being given the trade name of Alnico. Typical properties of this alloy are given in Fig. 7.5 and in Table 7.1, together with the approximate composition.

The dispersion-hardened alloys now in commercial use are superior to the martensitic steels in their $(BH)_{max.}$ value as may be seen by reference to Table 7.1, but a further important feature of the alloys is their freedom from the metallurgical instability which is a disadvantage of the latter steels. They are also much less affected by mechanical shock and by high temperature. The superiority of the iron-nickel-aluminium alloy over the martensitic tungsten and cobalt steels in the latter respect is illustrated in Fig. 7.4.

Apart from the iron-nickel-copper alloys, which, however, have a low $(BH)_{max.}$ value, the dispersion-hardened alloys are hard and brittle, and for this reason must be cast and ground to shape. Where the form or size of

magnet is unsuitable for casting some success has been achieved in employing the material in powdered form, compressed in a binding medium and sintered, which, however, reduces the retentivity of the magnet.

7.4. MAGNETICALLY ANNEALED ALLOYS

The improvement in permeability of some nickel-iron and other alloys brought about by allowing the material to cool down through the Curie temperature while a steady magnetic field was applied has been discussed in Chapter 4. Oliver and Shedden [14] appear to have been the first to try a similar treatment on materials of high coercivity. They cooled experimental cubes of Alnico of 4 cm. side from a temperature of 1,200° C. in a steady field of 4,400 gauss. The effect of this treatment was to make the material magnetically anisotropic, the value of $(BH)_{max.}$ for the direction in which the magnetic field had been applied being increased by 20 per cent and for the lateral directions decreased by 10 per cent over the values obtainable in the absence of the field. The treatment made no change to the coercivity, but raised the retentivity by $7\frac{1}{2}$ per cent for the field direction, and reduced it by about 9 per cent in the perpendicular directions. The effect may be qualitatively explained as before in terms of a preferred orientation of the domain magnetizations, the magnetostrictive strains set up on cooling through the Curie point, accompanied by some plastic relief of strain, causing, in the presence of a magnetic field, the domain vectors to favour the general direction of the applied field.

It was subsequently found [15] that a very much greater improvement could be obtained if the cobalt content of the alloy was increased with the particular object of raising the Curie temperature and thus of improving the chances of plastic flow occurring on cooling through this magnetic change point. For example, an alloy with the

composition 13·5 per cent Ni, 24 per cent Co, 8 per cent Al, 3 per cent Cu, and remainder iron, cooled from 1,250° C. to 600° C. at a rate of 1 to 5° C. per second in a magnetic field greater than 3,000 gauss, was found to have a retentivity of about 12,500, a coercivity of about 600 and a $(BH)_{max.}$ value $4{\cdot}79 \times 10^6$, the latter figure for the same alloy heat-treated with no magnetic field being about $1{\cdot}6 \times 10^6$. The principal effect of the magnetic treatment is to raise the retentivity by a very substantial amount for the working direction of the alloy, at the same time decreasing it considerably for the lateral directions. Alloys prepared in this way are now commercially available under various trade names, Ticonal, Alcomax, Alnico V. Curves are shown [16] in Fig. 7.5 for one of these materials which give the properties both in the working direction and perpendicular to it, and some data are also included in Table 7.1.

7.5. OTHER MATERIALS

A permanent magnet material prepared by mixing metallic oxide powders has been described by Kato and Takei [17]. The material consisted of equal quantities of iron oxide (Fe_3O_4) and cobalt ferrite ($CoFe_2O_4$) compressed and sintered at 1,000° C. This was then magnetized at a temperature of 300° C. and cooled down in the field. The hysteresis loop of this material, in Fig. 7.6, shows a retentivity of about 3,900 and a coercivity of about 590 with a $(BH)_{max.}$ value of approximately $1{\cdot}3 \times 10^6$. Its density is only 3·55 g./c.c.

It was found by Heusler (1898) that alloys made up of manganese, copper, and aluminium were ferromagnetic. Manganese appears to be an essential component, but the copper may be replaced by silver and the aluminium by tin. These alloys, consisting of non-ferromagnetic elements, are of great scientific interest though of little commercial utility. Fig. 7.7, however, refers to an

alloy [18] with the composition 86·9 per cent Ag, 8·8 per cent Mn, and 4·3 per cent Al, approximating to the formula Ag_5MnAl. On plotting the hysteresis loop, with the induction B as ordinate, this is seen to have a remanence of about 450 gauss and a coercive force, after applying a maximum field of about 14,000 gauss, of 460 gauss. It will be seen, however, that to reduce the intensity of magnetization J to zero a reverse field of about 5,500 is required, very much higher than the value of 460 to reduce

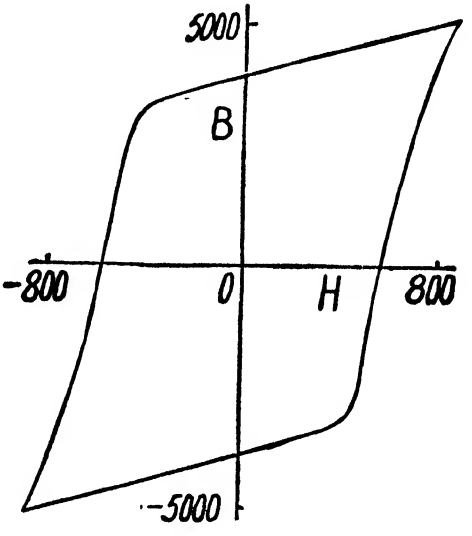

FIG. 7.6.—Hysteresis Loop of Kato and Takei's Oxide Permanent Magnet Material

B to zero. The value of the coercivity of the alloy would, according to the definition in Chapter 1, be based on the latter figure, although investigators sometimes quote values corresponding to the former figure as the coercivity. This is a rather extreme case which illustrates the care which must be taken when considering the claims made for different permanent magnet alloys of high coercivity, particularly where the retentivity is low.

Alloys of iron and platinum [19] and of cobalt and platinum [20] have also been found to give high values

of $(BH)_{max.}$. the former alloys, with equal atomic percentages of the two constituents, giving a retentivity of about 4,000 gauss and a $(BH)_{max.}$ value of about 2×10^6, and

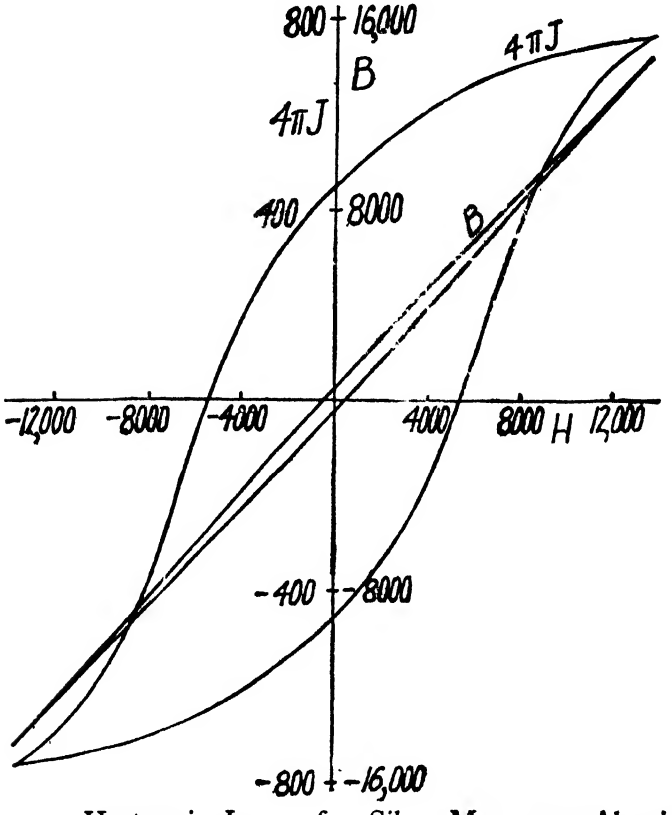

FIG. 7.7.—Hysteresis Loops for Silver-Manganese-Aluminium Alloy when plotted with B and with $4\pi J$ respectively as Ordinate (Potter)

the latter, also with equal atomic percentages, having a retentivity of about 3,000 gauss and a $(BH)_{max.}$ value of $2{\cdot}5 \times 10^6$.

REFERENCES

1. S. Evershed, *Journ. I.E.E.*, 1920, **58**, 780; A. Edwards and K. Hoselitz, *Elec. Rev.* 1944, **135**, 165; D. J. Desmond, *Journ. I.E.E.*, 1945, **92**, Part 2, 229.
2. Mme Curie, *Bull. de la Soc. d'Encouragement*, 1898, 3.

3. S. Evershed, *Journ. I.E.E.*, 1925, **63**, 725.
4. K. Honda, *Phys. Soc. Japan*, 1920, **2**, 32.
5. A. Kussmann, *Zeits. Ver. Deut. Ing.*, 1935, **79**, 1171.
6. T. Mishima, *Ohm*, 1932, **19**, 7; *Stahl u. Eisen*, 1933, **53**, 79.
7. K. S. Seljesater and B. A. Rogers, *Trans. Amer. Soc. Steel Treating*, 1932, **19**, 553.
8. W. Köster, *Arch. f. Eisenhwsn.*, 1932, **6**, 17.
9. A. J. Bradley and A. Taylor, *Magnetism*, Inst. of Phys., 1938, 91.
10. O. Dahl, J. Pfaffenberger, and N. Schwartz, *Metallwirtschaft*, 1935, **14**, 665; H. Neumann, *Metallwirtschaft*, 1935, **14**, 778; H. Neumann, A. Büchner, and H. Reinboth, *Zeits. f. Metallkunde*, 1937, **29**, 173.
11. *Bell. Lab. Record*, 1940, **19**, 36.
12. Brit. Pat. Spec. 568,418.
13. G. D. L. Horsburgh and F. W. Tetley, Brit. Pat. Spec. 431,660 and 439,543.
14. D. A. Oliver and J. W. Shedden, *Nature*, 1938, **142**, 209.
15. Brit. Pat. Spec. 522,731; A. T. van Urk, *Phillips Tech. Rev.*, 1940, **5**, 29.
16. *J.S.I.*, 1945, **22**, 56.
17. Y. Kato and T. Takei, *Journ. I.E.E. Japan*, 1933, **53**, 408.
18. H. H. Potter, *Phil. Mag.*, 1931, (7), **12**, 255; Brit. Pat. Spec. 535,168.
19. L. Graf and A. Kussmann, *Phys. Zeits.*, 1935, **135**, 36.
20. W. Jellinghaus, *Zeits. f techn. Phys.*, 1936, **17**, 33.

INDEX